ABSTRACT

Title of Dissertation: CONTINUOUSLY GRADED EXTRUDED POLYMER COMPOSITES FOR ENERGETIC APPLICATIONS FABRICATED USING TWIN-SCREW EXTRUSION PROCESSING TECHNOLOGY

Frederick Mitchell Gallant, Doctor of Philosophy, 2003

Dissertation Directed by: Professor Hugh A. Bruck
Department of Mechanical Engineering

A novel method of fabricating functionally graded extruded composite materials is proposed for propellant applications using the technology of continuous processing with a Twin-Screw Extruder. The method is applied to the manufacturing of grains for solid rocket motors in an end-burning configuration with an axial gradient in ammonium perchlorate volume fraction and relative coarse/fine particle size distributions. The fabrication of functionally graded extruded polymer composites with either inert or energetic ingredients has yet to be investigated. The lack of knowledge concerning the processing of these novel materials has necessitated that a number of research issues be addressed. Of primary concern is characterizing and modeling the relationship between the extruder screw geometry, transient processing conditions, and the gradient architecture that evolves in the extruder. Recent interpretations of the Residence Time Distributions (RTDs) and Residence Volume Distributions (RVDs) for polymer composites in the TSE are used to develop new process models for predicting gradient architectures in the direction of extrusion. An approach is developed for characterizing

the sections of the extrudate using optical, mechanical, and compositional analysis to determine the gradient architectures. The effects of processing on the burning rate properties of extruded energetic polymer composites are characterized for homogeneous formulations over a range of compositions to determine realistic gradient architectures for solid rocket motor applications. The new process models and burning rate properties that have been characterized in this research effort will be the basis for an inverse design procedure that is capable of determining gradient architectures for grains in solid rocket motors that possess tailored burning rate distributions that conform to user-defined performance specifications.

CONTINUOUSLY GRADED EXTRUDED POLYMER COMPOSITES FOR ENERGETIC APPLICATIONS FABRICATED USING TWIN-SCREW EXTRUSION PROCESSING TECHNOLOGY

by

Frederick M. Gallant

Dissertation submitted to the Faculty of the Graduate School of the
University of Maryland, College Park, in partial fulfillment
of the requirements for the degree of
Doctor of Philosophy
2003

Advisory Committee:
Dr. H. Bruck, Chairman/Advisor, Assistant Professor of Mechanical Engineering
Dr. D. Anand, Professor of Mechanical Engineering
Dr. A. Baz, Professor of Mechanical Engineering
Dr. D. Bigio, Associate Professor of Mechanical Engineering
Dr. R. Briber, Professor of Materials and Nuclear Engineering

DEDICATION

Dedicated to
My wife, Cynthia, and
two children, Adam and Kaitlyn

ACKNOWLEDGEMENTS

I would like to take this opportunity to recognize the support and contributions of some special individuals without whom I would not have been successful in my endeavor. Most important is the support, encouragement, and sacrifice made by my wife and children. They put my interests above their own needs and desires, yet they still supported me and encouraged me throughout this three-year period.

Thank you, Professor Hugh Bruck, my advisor, for your confidence, encouragement, support, and mentorship. You encouraged me through some tough periods with your leadership, patience, and direction. Following your vision of functionally graded energetic materials, I was able to achieve my academic and scientific goals.

I would like to also thank the members of my doctoral committee Professors Anand, Baz, Bigio, and Briber. Thank you for supporting my work and giving me technical direction during the proposal review and defense process. I would like to especially thank Dr. David Bigio for his mentorship, scientific insight, and allowing me to use his polymer processing facilities and work alongside his graduate students.

I would like to recognize the collaboration and hard work of many at NAVSEAIHMD. Dr. Suzanne Prickett was the lead project engineer who planned, coordinated and operated the twin-screw facility for this project with the assistance of Mr. Sharperson Johnson. I would not have made any progress without them. Thank you, Steve Mitchell, for your support of this project, funding arrangements, and vision. Mario Cesarec was responsible for the execution and research quality of the acoustic strand burning results. There would have been little fanfare to the research conclusions without his assistance.

There were many fellow graduate students that assisted me with class projects and my dissertation research. Thank you, Dr. Rajath Mudalamane, for your time and friendship. You helped me get established in the manufacturing facility and were a great source of ideas and fresh technical approaches. I would like to especially thank Mr. Arun Kota for his untiring assistance in materials characterization, especially the SEM and

pyrolysis. Thank you, Huiqing, Swami and Paul, for your friendship and assisting me with assignments.

I would like to recognize and show my appreciation to two excellent University of Mannheim internship students, Mr. Christian Rosenzwieg and Mr. Pedro Olivera. Thank you for helping me with the UMD extruder and improving the quality of my experiments.

Mitch Gallant
Waldorf, MD

TABLE OF CONTENTS

LIST OF TABLES

LIST OF FIGURES

1.0 Introduction

For a variety of applications, it desirable to determine material distributions meeting functional requirements that can vary spatially within a structure. One way to address this has been to join together different materials using techniques such as adhesion, diffusion bonding, and welding. This unfortunately gives rise to undesirably high stress concentrations at a weak interface when the structure that is susceptible to premature catastrophic failure during normal operating conditions. Another problem encountered is the concentration-directed migration of mobile ingredients during the operational life of the component that can alter the properties of the base materials to levels that are below those used during the design process. Attempts at controlling these issues have led to the concept of *Functionally Graded Materials* (FGMs), which are defined as materials that possess gradual variations in composition and/or microstructure (Suresh and Mortensen 1998).This thesis explores the application of functionally grading extruded polymer composites for propellant applications by varying the burning rate within the grain of a solid rocket motor.

FGMs represent one of the latest revolutions in materials science. They are being considered for employment in a wide variety of applications where conventional homogeneous composites are compromised against competing physical or chemical requirements. FGMS are microscopically inhomogeneous composites by design, in which the mechanical and other physical properties of the material are continuously or discretely graded from one surface to another. This is typically achieved in a single direction within a component by a continuously or gradually changing the composition of the materials. An often-cited examples are cutting tools and thermal barrier coating that possess gradients transitioning from a 100 percent ceramic surface to a 100 percent metallic interior to improve the wear or thermal resistance while maintaining the fracture toughness of the component [Suresh and Mortenson, 1998] To adequately design, study, and optimize FGMS, materials scientists must be able to understand the gradient architectures that can be created in manufacturing processes, as well as the

response of the gradient architecture to external stimuli, such as mechanical loadings and thermal shocks. Modern and future applications for these novel materials that are already under consideration include corrosion and radiation-resistant pipes for chemical plants and nuclear reactors, and thermally-resistant superstructures for transatmospheric vehicles.

The FGM concept requires the development of new material descriptions that can convey the variations in composition, microstructure, or their associated properties to a designer (Markworth *et al*, 1995) This description is known as the *gradient architecture*, Figure 1-1. Typical architectural parameters include layer thickness, *t*, and composition gradient, *p*. In designing FGMs, it will be desirable to determine the architectural parameters that optimize system performance for a component by modeling the relationship between the processing of a FGM, the gradient architectures that develop, their related properties, and the corresponding performance of the component.

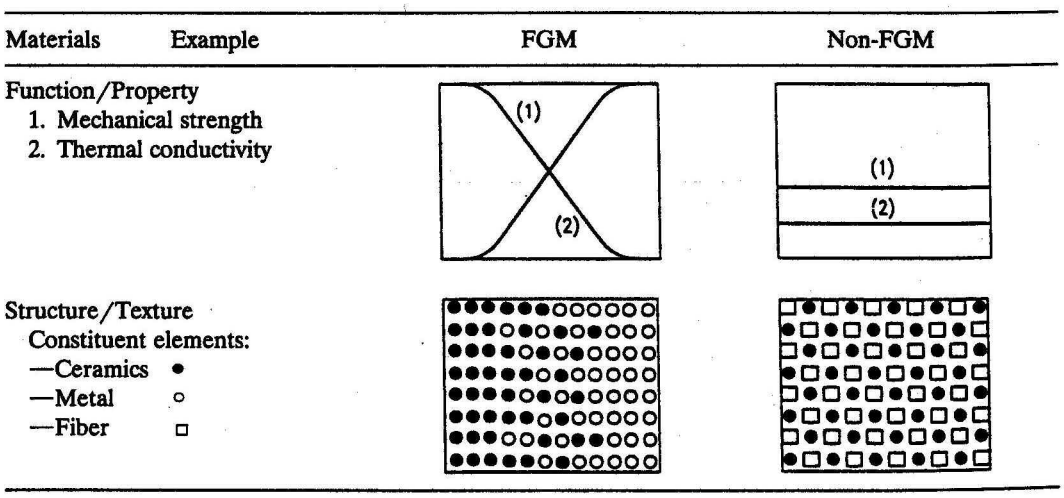

Figure 1-1. Illustration of Property Variation with Location and Microstructure (Reddy 1997).

1.1 FGM Concepts for Next Generation of Energetic Systems

FGMs are currently being applied to a variety of structural and nonstructural applications in non-military applications [Niino and Maeda, 1990; Suresh and Mortenson, 1998]. Recently, FGM concepts have become of interest to the military to

improve the performance of energetic systems such as propellants, by replacing geometrically complex features of the energetic portion of a gun or rocket motor, known as a *grain*, with simpler geometries that improve reliability while meeting the desired performance requirements,. In the case of a solid rocket propellant, the energetic portion is referred to also as a *grain*, it is hypothesized that the volume fraction of 30 and 200-micron ammonium perchlorate (AP) particles, V_{AP}, can be varied along the length of the grain to produce a corresponding variation in burning rate properties. It is important to realize that the burning rate is related not only to the volume fraction of AP particles, but the particle size distribution as well. Both of these parameters, among others, are available to the motor designer/propellant formulator.

One of the technical challenges to develop functionally graded propellants is the lack of a design methodology and manufacturing technology for processing continuously graded architectures in polymer composites. Attempts at been made to disperse microballoons in epoxy and urethane using a gravity casting technique to create continuous gradients over volume fraction ranges of 0 to 0.45 (El-Hadek and Tippur, 2002; Butcher *et al*, 1998). Therefore, it is necessary to develop a novel continuous processing technology for FGMs using an inverse design procedure that can be applied to propellants. A novel continuous processing technology that has shown a great deal of promise for solid rocket propellants is known as twin-screw extrusion (TSE) (Muscato, Michienzi et al. 1999). TSE processing can be applied not only to the fabrication of continuously graded solid rocket propellants, but to the fabrication of continuously graded extruded polymer composites for non-energetic applications as well.

1.1.1 The Inverse Design Procedure

For solid rocket propellants, it will be desirable to tailor the burning rate performance in a monolithic rocket motor utilizing new knowledge of the TSE process based on the gradient architectures that can be achieved by operating the extruder in a transient state. Because the conventional design of rocket motors utilizes homogeneous and not graded materials, the current focus of designers is on determining complex geometries that conform to the desired burn rate performance instead of varying the burn rate properties through the gradient architecture of the grain. The focus on gradient

architectures instead of complex geometries necessitates a new approach to designing energetic systems using continuously graded extruded polymer composites. The Japanese have proposed such an approach, and it has been termed the "*Inverse Design Procedure*" (IDP) [Niino and Maeda, 1990]. Thus, it is necessary to develop an IDP that will ultimately serve as a tool for the designers and manufacturers of solid rocket motors. Using the IDP, an entirely new methodology for designing energetic systems will be available for advanced energetics concepts, where the in-flight performance of a rocket motor (simply that part of a rocket consisting of the propellant grain, its case, and a nozzle) can be specified without having the constraint of geometrically complex designs that can not produce the desired performance either because of manufacturing or material limitations. Employing the IDP, the gradient architecture that achieves the specified performance can be easily predicted with or without geometric constraints, as well as the operating conditions that are necessary to create it using a given manufacturing process.

In the IDP, the specified performance is defined through an objective function, and the inverse problem is solved using mathematical optimization techniques to obtain the system parameters that satisfy the objective function. To design for manufacturing a component using the inverse design process, the designer must specify the choice of the objective function. Materials are then selected from a database of available materials that can potentially satisfy the requirements for a given application. These are then used to get the optimal material distribution that satisfies the target requirements. This is done for different selections of materials and the best design is picked from among these. The complexity and capability of the manufacturing process also influences the decision on the selection of the best design. In the case when the material selected is a FGM, the problem gets more complicated since there are an infinite number of gradient architectures that must be considered for every material combination. .

These complications are simplified by choosing a single material combination and assuming that an optimal gradient architecture exists along one direction of the component. Determining the optimal gradient architecture for a given set of specifications require the use of optimization methods to solve for the gradient. Various optimization techniques are available to arrive at the solution that achieves the best

value for the defined objective. Given the inherent complexity in the architecture of FGMs, the Genetic Algorithm optimization method has been demonstrated to be a robust and efficient technique for determining the optimal gradient architecture [Surendranath *et al,* 2002]

The inverse design procedure can be summarized as follows in Figure 1-2:

1. Define the required target performance or the system objectives
2. Select the material components for the gradient architecture
3. Determine the gradient architectures that evolve in a manufacturing process, such as TSE, for a given set of operating conditions.
4. Evaluate the relationship between the microstructures in the gradient architecture and their associated physical properties.
5. Evaluate the optimal gradient architecture using mathematical optimization techniques, such as Genetic Algorithms.
6. Fabricate the component with the optimal gradient architecture .
7. Test the performance of the component for desired performance
8. If the desired performance is not achieved, reassess processing/structure/property relationship for the gradient architecture or the performance modeling of the gradient architecture.

Critical to the IDP are appropriate processing models that describe the relationship between operating conditions and the gradient architectures that evolve in a specific manufacturing process, such as TSE. These models will define the limits that restrict the evolution of the microstructures, and therefore constrain the range for the architectural parameters over which a gradient architecture can be fabricated. Each manufacturing process will have its own set of constraints that must be determined experimentally in order to develop the appropriate processing models.

1.2 Project Hierarchy

The research described herein primarily addresses the pieces of the inverse design highlighted by red in Figure 2. The research approach is multidisciplinary, and was primarily sponsored by an Office of Naval Research Young Investigator's Program (ONR YIP) granted to Professor Hugh A. Bruck with additional in-house research funding and support from the Indian Head Division of the Naval Surface Warfare Center (NAVSEAIHMD) for the energetic materials portion of the program. This research

program was facilitated by a collaborative research agreement between UMD and NAVSEAIHMD that is administered through the Center of Energetic Concepts Development (CECD). The research was conducted at both the College Park campus of UMD and in the unique processing facilities of NAVSEAIHMD with the inert/energetic ingredients demarcating the two facilities. The research was conducted in three areas: processing science, materials characterization, and property/performance models. This thesis addresses makes contributions in the first two areas that also have an impact on the third. Contributions from all three areas provide the models and computational tools for the inverse design procedure.

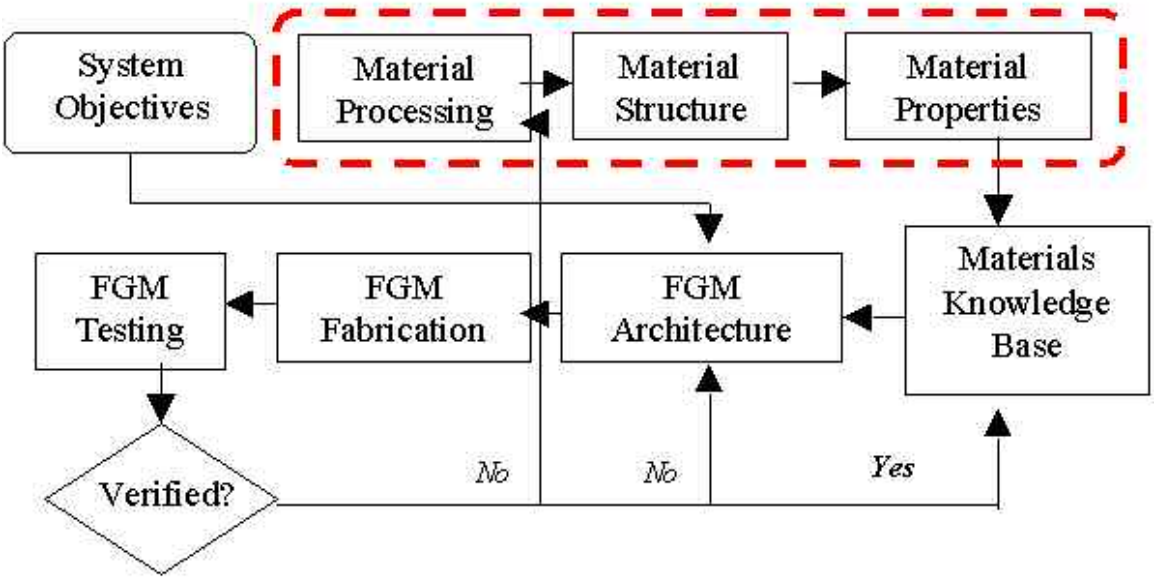

Figure 1-2. Flowchart illustrating the Inverse Design Procedure (Bruck *et al*, 2002).

1.2.1 Research Issues

This thesis addresses a number of fundamental questions relating to the operation of a twin-screw extruder in a transient state and to the microstructures of highly filled polymer composites that evolve during this process. These questions include:

1. How does transience in the operating conditions during processing affect the gradient architecture of the extruded composite?

2. Can this evolution be predicted using a quantifiable process model based on concepts such as the Residence Time Distributions (RTD) or the Residence Volume Distributions (RVD)?
3. What characterization techniques have to be developed to adequately describe and quantify the gradient architecture in the extruded material?
4. How are these gradients related to performance as measured by the burning rate?

1.3 Intellectual Contributions

Answers to the fundamental questions that are addressed by the research effort described in this thesis have resulted in the following scientific and technical knowledge:

- The relationship between the composition gradients that evolve in the TSE and the operating conditions for the extruder has been characterized through new process models
- The applicability of RTDand RVD characterization of the TSE process has been extended to polymer composites
- Techniques for quantifying the gradient architecture of extruded polymer composites have been developed
- The dependence of the burning rate performance on the microstructures in the gradient architecture have been characterized
- The new process models and characterized properties provide the basis for establishing an IDP that provides the operating conditions to meet a desired performance objective for a given energetic formulation and TSE screw configuration

1.4 Impact on Industrial Practices

The research described in this thesis will also have a broader impact commercial and military applications for both energetic and non-energetic of FGMs as follows:

- Establishes a new technology area for producing tailored energetic systems for commercial, as well as military, applications
- Establishes new techniques for fabricating FGMs using the transient attributes of continuous processing technologies
- Describes mixture experiments with operating conditions that are of great interest to energetics manufacturing facilities such as NAVSEA-IHMD

- Presents new characterization techniques for energetic and non-energetic extruded polymer composites

1.5 Organization of Dissertation

The following sections will address these questions by presenting data from work in-progress and plans for work based on indications given in the literature. Chapter 2 contains a description of the twin-screw process, associated processing equipment and instrumentation, and proposed methods for characterizing the process through the study of RTDs. Chapter 3 describes the TSE experiments conducted on inert and energetic formulations to characterize the RVDs and RTDs for the materials and process. Chapter 4 describes experiments where variations in process conditions through step and ramp changes in feed conditions are characterized in order to develop a convolution process model for describing the gradient architecture that evolves. Chapter 5 describes the characterization of the gradient architecture for the inert formulations using optical, mechanical, and microscopy techniques. Chapter 6 will describe the characterization of combustion properties over a range of compositions for the homogeneous energetic formulations, and its relationship to the burning rate response for graded energetic formulations. The final section will summarize the accomplishments of the thesis and discuss research issues that have been uncovered during the course of the thesis that have potential for future investigation.

2.0 Continuous Processing Using a Twin-Screw Extruder

Twin-screw extrusion processes are utilized to manufacture a number of consumer and industrial goods, from snack foods and medical tubing to plastic pellets and military propellants. The process is a continuous type in that the twin-screw extruder will produce a product as long as the ingredient supply is maintained. Because this type of process has so many advantages over batch type, it has found widespread utility across diverse industries. For most however the advantages are universal: economy, quality, environment, flexibility, and safety. In the case of energetic materials, all these advantages have been documented (Staub, Neuenschwander et al. 1989) (Muscato, Michienzi et al. 1999). Some of these advantages illustrate why the twin-screw extruder shows great promise for producing functionally graded materials.

2.1 The Twin-Screw Extruder

First a description of the equipment is necessary. The extruder consists of two screws, typically fully intermeshing, which run through temperature-controlled barrels. The barrels are modular in design and specialized for feeding solid and liquid ingredients, vacuum, or other functions. They are interchangeable allowing a configuration best suited to a particular process. Furthermore the screws consist of various segmented elements that slide onto the screw shafts allowing for customizable screw designs. Like the barrel sections, various screw geometries are available which are utilized for conveying ingredients, gentle and high shear mixing, devolatilization, and many others. Hence the mixer is highly configurable and thus very flexible allowing for the optimization of many types of processes. In less time than a typical work shift, the mixer and its auxiliary equipment can be reconfigured for a completely different product.

This flexibility lends itself to facility expenditure savings. As with the case of naval gun propellants, the discrete batch process required a number of individual process steps, each with its own facility, equipment and operators. The continuous process with a twin-screw extruder eliminates some steps and allows others to be combined. The result is a great reduction in the number of facilities required and a continuous operation; this is a savings of resources and operating costs. In that the mixing/extrusion /cutting operation is remotely operated, the safety of the process is much greater by reduced operator exposure to hazards and reduced quantities in a mixing state at any point in time.

Furthermore the continuous process yields a more consistent product thus improving overall quality. There is significantly less variation in material, and the efficiency of mixing is better than batch methods. The process lends itself to on-line analysis allowing for the quick detection of anomalous conditions or material automatically diverting it to waste. In the batch process this is impossible until later in the production after a large quantity of potentially bad product has been made.

The extruder is only the heart of the process as shown in Figure 2-1. Various ingredient feeders support the process. The quality of the extruded product is directly influenced by the accuracy of the ingredient addition. For this reason, only the most accurate feeding technologies are utilized. These commonly include loss-in-weight control for solid ingredients and flow metering control for liquids.

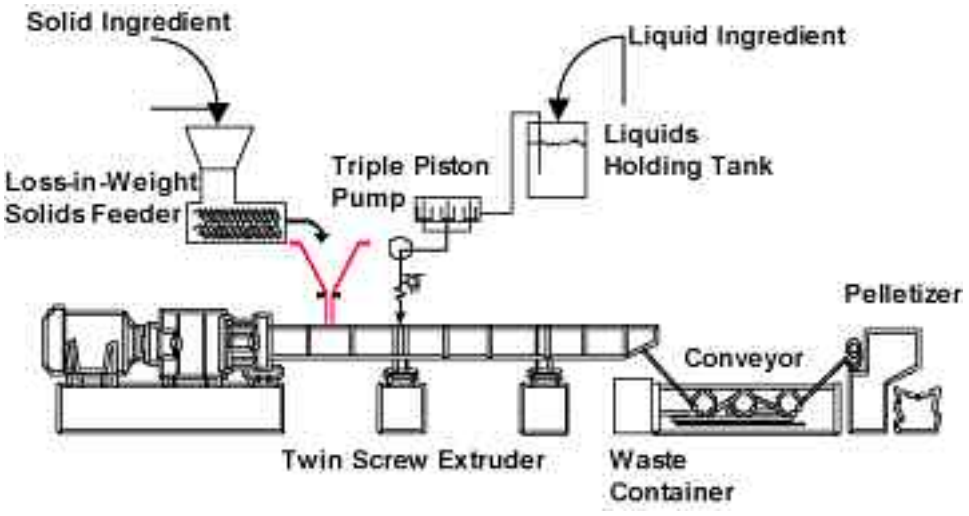

Figure 2-1. Twin-screw extrusion process

Other support equipment includes product collection. For the example in Figure 2-1, the extruded strand is conveyed to a pelletizer where it is cut by a rotating blade into short *pellets*. Not shown are the temperature control units for the extruder barrels and the process control system for the facility.

2.1.1 Modeling of TSE Process

There are a number of research issues related to TSE processing that must be addressed in order to develop a predictive model for continuously extruded polymer composites. These include:

1. Developing techniques for quantitative characterization of the gradient architecture
2. Characterizing the effects of solid ingredients on conventional TSE process models that have been developed for polymers
3. Study of the coupling between the operating conditions and the gradient architecture that evolves in the TSE process.

The physical basis for the TSE process is the transport of material through a fully intermeshing twin-screw extruder is accomplished by screw geometry and screw motion (Rauwendaal 1986). In other words, the material flow is due to a combination of drag flow and pressure flow. The actual breakdown between each is highly dependent upon material properties, screw elements' geometry, and rotational speed. In the case of energetic processing, the TSE is used as a mixer (or compounder) of ingredients, deaerator, and extruder in the same process step as material travels through the barrels. This aspect alone can result in evolving material properties that are difficult to estimate and are dependent upon time and location in the process. Therefore, calculations of drag flow and degree of fill are subject to approximation. For these reasons, the quantitative residence time of the system becomes a convenient measurement of the cumulative effect of all process and material parameters on the transport and mixing of the material in the TSE process. This has lead to the concept of the Residence Time Distribution (RTD), and its volumetric equivalent, the Residence Volume Distribution (RVD), as common descriptors for the physics of the TSE process. These are typically expressed as normalized functions in the following forms:

$$f(t) = \frac{c(t)}{\int_0^\infty |c(t)|\, dt} \quad (1)$$

$$g(v) = \frac{c\left(\frac{v}{Q}\right)}{\int_0^\infty \left|c\left(\frac{v}{Q}\right)\right| dv} \quad (2)$$

where *f(t)* is the normalized RTD, *g(v)* is the normalized RVD, *Q* is the throughput, *t* is time, *v* is volume, and *c* is the response function associated with the amount of material that is located at a designated position in the extruder at the time, *t*, or volume, *v*.

2.1.2 Screw Geometry and Degree of Fill

The effects of the TSE process on microstructural evolution is directing related to the nature of the screws themselves. The geometry used for the screws is highly flexible in that individual element pairs of different shapes can be added together to result in specialized combinations for different material formulations. Figure 4 is a photograph of screws that have been removed from the barrels immediately after a mid-operation stop. Note the differences in geometry in regards to pitch, direction, and shape.

The direction of flow through the barrels is from the left to the right as looking at the picture. This picture is a good illustration of the state, mixing and distribution of material in the process at any given time. In general, twin screw extruders are *starved fed*, i.e., the screw channels are not completely full in the locations where ingredients are added in order to promote mixing. However the degree of fill in the screws downstream of ingredient addition is variable depending upon the geometry, ingredient throughput rate, screw speed, and time, refer to Figure 2-2. Places of high fill, including 100 percent, occur in sections where there are mixing and left-handed screw elements. There is material located on the conveying screws elements, though the degree of fill is significantly less.

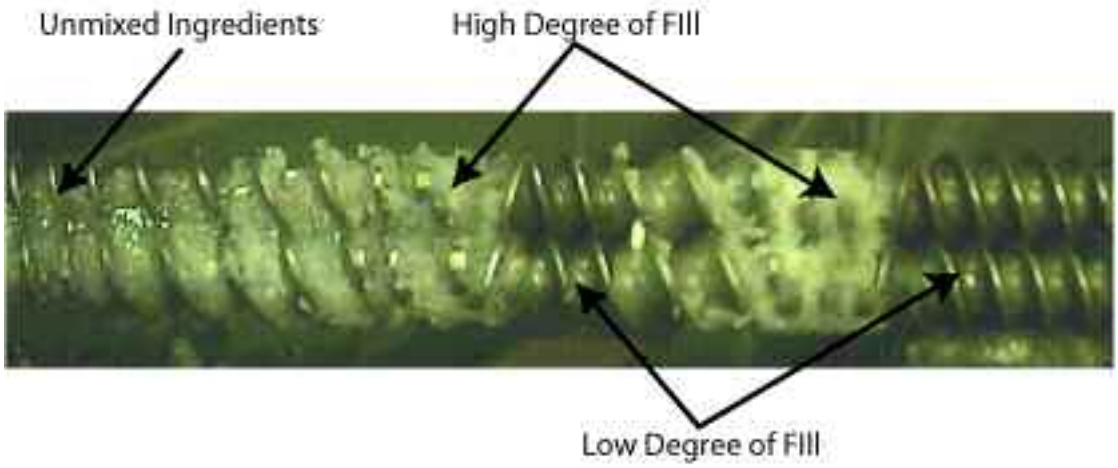

Figure 2-2. Picture of unmixed and mixed material on twin screws after process has been halted and the screws extracted

2.2 Distributions & Process Modeling

Physically the RTD is a characteristic of the process that is studied to quantify the dampening as a result of backmixing that occurs in the extruder (Rauwendaal 1986). Under normal and steady operating conditions there is a continuous supply of material conveyed to the mixing zones, and an equal amount conveyed away. Much of the literature for the twin-screw process has focused on characterizing the process operating in steady-state. The basis for characterizing the steady-state transport of material within a twin-screw extruder has been the residence time distribution. The concept of distribution functions and age distributions is attributed to the classical work of Danckwerts (Danckwerts 1953), including the experimental method of tracer addition for determining the residence time distribution. In the following five decades RTD studies have been performed on all varieties of extruders, and equally varied are the types of tracers and experimental techniques employed. Most literature has limited applicability and merely reports the material extruded or reacted, the screw configuration, and the resulting experimental data with little discussion in regards to the mechanisms or general relationships that advance the state of knowledge for the physics of the process.

In an excellent review of this body of work, Gao reports that the basis for RTD studies has been to characterize the ability of the process to dampen disturbances, such as ingredient variations, feeder upsets, etc (Gao, Walsh et al. 1999). The answer is dependent upon the time scale of the disturbance. The method of tracer introduction is

generally the impulse or spike by concentrated injection of solids introduced onto the rotating screws. However this FGM project will be specifically interested in step inputs as much as the impulse inputs. *Step inputs of the ingredients will be the primary mechanism for generating the gradient in the extrudate, since they can produce the most abrupt change in material composition and can be easily superposed to create more complex feeding conditions, such as a ramp or higher order change in feed rate.*.

Previous studies that have focused on co-rotating twin-screw extruders are most germane to this investigation. There are significant differences in operation and transport among the various classifications of twin-screw extruders. However methods to experimentally determine the characteristics of material transport can be universally applied, but the interpretations and mechanisms will depend on the classification. Furthermore, most of the literature regarding transport has focused on time-based concepts. Gasner *et al* expressed the residence distribution in different domains beyond time in a corotating twin-screw extruder, i.e., as functions of screw revolutions and material volumes (Gasner, Bigio et al. 1999). Gasner used published data to illustrate these ideas. It has been these alternative domains that have yielded important insight into the similarities between processing conditions which are essentially to developing a unified model of the TSE process.

2.2.1 RTD Process Models

In a more complete study, Gao *et al* have developed more general domain transformations, and conducted experiments to illustrate their applicability (Gao, Walsh *et al*. 1999) (Gao, Walsh et al. 2000). The transient process models are based on the models describing the transport of a disturbance through a series of perfect mixers including a dead time. One mixer is a first order model; two mixers in series is a second order model etc. A third order model was used by Gao *et al* with the interpretation that the screw geometry could be described as a series of mixers in series. The two mixing zones and the combined metering zones attribute to the employment of a third order model.

In the Laplace domain, the first order model with a dead time is given by,

$$M(s) = \frac{a}{s+a} e^{-ts} \qquad (3)$$

Likewise, the third order model with a dead time is given by,

$$M(s) = \left(\frac{a}{s+a} \right)^3 e^{-t_d s} \tag{4}$$

The inverse Laplace transform for this expression is the same as that used by Gao *et al* (Gao, Walsh et al. 2000) to fit normalized RTD data for a specific screw configuration.

$$\mathcal{L}^{-1}\left[M(s)\right] = f(t) = \frac{a^3}{2}\left(t - t_d\right)^2 e^{-a\left(t-t_d\right)} \tag{5}$$

It consists of two parameters, the delay time and a shape factor. Gao *et al* showed how these parameters can be estimated from knowledge of the screw geometry and a set of constants determined experimentally. In other words, a characterized RTD from one set of conditions can be used to predict the residence time at various other conditions given the same screw geometry profile. The power in this is that a certain desired microstructure in a FGM rocket grain could be directly related to a specific RTD. Then the conditions to achieve that RTD could be estimated using Gao's set of relationships as defined in the following.

The delay time, t_d, is defined as the time from tracer introduction to detection by the probe. It can be determined from the mean residence time, t_m, and the shape factor, a, by the this expression,

$$t_d = t_m - \frac{3}{a} \tag{6}$$

Gasner reports that t_m is the result of additive effects of feed rate (of ingredients to the process), expressed in the form of the volumetric throughput, Q, and extruder screw speed, N, as follows by calculating the coefficients, A and B, from experimental data.

$$t_m = \frac{A}{Q} + \frac{B}{N} \tag{7}$$

However Gao shows that these are not coefficients but quantities that can be determined from screw geometry. In other words the mean residence time is the sum of flow through the filled and partially filled sections of the screw (Figure 4). The filled quantity, A, is based on the length of the mixing sections and conveying sections with 100 percent screw fill as given by equation (8). (Note that mixing sections are typically assumed to be 100 percent filled, but this assumption should be tested.)

$$A = A_f L_m + V_p$$

where,

A_f = free cross - sectional area of the screws

L_m = length of mixing section

V_p = filled volume in a conveying section due pressure back flow, e.g., at the die

(8)

Rauwendahl calculates A_f by (Rauwendaal 1986),

$$A_f = D^2\left[\left(p - \tfrac{1}{2}\right)\alpha_i + \left(p + \tfrac{1}{2}\right)\sin\alpha_i \cos\alpha_i - \pi\cos^2\alpha_i + \left(\pi - 2p\alpha_i\right)\cos\alpha_i\right]$$

where,

D = diameter of the screws

p = number of starts on screw (aka lobes)

α_i = angle of intermesh

(9)

The quantity, B, is the unfilled parameter; it is calculated from the geometry of the unfilled screw flights as follows (Booy 1980) (Gasner, Bigio et al. 1999) (Gao, Walsh et al. 2000),

$$B = \frac{2A_f L_c}{(2p-1)\pi DWHF_d \cos\phi}$$

where,

L_c = length of the partially filled conveying screws

W = screw channel width

H = screw channel height

F_d = screw shape factor (Booy 1980)

ϕ = helix angle of screw flights

(10)

The other parameter in (6) is a curve shape factor, *a*; and, it is based on the volumetric throughput rate, *Q*, and a coefficient, *C*, that must be experimentally derived.

$$a = CQ \tag{11}$$

2.2.2 The RVD Process Model

In the volume domain, equation (12), the locations of the residence volume distributions are independent of mass throughputs and only dependent upon screw geometry and operating conditions such as extruder screw speed or temperatures. Furthermore, the shape of the RVD curve is independent of the extruder screw speed as

well. In this manner, Gao showed that a universal process model could be developed independent of the operating conditions, and that screw designs indeed would could uniquely determine the effect of processing on microstructural evolution, thereby resulting in a the possibility of utilizing shape factors to "*fingerprint*" the process. This being true, it is then possible to predict the RTD for different operating conditions once the RVD is established for a specific screw design. This transformation from the time domain to volume is important for two reasons. The first is the power of one function to predict the transient material response for any throughput. The second is the convenience of expressing the screw mixing function and the gradient characteristics in the same manner, as functions of volume.

$$g(v) = \frac{c\left(\frac{v}{Q}\right)}{\int_0^\infty \left| c\left(\frac{v}{Q}\right) \right| dv} = \frac{e\left(\frac{v}{Q}\right)}{Q} = \frac{a_v^3}{2}\left(v - v_d\right)^2 e^{-a_v\left(v - v_d\right)} \tag{12}$$

The delay volume, v_d, is given by,

$$v_d = t_d \times Q = A - \frac{3}{C} + B\frac{Q}{N} \tag{13}$$

and the RVD curve shape factor, a_v, shown below.

$$a_v = \frac{a}{Q} = C \tag{14}$$

2.2.3 Different Order RD models

Although this investigation initially focused on Gao's third order model, it was found to be incomplete in describing the residence response for the particular screw design used in this investigation for inert composite formulation. Exploring models of lower and higher orders provided a much better description of the residence responses. The n^{th}-order model can be expressed as,

$$M(s) = \left(\frac{a}{s + a}\right)^n e^{-t_d s} \tag{15}$$

The inverse Laplace transform for this expression given in terms of volume is,

$$\mathcal{L}^{-1}\left[M(s)\right] = f(v) = a_v^n \left(v - v_d\right)^{n-1} e^{-a_v\left(v - v_d\right)} \tag{16}$$

This is a function that describes the residence volume distribution for a n^{th}-order ideal mixer with a dead time. The volume delay, v_d, is a locating factor for the function, and the RVD shape factor, a_v, is a parameter that governs the shape of the distribution.

Higher order models beyond the third were derived in a similar manner to describe the RVDs produced by the extruder at NAVSEAIHMD. The implementation of the models is discussed in Chapter 3 and implication on the structure of the gradient in Chapter 4. The fourth and fifth order models are respectively given by,

$$M(s) = \left(\frac{a}{s+a}\right)^4 e^{-t_d s} \tag{17}$$

$$M(s) = \left(\frac{a}{s+a}\right)^5 e^{-t_d s} \tag{18}$$

The inverse Laplace transforms in the volume domain are,

$$\mathcal{L}^{-1}[M(s)] = f(v) = \frac{a_v^4}{6}(v - v_d)^3 \, e^{-a_v(v-v_d)} \tag{19}$$

$$\mathcal{L}^{-1}[M(s)] = f(v) = \frac{a_v^5}{24}(v - v_d)^4 \, e^{-a_v(v-v_d)} \tag{20}$$

These are new representations for RVDs that are being proposed for describing the TSE process for the extruders configured in this research investigation. The application of these new higher order RVD models to continuous processing data is given in Chapters 3 and 4, where comparisons are made with the third order model as well. There are useful extensions to these functions to describe the distribution in more convenient terms, as will become apparent in the development of a relationship between the RVD and the gradient architecture that evolves in the TSE process.

2.2.4 Convolution of the Residence Distribution Models

One of the most important research questions was if the description of the gradient could be related to some process characteristic. The best characterization method for a process is the residence distribution (RD) in time (Danckwerts 1953), (Levenspiel 1989), and (Fogler 1999) or volume (Gao, Walsh et al. 1999) and (Gasner, Bigio et al. 1999). The results of the functionally graded energetic material research effort have shown that a convolution of a RD model with a step input yields a good estimate of the gradient evolution.

The behavior of a linear, continuous, time-invariant system with input signal, *u(t)*, and output signal, *y(t)*, is described by the *convolution integral* (Nise 2000) and (Fogler 1999).

$$\tilde{y}(t) = \int_0^t \tilde{\Phi}(t-\tau)\tilde{B}\tilde{u}(\tau)d\tau \tag{21}$$

The description of the second order RD model, where *x* can be volume or time, is given by,

$$f(x) = a_x^2\left(x - x_d\right)e^{-a_x\left(x-x_d\right)}u(x_d) \tag{22}$$

and the convoluted function, *F(x)*, or *cumulative distribution function*, for a second order system is given as,

$$F(x) = u(x_d)\int_0^{\infty} a_x^2\left(x - x_d\right)e^{-a_x\left(x-x_d\right)}dx \tag{23}$$

Letting $x_{delay} = 0$ and solving the integral, (23) reduces to,

$$F(x) = 1-(1+a_x x)\,e^{-a_x x} \tag{24}$$

This form is acceptable because *F(x)* has a value of 0 until the delay time or delay volume by the definition of the step function. The convolution functions for the first, second, and third order systems are shown in Table 2-1. These functions were used to describe the response of the process to a step input (Chapter 5).

Table 2-1. Convolution functions for first, second, and third order ideal mixer systems.

Order	RD Model	Convolution of RD Model with Step Input ($x_d = 0$)
First	$f(x) = a_x\,e^{-a_x\left(x-x_d\right)}u(x_d)$	$F(x) = 1-e^{-a_x x}$
Second	$f(x) = a_x^2\left(x - x_d\right)e^{-a_x\left(x-x_d\right)}u(x_d)$	$F(x) = 1-(1+a_x x)\,e^{-a_x x}$
Third	$f(x) = \frac{a_x^3}{2}\left(x - x_d\right)^2 e^{-a_x\left(x-x_d\right)}u(x_d)$	$F(x) = 1-\left(1+a_x x+\frac{a_x^2 x^2}{2}\right)e^{-a_x x}$

A general relationship between the convolution of the residence distribution function, *f(x)*, and the measured response function, *h(x)*, can also be developed using the following form of the convolution integral,

$$h(x) = \int_0^{\infty} g(x-x')u(x')dx' \tag{25}$$

For an impulse input, *u(x) = H(x)-H(x-ε)*, where *H(x)* is the Heaviside Step Function and ε is a perturbation, the following response function is measured,

$$h(x) = \int_0^\infty g(x-x')[H(x') - H(x'-\varepsilon)]dx'$$

$$= \int_0^\infty g(x-x')dx' - \int_0^\infty g(x-x')H(x'-\varepsilon)dx'$$

$$= \int_0^\infty g(x-x')dx' - \int_\varepsilon^\infty g(x-x')H(x')dx'$$

$$= \int_0^\varepsilon g(x-x')dx' \qquad (26)$$

But the perturbation can be assumed to be infinitesimal, yielding the following relationship between the residence distribution function and the measured response function,

$$h(x) \approx g(x)\varepsilon \qquad (27)$$

The normalized response, *h(x)*, is therefore given by,

$$\bar{h}(x) = \frac{h(x)}{\int_0^\infty h(x')dx'} \approx \frac{g(x)\varepsilon}{\int_0^\infty g(x')\varepsilon dx'} = \frac{g(x)}{\int_0^\infty g(x')dx'} \qquad (28)$$

which is identical to the definition of the normalized residence distribution function. Therefore, the normalized residence distribution function can be determined from a small perturbation to the input of the twin-screw extruder. However, it is important to note that if the perturbation is too small, it can not be detected, while a large perturbation will deviate significantly from the approximate relationship expressed in equation (27) and will require the use of the exact relationship expressed in equation (26).

For a unit step response, *u(x) = H(x)*, the following relationship is obtained,

$$h(x) = \int_0^\infty g(x-x')H(x')dx' = \int_0^\infty g(x-x')dx' \qquad (29)$$

using the transform, $\bar{x} = x - x'$, equation (29) can be rewritten as,

$$h(x) = -\int_{x}^{x-\infty} g(\bar{x})d\bar{x}$$

$$= \int_{x-\infty}^{x} g(\bar{x})d\bar{x}$$

$$= \int_{-\infty}^{x} g(\bar{x})d\bar{x} \qquad (30)$$

For the TSE process, $g(x)=0$ for $x<0$, yielding,

$$h(x) = \int_{0}^{x} g(\bar{x})d\bar{x} \qquad (31)$$

Therefore, the gradient architecture that is attributed to a step change in the input to the extruder can be easily predicted by integrating the measured response from a perturbation to the input.

3.0 Residence Distribution Experiments

3.1 Residence Distribution Experiments of KCl/Elastomer Composite in UMD 28 mm Twin-Screw Extruder

3.1.1 Facility Description

For this research investigation, a special TSE facility was assembled in the Polymer Processing Laboratory at the University of Maryland that was capable of controlling the evolution of gradient architectures in polymer composites. A laboratory scale Werner & Pfleiderer model ZDSK-28 twin-screw extruder featuring co-rotating fully-intermeshing screws was the focal point of the experimental set-up. The extruder is shown in Figures 3-1 through 3-3. A twin-screw extruder is classified by the degree of screw-to-screw

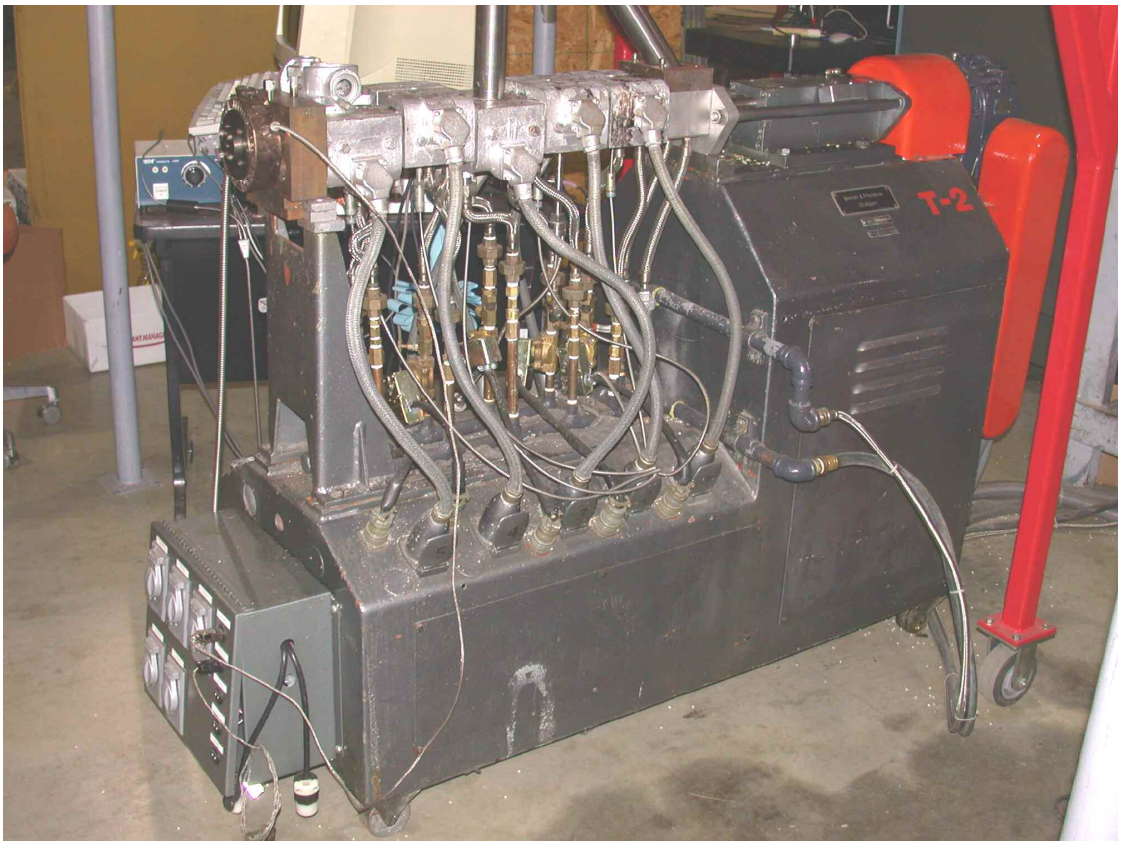

Figure 3-1. The ZDSK-28 twin-screw extruder at the University of Maryland is a laboratory-sized extruder.

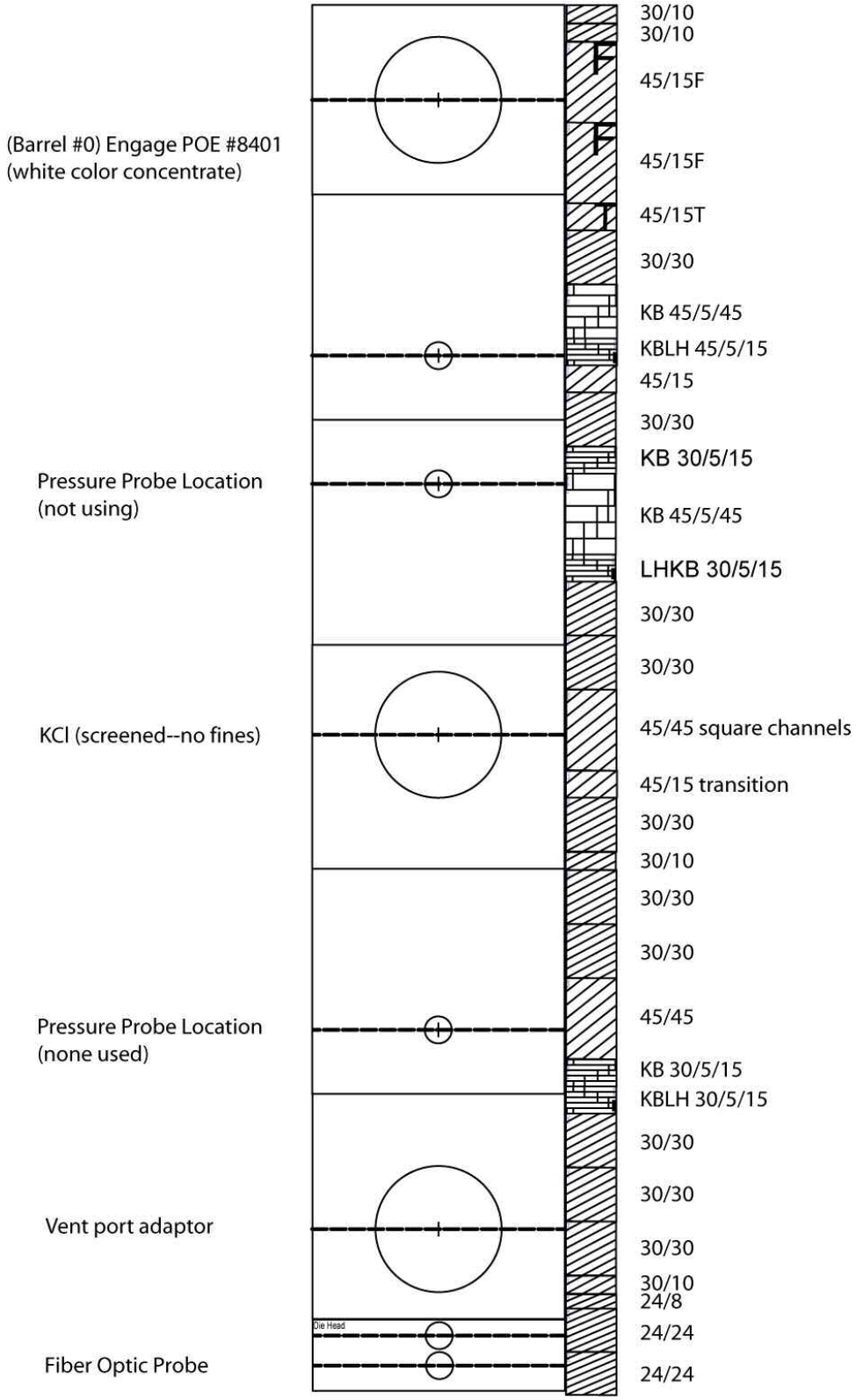

Figure 3-2. Screw Design, Barrel Configuration, and Feed Locations for the experiments conducted on the KCl-filled Elastomer.

intermesh and direction of rotation. The screws in this extruder have a nominal diameter of 28 mm with an overall length to diameter ratio greater than 26, which results in longer residence times and more options for screw element combinations to control the mixing and transport processes. The extruder also consists of six interchangeable sections, commonly referred to as barrels, with three for feeding solids or devolatilization and three with one instrumentation port each. The barrels were heated electrically and water-cooled. Five temperature zones are possible in the processing section, one barrel per zone. The temperature can be controlled from ambient to above 220 C (425° F).

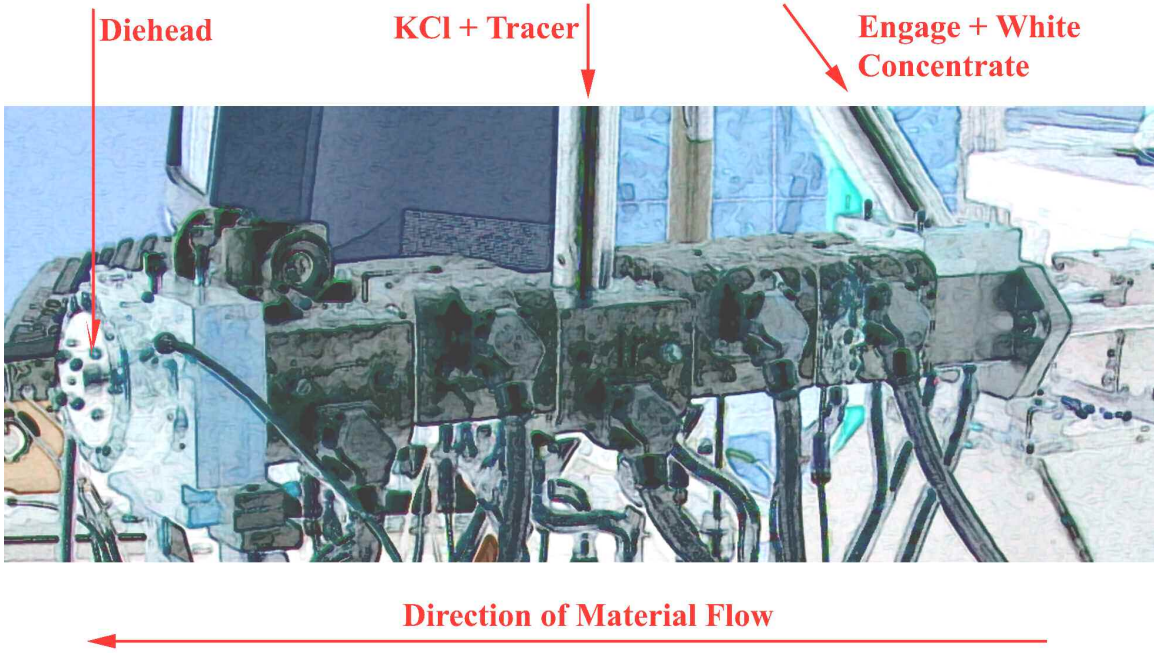

Figure 3-3. This diagram of the ZDSK-28 shows the feeding locations and the staged mixing zone layout of the barrels.

The ZDSK-28, prior to this project, had been on loan to a company. The extruder was installed in the Polymer Processing Laboratory in the University of Maryland's Manufacturing Building as the first stage of this research. A suitable die for extruding filled composites was designed by Gallant and produced for this research. A view of the extruder's exit before the die project is shown in Figure 3-4. Note how far the screws extend from the last section of the barrel; this plate is referred to as the *diehead*. The unusually high distance of the screw extension had to be considered in the new design.

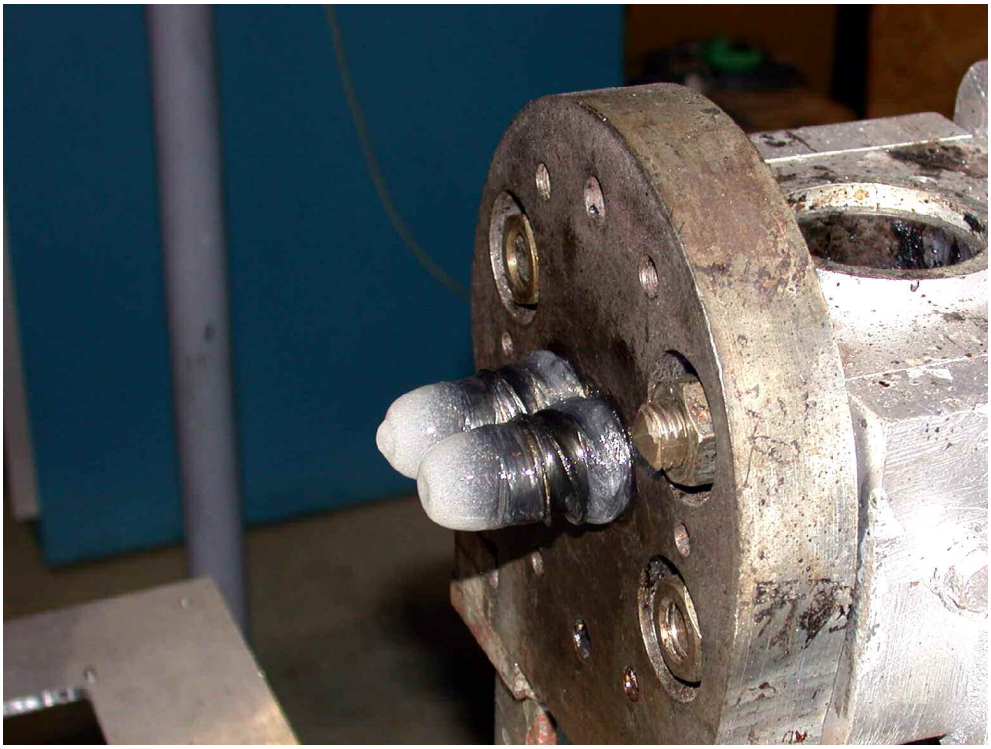

Figure 3-4. This is a picture of the original thin *diehead* for the ZDSK-28 extruder before the design and fabrication of the new assembly. Note the presence of polymer melt on the screws and screwtips.

The approach taken was to maximize the flexibility in future utility of the die hardware at a minimum cost. Three functional pieces comprised the new die. The first was a new diehead (Figure 3-5) that was significantly wider than the original so as to cover the extending screws leaving only the screwtips exposed. The new die was bored with two in-line instrumentation ports. One of the ports was used in this research for the fiber optic probe; the other was available for potential use with a pressure transducer. However, there was not a pressure transducer available for this project.

The second piece is the adapter and is shown in Figure 3-6, commonly referred to as the *eight-to-round* because of its function. This piece houses the screwtips and directs the flow from the figure eight of the barrel to a round hole that comprises the die entrance. This piece was designed to accomodate an wide variety of dies—the hardware that forms the final shape of the extruded product. For this research, three dies (Figure 3-7) with different shapes, round, square and rectangular, were designed and produced. A view of the assembled die hardware with the ceramic heating band for temperature control is shown in Figure 3-8.

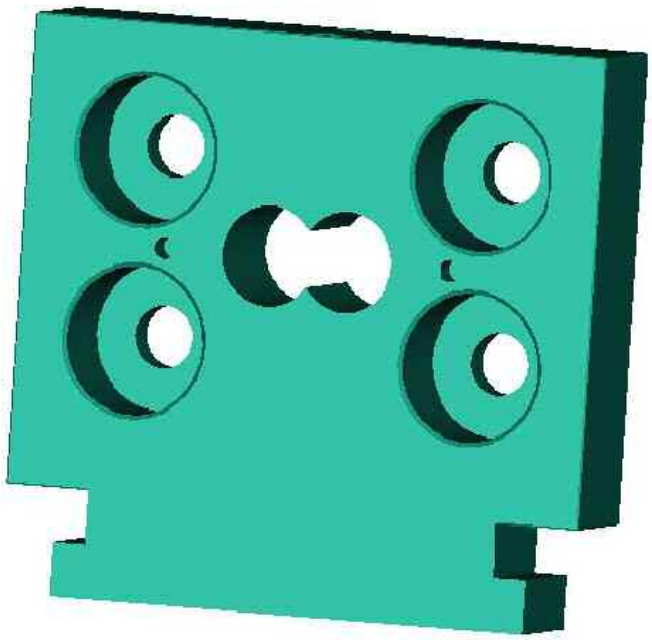

Figure 3-5. Design for the replacement diehead that is significantly wider than the original one shown in Figure 3-4.

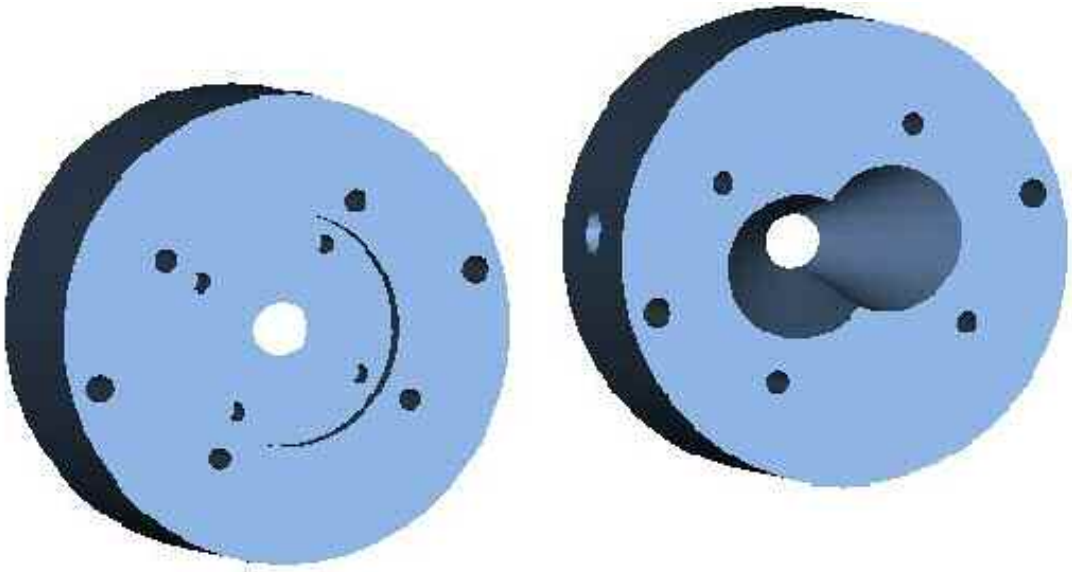

Figure 3-6. Eight-to-Round Adapter for the New Die Assembly.

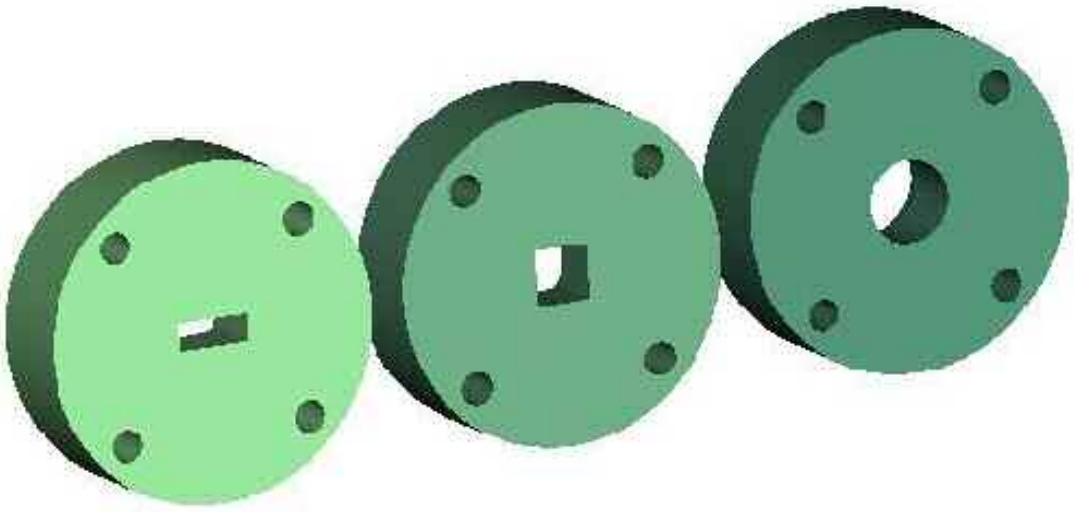

Figure 3-7. Three Dies Used for this Research on the UMD Extruder.

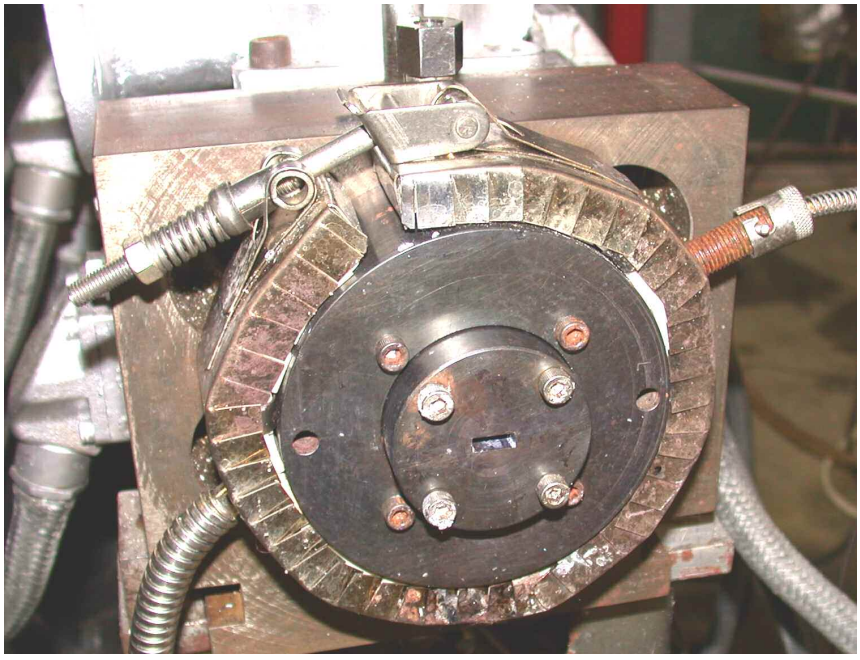

Figure 3-8. This is a picture of the replacement die hardware fully assembled and attached to the ZDSK-28 twin-screw extruder.

3.1.2 Feeding Solid Ingredients

The solids feeding equipment was upgraded as part of this project. This project had a requirement for strict feeding rate control and verification of feeder stability that could be provided by loss-in-weight control. The laboratory consisted of three feeders, two volumetric and one loss-in-weight. Two of these were operational. Each of the three

feeders was a laboratory scale twin-screw type; a type that exhibited better accuracy than the single screw or vibrating tray varieties. A control system and weighing platform upgrade was purchased and installed to yield three loss-in-weight feeders with a modern integrated control system. A mobile feeder platform was designed and purchased that allows the feeders to be used with any of the extruders in the Polymer Processing Laboratory.

3.1.3 Polymer: Polyolefin Elastomer

The polymer chosen for this project is DuPont Dow Engage 8401, a high melt index polyolefin elastomer (POE). It is a copolymer of ethylene and octene with a melt index (at 190 C using 2.16kg) of 30 $\frac{dg}{\min}$ (300 $\frac{g}{\min}$) and a density of 0.885 $\frac{g}{cm^3}$. It is commercially available as free flowing pellets without the need for a partitioning agent. Some grades of Engage need a partioning agent to reduce surface tack; those grades were not suitable for this project due to that characteristic. Engage 8401 is clear in the melt state, which was a requirement, because there are more options with RTD tracer techniques for an optically clear matrix. The high melt index was desirable because it was felt that it would tolerate solids loading better than a higher viscosity grade.

Figure 3-9. Two twin-screw loss-in-weight feeders were used to feed the polymer (left) and the KCl (right) at UMD.

3.1.4 Solids Fill: Potassium Chloride

Potassium chloride is a useful substitute for ammonium perchlorate because of the similarity in density and its availability in a variety of sizes through purchase or captive grinding. For this project a drum of technical grade potassium chloride was obtained from NAVSEA-IHMD. This material was screened through a U.S. sieve size #60 corresponding to screen openings of 250 μm. The material remaining on the screen was used in the extrusion studies. In other words, the material passing through a 250 μm screen was not desirable. Large particle size filler is advantageous for microstructural analysis using optical microscopy, because it can be readily identified without making assumptions associated with smaller particle sizes.

3.1.5 ZDSK and Instrumentation Configuration

The sensor consists of a bifurcated fiber optic cable inserted into a probe that screws into a Dynisco-profiled barrel instrumentation port. One set of fibers was connected to a variable-output, unfiltered, white light source. The other set was connected to a photodiode (or similar). The voltage output from the photodiode was connected to a custom-built electronic signal conditioner that consolidates various sensor inputs and interfaces with a National Instruments eight-channel data acquisition PCMIA card, model DAQ-516. National Instruments LabView software was used to collect and display the data in real time.

A new LabView virtual instrument (VI) was created by the author for this effort that allows the user to select acquisition rates up to 1,000 Hz, eliminates missed data reads, and is more flexible. For the experiments conducted to date, all data was acquired at 250 Hz. For an extruder rotating at 150 RPM with tri-lobed screws and a sensor located between them at the nip region, there is a lobe entering the region at a frequency of 15 Hz. It is prudent to collect data at a rate at least an order of magnitude higher. For this reason among others, the new LabView virtual instrument was created to allow collection at the full capability of the hardware.

3.1.6 Screw Designs and Process Configuration for the 28 mm TSE

The screw designs were relatively uncomplicated, Figure 3-2 and Figure 3-10. The first design (not shown) consisted of a primitive melt zone after the polymer feed port and a generic mixing section after the second feed port. The second design, #310 in Figure 3-10, added a left-handed mixing element to increase retention and melt in the

first mixing zone; this is done out of prudence and convention more than any specific observation in this case. The second design further increased the retention in the second mixing section by adding neutrally-staggered elements, so called because there is no helical arrangement.

Figure 3-2 is a diagram of the extruder barrel configuration for process experiments conducted to date. A screw configuration is shown in this figure as well. The direction of transport in the diagram is from the top to the bottom. The composite is compounded continuously in a two-stage system. The first stage is the polymer feed and mixing zones. The feeding barrel was keep at ambient temperature by cool water circulation to prevent premature melting and blockage of the feed port. The following three barrels were set at 450° F, and the screw geometry was arranged as to ensure complete melting and incorporation of a white color concentrate.

The relatively high temperature was necessary to minimize accumulation of polymer in the open KCl feed port. The mechanism for the accumulation was attributed to the degree of fill in the screw channel and the melt viscosity mollified by screw speed and process temperature respectively. For these reasons the process temperature and screw speed were kept at high settings for the RTD and gradient experiments. Later it became apparent that a third cause may be a factor, i.e., the proximity of the third set of kneading element to the KCl feed port. However more experiments and pressure measurements would be necessary to verify this hypothesis.

The negative effect of a high processing temperature was detrimental to strand integrity at the die. As it was necessary to collect extruded strands for gradient analysis, dimensional integrity was very important. The extruder barrels and die following the solids addition were set at lower temperatures to affect an increase in extrudate viscosity. Although extruders are poor heat exchangers, this did have the desired effect, and improved the quality of the extruded strands.

In the three screw designs evaluated for RVD characterization and production of gradient architectures (see Figure 3-10), the screw configuration for the polymer-melting portion did not change. This section of the screw performed its function well, and was not used to control the evolution of the gradient architecture. The mass throughput of polymer was not changed either—only the mass throughput of the solids

filler. Only the screw configuration beyond the solids feed port was of analytical significance. The effects of these configurations are discussed in a later section.

3.1.7 Typical RTD Response

To measure the typical RTD response, the best results were obtained by premixing a while color concentrate with the colorless Engage POE. Pellets of black color concentrate were used as tracer, and a black-colored filled thermoplastic was used as the second component for the step response tests. A sample of white TiO_2 concentrate #32-701 was obtained last year for this type of study from Uniform Color Company, Holland, MI. The white titanium dioxide compounded with a proprietary polymer that a representative of the company assured was compatible with POE. Experimentation at UMD demonstrated this claim; no separation was detected and the concentrate was readily miscible with the POE in the melt state. A letdown ratio of 24:1 is recommended for this material; however, a ratio of 20:1 was used for these experiments for reasons of ensuring a saturated color.

This ratio was quite adequate to provide complete saturation of the POE. One concern was that non-uniform blending of the white concentrate in the POE was affecting the stability of the baseline. The baseline was shown to be unaffected by additional white pellets in sensitivity tests. It was found that minor baseline drift was inherent to the electronics.

The residence time experiments were conducted against the white background using Reed black color concentrate as the tracer. The black color concentrate had been used in other studies in the UMD Polymer Processing Laboratory and was quite compatible with the POE. The physical form of the Reed black was a uniform round pellet. The mass of five pellets ranged consistently from 0.10 to 0.13 g.

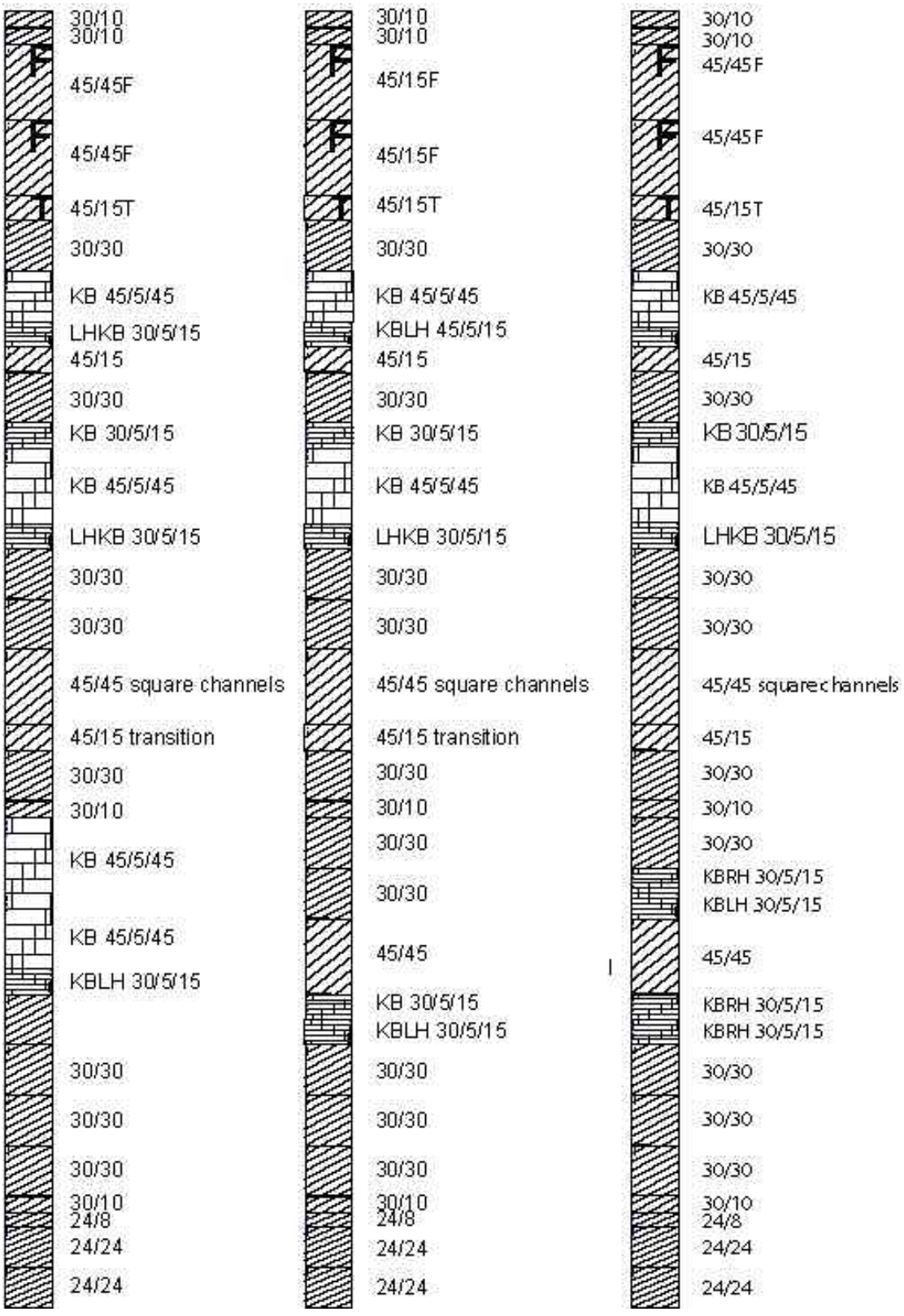

Figure 3-10. Three ZDSK-28 Screw Designs Used with KCl-Filled Composite

A typical RTD experimental response is shown in Figure 3-11. The absorbance was measured as a voltage signal and was plotted as a function of time. Initially there was no tracer in the process section except for the solids feed port. The tracer melted and dispersed with the white-colored POE and the KCl as it passed through the second mixing section. The reflectivity of compounded material was measured at the sensor. There was a corresponding decrease in the signal as expected as the color darkened. Then as the bulk of the tracer moved further down the process section, its strength began to wane until the entire amount of black tracer was clear of the mixing section. Note that time zero was the addition time, which is a normal convention for graphing and analyzing this type of data.

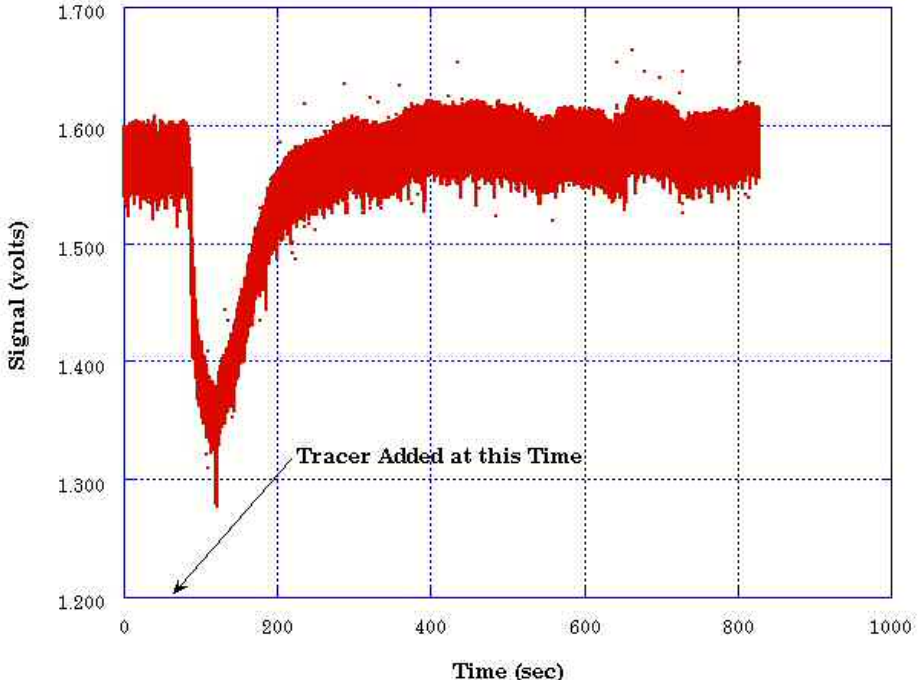

Figure 3-11. This is a plot of the unfiltered experimental process response to impulse input of five pellets of black tracer. Extrusion conditions were 6 lbs/hr, 95 rpm screw speed, and 40 percent by weight KCl. (Test 0725/1504)

3.1.8 Filtering of Experimental Data

The data was processed with a Butterworth filter to remove periodicities and screw noise. An example is shown in Figure 3-12. The filter introduces a transient that quickly damps out, which is apparent in the first 30 seconds or so. This was not a problem because each dataset contained a lead time to establish a baseline before the tracer was introduced. Note that this plot does not include the data beyond 330 sec, but the signal

eventually returns to the baseline at a later time. Figure 3-12 shows the translation of this data so that it represents a conventional RTD with a positive displacement in the signal, and the baseline shifted to zero. Whenever circumstances permitted, the general experimental procedure was to collect three RTDs for each condition of interest and average the filtered signals. This increased the precision of time measurements and smoothed the tails of the curves to some extent.

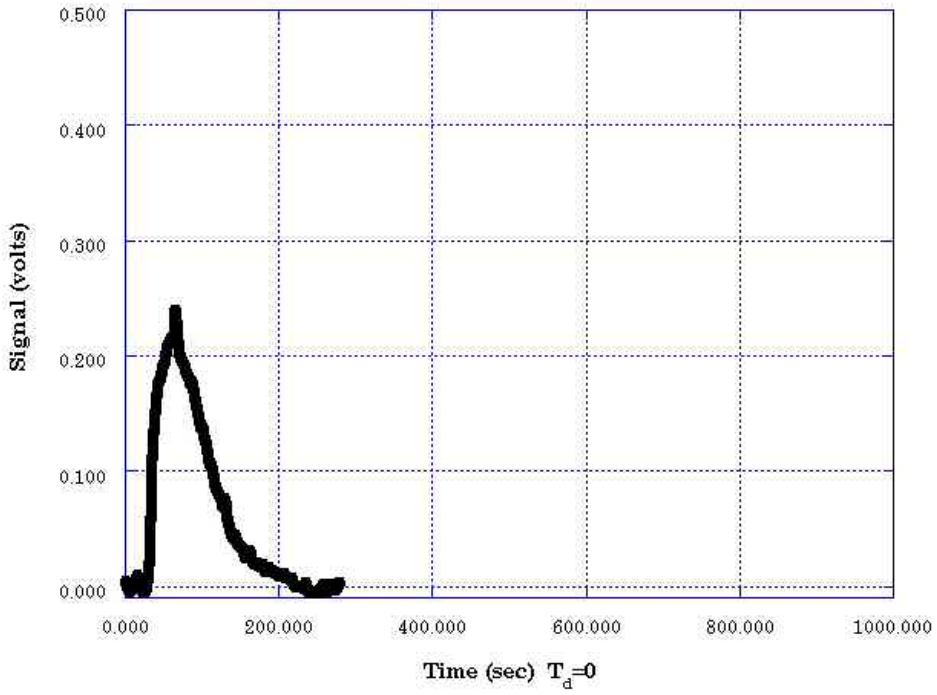

Figure 3-12. The filter effectively smoothes the noise in the signal without sacrifice to details and idiosyncrasies. The signal was inverted for the plot, as this is the convention for RTD plots. (Test 0725/1504)

3.1.9 RTD Characterization and Sensitivity Analysis

The RTDs collected illustrate the classical response of a twin-screw extruder to an impulse input disturbance such as a one-time *injection* of tracer. There was one exception to typical RTD measurements. The tracer was added more than halfway down the processing section of the extruder. Typically RTDS are conducted for the full length of the processing section. This coupled with the low value of *Q/n* in the polymer composite studies at UMD resulted in a very small residence time. The following observations are based on these rather limiting conditions; however the RTD experiments still exhibited conclusive data that was in agreement with conventionally

acknowledged process effects. These are illustrated in the following figures. For example it is well understood that an increase in mass throughput results in a decrease of the delay time, shown in Figure 3-13 as a comparison between 3 and 6 lb/hr. The trace for the 3 lb/hr RTD was significantly delayed with respect to the two 6 lb/hr measurements.

Although the fiber optic probe was located near the screw tips immediately preceding the eight-to-round die adapter, it was important to identify any die effect on the RTD measurements. Figure 3-13 includes two RTDs for the same composition, 50 percent filler, and operating conditions, 6 lb/hr and 180 rpm screw spreed, with the die geometry as the only difference. There was no effects on the RTD due to the die geometries used in this project. Similarly, the composite process exhibited the expected screw speed effects on the RTDs. As the screw speed was reduced, the corresponding effect was an increase in the delay time. Of throughput and screw speed, throughput was generally the dominant factor.

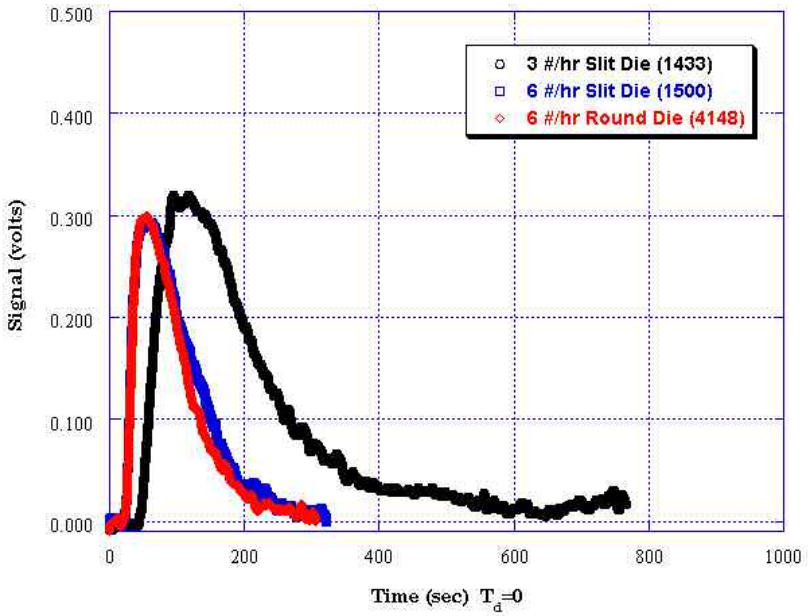

Figure 3-13. This figure compares the effects on the RTD for mass throughput and die geometry given the same solids concentration of 50 percent by weight.

To ensure that there was no effect of the die geometry at these operating conditions, an error analysis was conducted to determine if the *tail* of the RTD for the slit die was significantly different than that for the round die. The conditions for the RTD measurements were: 6.00 lb/hr, 50 percent filler, and 180 rpm screw speed. Calculating

and plotting the confidence intervals for the round geometry was the method used for this. Since there were two observations for the round die (the green and red traces), a reasonable choice of a two-sided 100[1-(α = 0.10)] percent *confidence interval* for the mean was made for the type one error. The type one error occurs when a sample is rejected that is actually acceptable.

Figure 3-14 shows that the great majority of the signal for the slit die (the blue trace) lay within the 90 percent confidence interval for the round die. The two round-die data sets were averaged (the black trace). The short segment of the curve where the blue trace is significantly beyond the 90 percent confidence intervals would fail (or lie within) if the analysis were conducted at 95 percent. (A higher the level of significance results in wider confidence intervals.) While the selection of confidence intervals after the data are collected is subject to bias, the important point is a quantitative judgment of an assignable cause. There either were not enough observations (two RTDs), or there was no die effect at these conditions. The hypothesis of too few measurements of the RTD can be eliminated by the next example of confidence interval analysis for a case where three observations of the RTD were available.

To eliminate the possibility of too few observations, confidence intervals for another set of conditions (but the same screw design) were calculated and plotted for a case where there were three observations of the RTD, see Figure 3-15. Note that the tail of the RTD typically has relatively wide confidence intervals. Therefore it can be determined by analogy that there was no die effect on the RTD for the given experimental configuration and conditions for Figure 3-15. Akin to no measurable effects of the die, the same conclusions can be made as to the repeatability of the RTD measurements made on different days.

The extruder screw speed has an effect on the residence time as well, but is much less significant than the mass throughput. An example of this effect is shown in Figure 3-16 for the case of a difference of 95 and 180 RPM with all other operating conditions being identical. A higher extruder screw speed has the expected effect of decreasing the delay time.

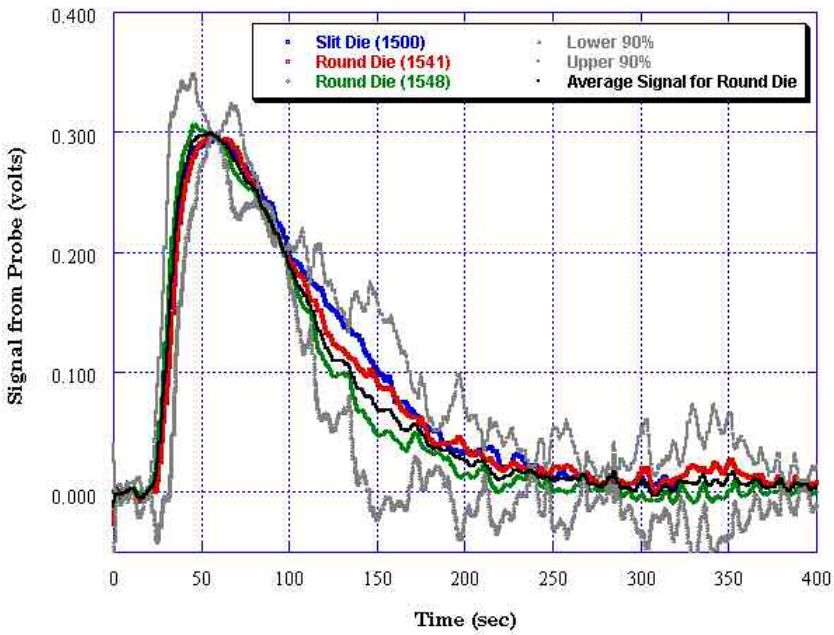

Figure 3-14. The confidence intervals for the round die (green and red traces) were plotted with an RTD for the slit die (blue trace). At a 90% level of significance, the slit die RTD was within the confidence intervals for the round die at identical conditions.

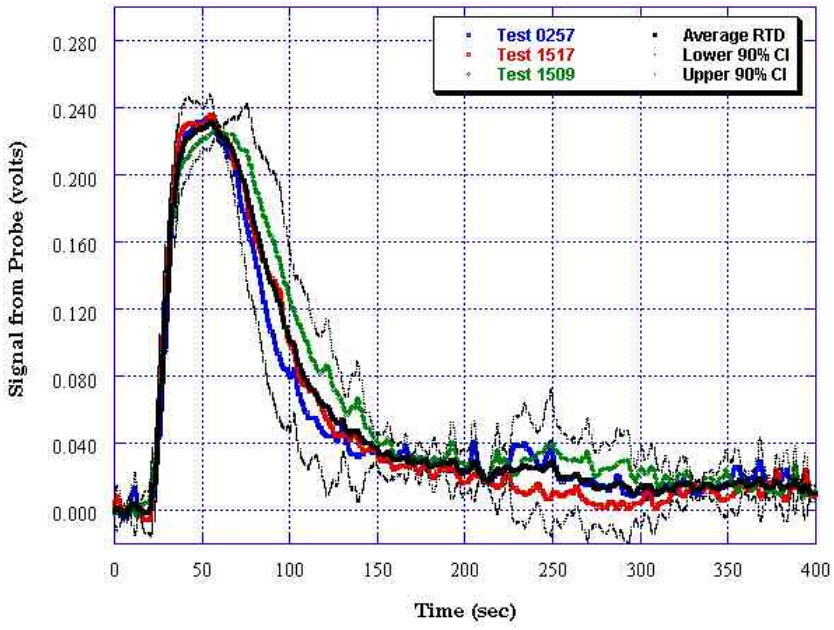

Figure 3-15. The confidence intervals are shown for three RTDs collected at identical processing conditions. The configuration was: a round die, 6.00 lb/hr, and 40 percent filler.

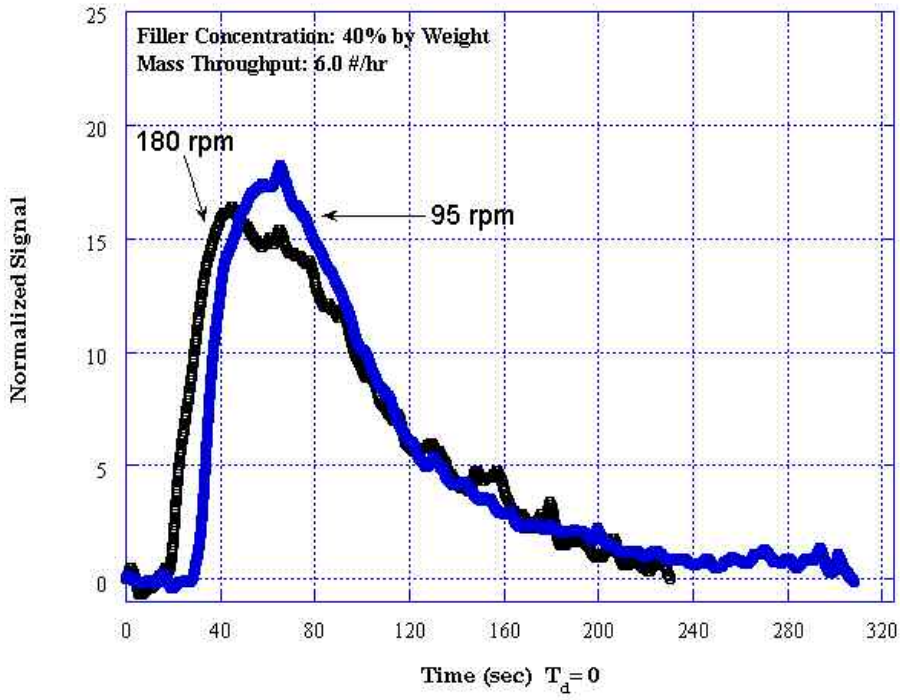

Figure 3-16. This plot shows a comparison of the screw speed effect on the RTD for 40 percent filled composite at a mass transport rate of 6.00 lbs/hr.

As a point of future study, the degree that screw speed can influence the evolution of the gradient architecture will be studied. This project documented for the first time some interesting effects of screw speed on the burning rate. These are discussed in Chapter 4. This effect was not amenable to study using the inert or the live formulation, because a change or disturbance in the screw speed affects the entire length of the screw immediately. In the case of a two-staged continuous process, an abrupt shift in screw speed would create a temporary transport disturbance upstream of the solids addition port. Depending upon the direction of the shift, the effect could be a temporary abundance or scarcity of polymer in the solids mixing portion of the screw. This could lead to a dangerous situation in the case of processing energetic material. However there could still be merit to future investigations in considering the effects of small or incremental changes to the screw speed given the right formulation and configuration.

The RTDs for the inert thermoplastic composite were fitted to first and higher order models to determine fit parameters that could be used to estimate process and material property responses. The first order functions fit poorly. The second order RTD function (14) fit the data very well, and the third order was somewhere in between. For the

conditions that were later used as starting points for creating gradients, the best-fit parameters to these functions are given in Table 3-1.

Table 3-1. Best-fit parameters for models of RTDs used as starting conditions for constructing gradients with the thermoplastic inert composite. The second order shape factor was the best fit in each case.

ID	Throughput (lb/hr)	KCl Content (% by wt.)	Delay Time, T_d (sec)	Model Order	Shape Factor, a_t
0723/1612	3.60	0	20.756	1	0.0091
"	"	"	"	2	0.0265
"	"	"	"	3	0.0427
0729/Norm1515	6.00	40	17.180	1	0.0102
"	"	"	"	2	0.0288
"	"	"	"	3	0.0460
0725/Norm162237	9.00	60	18.900	1	0.0153
"	"	"	"	2	0.0430
"	"	"	"	3	0.0676

3.1.10 Conversion to RVDs

As discussed previously, the RVD is more significant in characterizing the process, mixing characteristics, and screw geometry. The data was always collected as RTDs, then filtered and averaged as discussed above. Conversion to RVD was accomplished by first converting the mass flow rate to volumetric units paying particular attention to the effect of KCl concentration on the theoretical maximum density of the composite. Some sample conditions are shown in Table 3-2. Note that the volumetric flow rate decreased with increasing KCl given no change to the weight throughput. After calculating the theoretical volumetric throughput, it was a trivial operation to transform time to volume. The voltage signals were then normalized with respect to volume. Note the RTD curves were not normalized. In this writing all the RVD curves are presented as normalized data in order to make direct comparisons to the material composition.

Table 3-2. Volumetric feedrates for some combinations of throughput and filler concentration.

Engage Feedrate (#/hr)	KCl Feedrate (#/hr)	Total Throughput (#/hr)	%KCl (by wt.)	TMD (g/cm^3)	Mass Flow (g/min)	Vol. Flow (ml/min)	Vol. Flow (liter/sec)
1.65	0.00	1.65	0.00%	0.885	12.5	14.1	2.35E-04
1.65	1.35	3.00	45.00%	1.179	22.7	19.2	3.21E-04
1.20	1.80	3.00	60.00%	1.326	22.7	17.1	2.85E-04
0.90	2.10	3.00	70.00%	1.447	22.7	15.7	2.61E-04
1.75	3.25	5.00	65.00%	1.384	37.8	27.3	4.55E-04
1.50	3.50	5.00	70.00%	1.447	37.8	26.1	4.36E-04
3.60	2.40	6.00	40.00%	1.137	45.4	39.9	6.64E-04
3.00	3.00	6.00	50.00%	1.225	45.4	37.0	6.17E-04
2.70	3.30	6.00	55.00%	1.273	45.4	35.6	5.94E-04
1.80	4.20	6.00	70.00%	1.447	45.4	31.4	5.23E-04
3.60	5.40	9.00	60.00%	1.326	68.0	51.3	8.55E-04

Note that in the time domain, the system response to an impulse is variable in location and shape depending upon mass throughput, screw speed, rheological properties, etc. In the volume domain the throughput effect is nullified (Gao, Walsh et al. 1999). This is highly significant for the determination of a process indicator that can serve as a predictor for characterizing the gradient architecture. A step change in the solids (KCl) feeding rate to produce a gradient will have two dynamic effects: one being a differential change in the mass and volumetric throughputs, and the second being a differential change in the filler concentration. The first changes the RTD but not the RVD as discussed above. If the second caused a shift in the location of the RVD, then the RVD would have proved difficult to use as a predictor for the gradient architecture. These effects are discussed in the following.

Figure 3-17 is the same data in Figure 3-13 but now plotted as a RVD. The location and shape of the volume distributions are now identical. This is attributed by the RVD's independence from throughput. Note that no die or delay effect is apparent in the volume domain either.

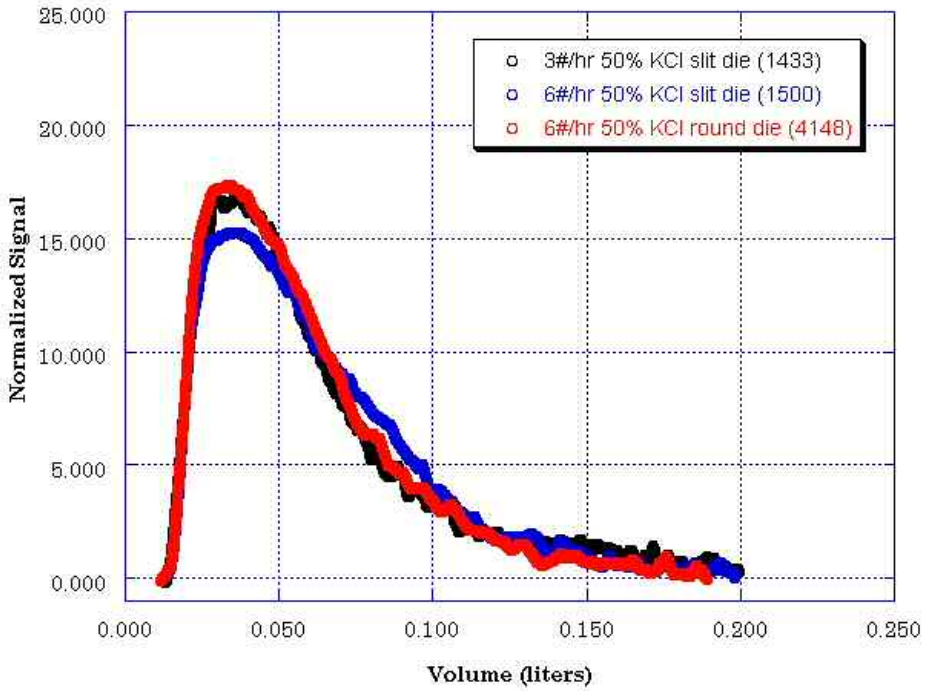

Figure 3-17. The null effects on the RVD for mass throughput and die geometry.

Similarly, the effects of concentration on the RVD were investigated. The results are presented in Figure 3-18. The most important result that can be observed in this figure was the absence of a shift in the location of the curves. However, there was a slight increase in the delay volume for the highest throughput that also represented the highest filler concentration. The discrepancy in the height of the peaks was attributed to the noise in the tails. Since these data were not replicated for the most part, the usual noise in the tail more strongly affected the normalization and thus peak height. The 60 percent data was plotted as the average of two RVDs. The other two traces, the zero and 40 percent data, consisted of only one observation, which likely contributed to some inaccuracy in determining the volume delay.

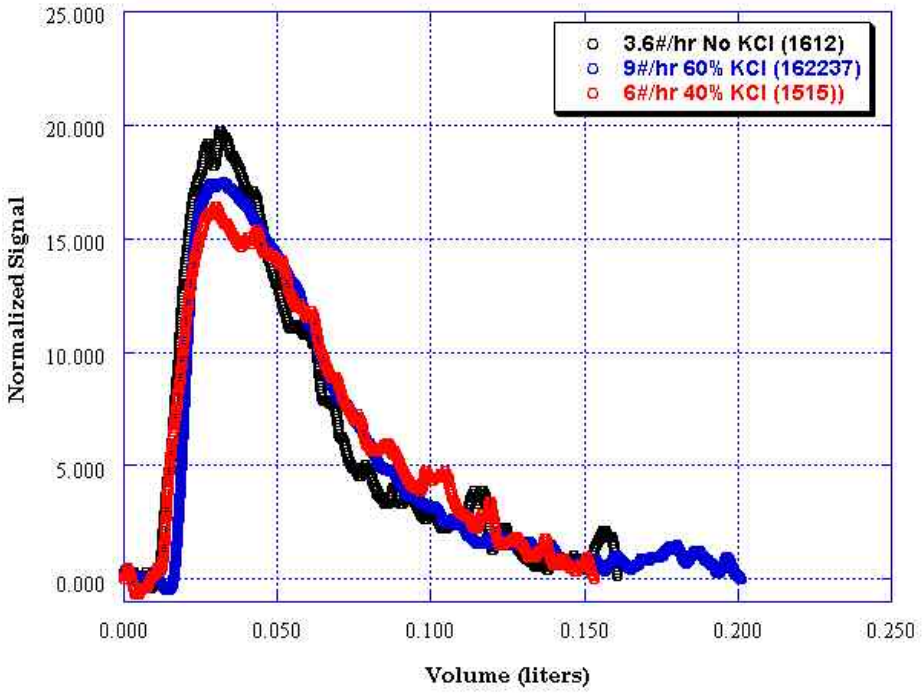

Figure 3-18. Comparison of effects on the RVD for filler concentration (by weight) and throughput.

The effect of screw speed can be detected in the volume domain at steady state. This was not unexpected. Furthermore this represents the first validation of the effect of screw speed on the RVD using a filled system, see Figure 3-19. There are many similarities of this figure with the corresponding RTD figure using the same dataset. The lower screw speed resulted in a longer volume delay and a decreased rate of peak development. The overall physical effect of lower screw speed on the microstructural evolution is a slower transport rate in mass and volume.

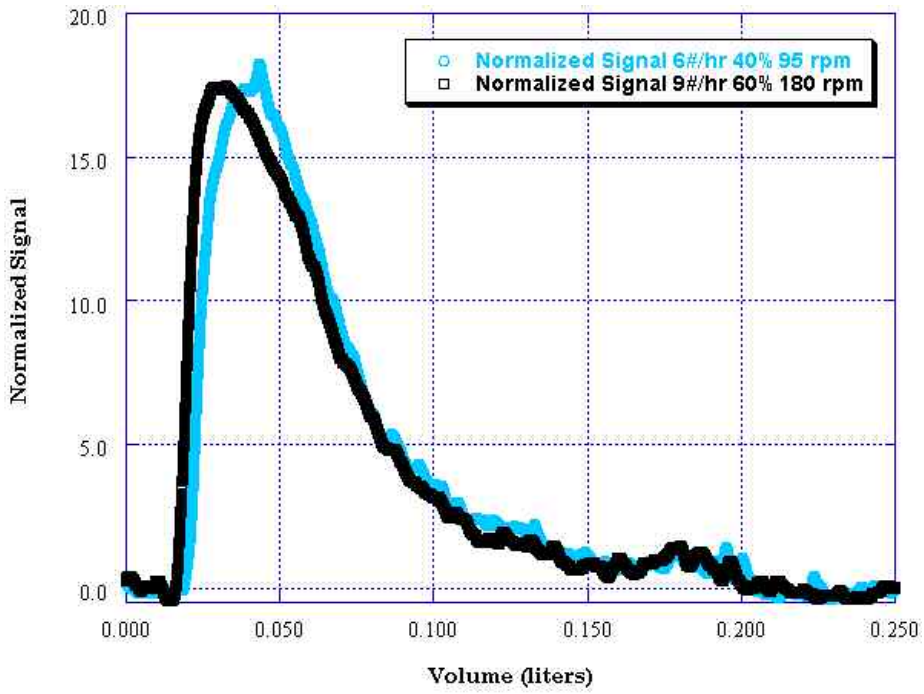

Figure 3-19. Comparison of the RVDs for two extruder screw speeds.

The power of the RVD is that while the RTD yields a unique fingerprint of the operating conditions, the RVD yields a unique fingerprint of the TSE process. The response of the system to an impulse (disturbance) over a range of conditions, such as mass throughput and filler concentration, can be predicted once the RVD is defined for one screw configuration.

3.1.11 Fitting RVDs to Second Order Process Model

The experimental RVDs were fit to a second order process model, Equation (13), based on the inverse Laplace transform of a model for two perfect mixers in series with a dead time. The second order model was found to fit the data much better than a first or third order model. It is important to remember that this process model permited the process to be represented as an ideal abstraction of a physical process. However, the advantage of this representation is the capability of the process model to describe the behavior of a complex process with few parameters.

The second order model fit the data for the KCl-based elastomeric composite very well. Two parameters were necessary for the model in Equation (13): the volume delay and a constant term. The values for some typical RVDs are given in Table 3-3. This data

was from one screw design only. The terms for the constant, a_v, are similar and of the same order. The volume delays are also reasonable.

The longest delay was for the lower screw speed. As anticipated, the RVD is not independent of the screw speed but is relatively insensitive to throughput. A rigorously designed experiment would reveal any relationship to the process parameters. However the primary objective was to determine a model that best characterizes the data.

Table 3-3. The second order model parameters for KCl/Engage RVDs at various process conditions were similar for a range of filler content, screw speed, and throughput.

Total Throughput (#/hr)	%KCl (by wt.)	Extruder Screw Speed (RPM)	Constant a_v	Error for Constant a_v	Vol. Delay, v_d (liters)	Probability Model Fits Data
3.60	0.00%	180	50.01	±0.04	0.01102	>99.99%
6.00	40.00%	95	47.51	±0.03	0.01836	>99.99%
6.00	40.00%	180	43.14	±0.03	0.01142	>99.99%
9.00	60.00%	180	50.22	±0.05	0.01616	>99.99%

The strengths of the second order mixing model with a dead time as a RVD process model can be seen in Figures 3-20 and 3-21. In fitting this type of data, it is difficult to fit both the peak and the tail simultaneously. The example in Figure 3-20 has excellent resolution of the curve's tail but peaks slightly too late. Other model fits have excellent agreement with the curve maximum, but may fit the tail at a slightly steeper slope. The curves in Figure 3-21 are the fitted estimates for the experimental RVD data in Figure 3-18. The agreement of the measured data with the model predictions is excellent, as can be seen in Table 3-3.

Overall the second order model fits are excellent, especially compared to a third order model as shown in Figure 3-22. The fit for the third order does not model the RVD onset slope, the peak intensity, or the tail. The screw geometry is hypothesized to control the order of the model, but experiments with more mixing sections need to be conducted to affirm this.

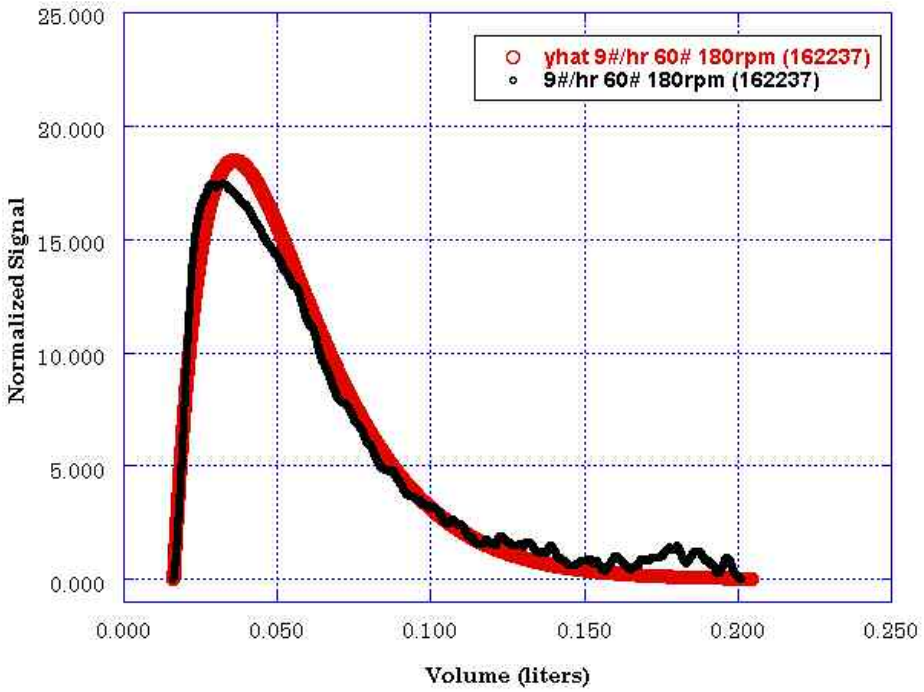

Figure 3-20. This is an example of the goodness of fit for the second order process model to describe a RVD. The thin line is a RVD for 9.00 lbs/hr, 40 Percent KCl, and 180 rpm extruder screw speed. The wider, smooth line is the second order model prediction.

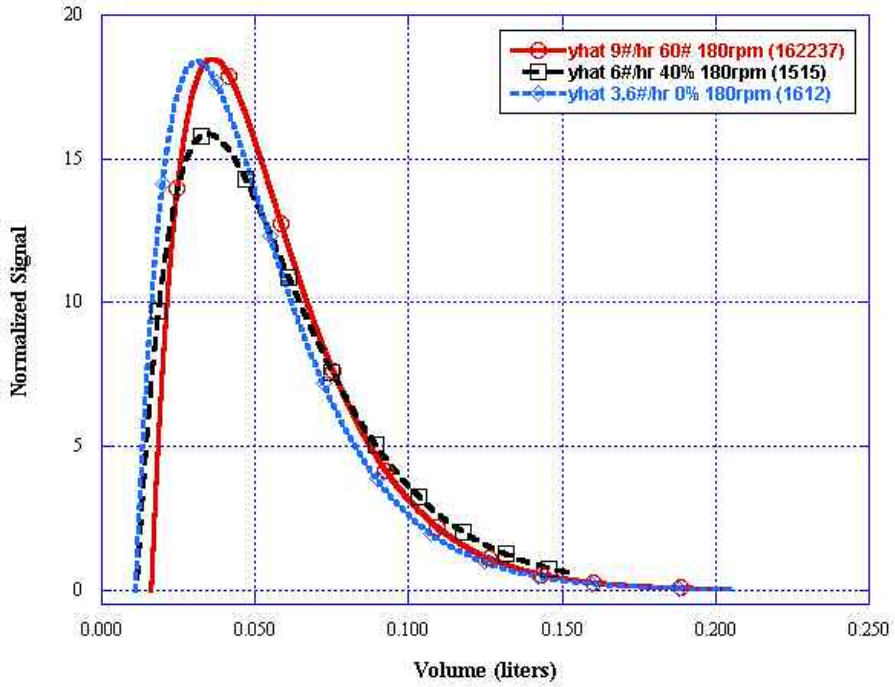

Figure 3-21. A set of second order model fits for RVDs at various throughputs and filler concentrations.

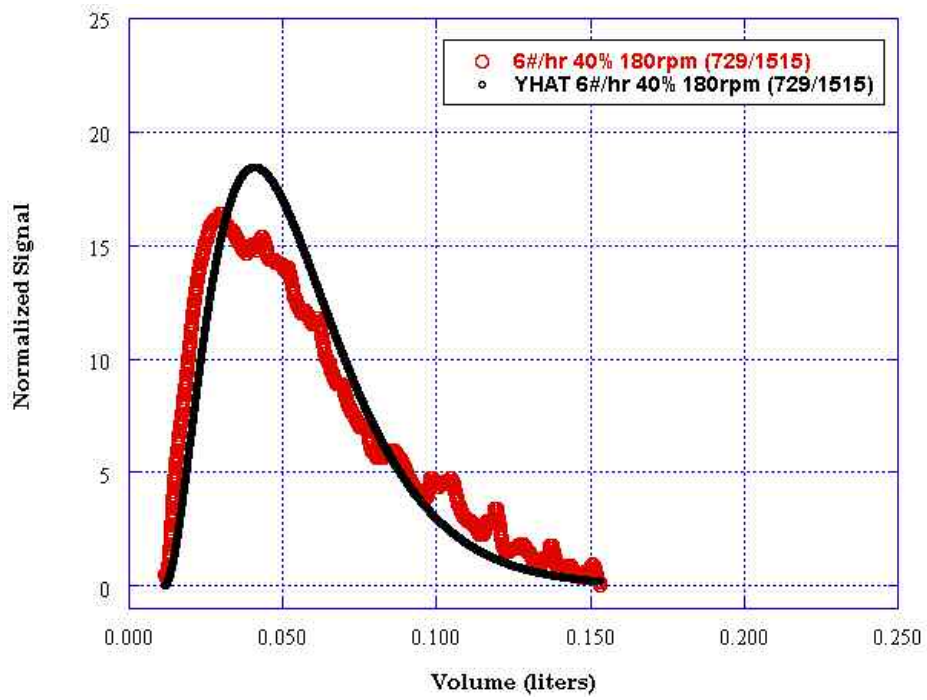

Figure 3-22. The third order ideal mixer model was not the best representation as seen in this example comparison of the experimental response to the model.

3.2 Residence Distribution Experiments of Rocket Propellant Simulant in NAVSEAIHMD's 40 mm Twin-Screw Extruder

The TSE facilities at UMD offered the opportunity to conduct processing research efficiently and inexpensively using inert formulations. The facility is more oriented toward process research on a laboratory scale: the controls are located adjacent to the processor, the manpower demand is much lower, etc. Furthermore, highly-filled composites, whether energetic or inert, are physically similar and the process approaches are the essentially the same. The Polymer Processing Laboratory at UMD offered all these advantages. The only limitation of the facility was the inability to study the process science on energetic formulations. For these studies, a special facility had to be utilized that was configured for safely processing these materials.

The Navy is the by far the most progressive of the armed services in the research and technology of energetic materials and ordnance. The first U.S. experiments with energetic material in a TSE were conducted at NSWC facilities in Silver Spring, MD Presently there are three world-class energetic continuous processing operations at NAVSEAIHMD. All project experiments with energetic materials were conducted in the pilot facility there. In addition, there were internal Navy requirements to conduct some

trials with an inert propellant simulant before the process experiments with am energetic propellant formulation could proceed. The results of the RTD experiments using this simulant follow. The RTD trials conducted with energetic material, as well as the details of other experiments, are described in later sections.

3.2.1 Facility Description

A unique facility has been assembled at NAVSEAIHMD to address the specific needs for processing energetic polymer composites in a TSE (Gallant 2000). The extruder employed in the facility was a Werner & Pfleiderer ZSK-40 (mm) featuring segmented and cantilevered screws. It has a process length to diameter (L/D) ratio of 28, which is similar to that employed at the UMD facility. The six barrels were temperature controlled by five temperature controllers. The extruder barrel featured open ports for introducing the two solids and an additional port for vacuum deaeration. Many of the barrels are bored to allow for the insertion of temperature and pressure sensors to measure the physical state of the propellant during processing. Five combined sensors were used in process-critical areas in the barrel and at the die. The 40-mm extruder features a hydraulically clamped die holder that operates similar to a door. This is a safety feature unique to this extruder, which causes the door to open should the die pressure exceed the clamping pressure, thus relieving the pressure instantly.

Four feed streams were required to process this simulant, one of the most complex feeding schemes used to date at NAVSEAIHMD. Two feed streams were solid ingredients, and the other two were blends of liquid ingredients. The solid ingredients were fed to the extruder using K-Tron models T-37 and T-20 loss-in-weight twin-screw and single-screw feeders respectively. More details of the feeding arrangements that were not essential to this investigation can be found in NAVSEAIHMD technical documents (Gallant, Newton et al. 1999) (Newton, Gallant et al. 1999).

3.2.2 Ingredient/Formulation Discussion

The nominal formulation of the inert composite is given in Table 3-4. It is very similar to the energetic formulation given in the subsequent section. In the processing experiments, the concentration of filler was varied over a range 79.3 to 87.2 percent by weight. The binder ingredients were adjusted proportionately. This formulation has an unusually high number of individual ingredients. In order to feed these to an extruder, it was first necessary to blend them to suit the number of feeders available as well as other

considerations such as process safety, chemical compatibility, storage stability, etc (Newton, Gallant et al. 1999). The ingredients were fed in four feed streams using two loss-in-weight solids feeders, one gear pump, and one triple-piston pump.

Table 3-4. Formulation for the Inert Composite. The Functions of the Ingredients are Given as They Pertain to the Energetic Composition.

Ingredient	Weight Percentage	Function
Potassium chloride (coarse)	57.59	Oxidizer
Potassium chloride (fine)	26.28	Oxidizer
Zeon Chemical HyTemp® 4404	10.20	Binder
Dioctyl adipate	2.78	Plasticizer
3M Dynamar® HX-752	0.32	Bonding agent
Isophorone diisocyanate	0.33	Curative
Graphite	0.50	Extrusion aid
Zirconium carbide	0.50	Combustion modifier
Iron oxide	1.50	Ballistic modifier

3.2.3 Process Configuration and Screw Design for the 40 mm TSE

The extruder configuration, feeding locations, and screw design for the inert and energetic propellant are illustrated in Figure 3-23. Note the similarity with the barrel layout used for the KCl composite processing at UMD in Figure 3-2. The KCl composite process was configured to represent the propellant compounding strategy. The binder ingredients were compounded first, and then the fillers were added mid-process to a homogeneous binder. Some major differences follow. The HyTemp elastomer was not thermoplastic, but rather a partially cross-linked polymer that was theromoset to increase the cross-link density. Thus barrel temperatures were much lower than the KCl composite. There were liquid ingredients in the Navy formulation. The Navy process included deaeration by vacuum over the barrel (see Figure 3-23); this improved the density and the performance of the product.

Additionally, the screw designs were different between the two research sites. The Navy design was optimized for this particular propellant formulation. A different

formulation was used at UMD, thus requiring an appropriate design. Furthermore, the screw configuration for the KCl composite was varied as an experimental factor for investigating the effects of the filled material on the RVD process model.

3.2.4 Dye Tracer Technique and On-line Data Collection Method

In the early 1990s, a Navy continuous processing project used fiber optic probes mounted in the process section and die to detect the presence and concentration of a blue dye in the process stream. The calibrated microencapsulated sensor (CAMES) instrumentation, or CAMES probe as it has come to be known (Figure 3-24), was custom built by MACH I, King of Prussia, PA. It operates on the principal of absorbed and reflected light and consists of a bifurcated optical fiber with a tuned LED source and highly sensitive photomultiplier. Because the formulation is colored a deep red due to the concentration of highly absorbing iron oxide, a concentrated organic blue dye was used for the RTD studies. The dye was Automate™ Blue 8A liquid dye from Rhom & Haas Co., Philadelphia, PA. It is a solution of mixed dyes in predominately xylene. One gram of the solution was added to a small mixture of the filler, a viscous polybutadiene resin, and fumed silica to form a semi-soft pill to drop into the solids feeding port of the extruder.

For inert operations at UMD, the tracers were added manually. For energetic operations, it was essential that the addition be conducted remotely using an in-house designed rotating table. Before the device could be used with propellant, it had to be used once in a full operation with an inert formulation as required by NAVSEAIHMD safety regulations. This provided the opportunity to collect RTD data on the inert formulation for comparison with the propellant. The data were acquired using a PLC-based supervisory control system at the low frequency of one Hertz. There was no capability for higher acquisition rates without adding specialized equipment. The signal did not contain noise or oscillations in the signal. Therefore, post filtering of the signal was unnecessary.

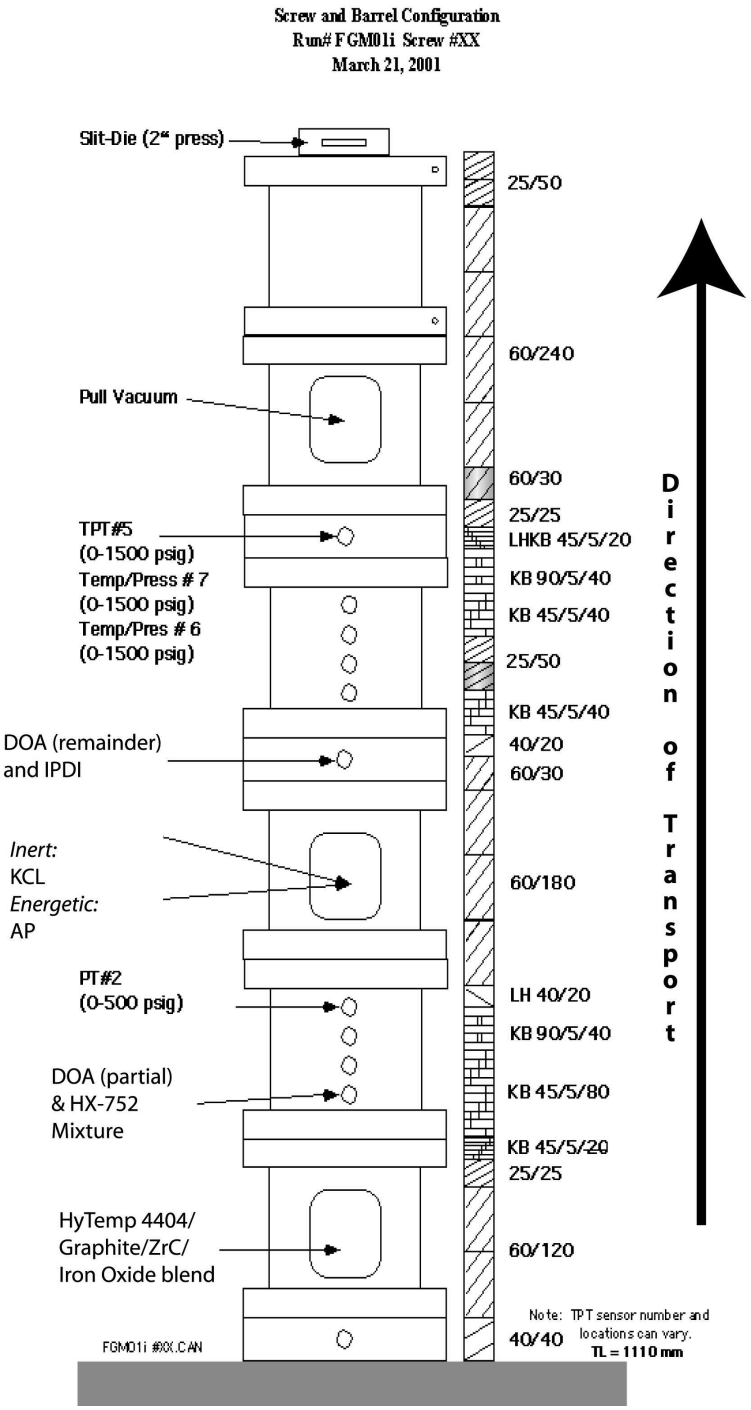

Figure 3-23. Extruder barrel configuration, screw design, feeding locations, and instrumentation sites for the ZSK-40 TSE at NAVSEAIHMD are illustrated. The Numbers next to the screw are for geometry descriptions, and TPT is a temperature-pressure transducer.

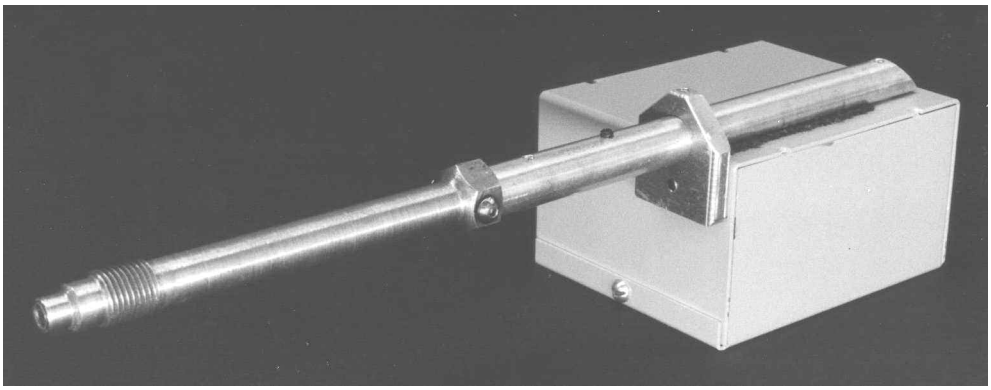

Figure 3-24. A fiber optic probe, referred to as the CAMES probe, was used at NAVSEAIHMD to detect concentration of tracer in RTD and other processing experiments.

3.2.5 Typical RTD Response by Location

Since there were two CAMES probes available, one was positioned at the screw tips for the conventional response measurements. The second was positioned over the discharge location from the filler mixing zone, see Figure 3-23. At this time the data from the mid-process probe was not treated or analyzed; however, it bears mentioning for future reference. Figure 3-25 is a plot of the untreated RTD data for the process condition of 30.00 lbs/hr with the lower filler concentration. The barrel and die signals were acquired as two channels, and three drop-times are indicated.

The response data was averaged for each condition; an example is given in Figure 3-26. One exception was the high throughput data. Due to a low supply of KCl, there was only enough material for one reading. However, given the consistency of the replicates for the 30 lbs/hr data, the same would have been reasonable to expect from the 50 lbs/hr data.

3.2.6 Discussion of RTD Data

The conditions and measurements for the simulant RTD study are summarized in Table 3-5. The volume of filler was identified as *low (L)* or *high (H)* in the table and was based on equivalent volume loading of ammonium perchlorate in IH-AC3 with the lowest and highest burning rates. Representative responses for the RTDS are provided in Figure 3-27. The positive effect of throughput on the RTD is obvious in this system. The effect of filler concentration was more subtle and could be a point for future study.

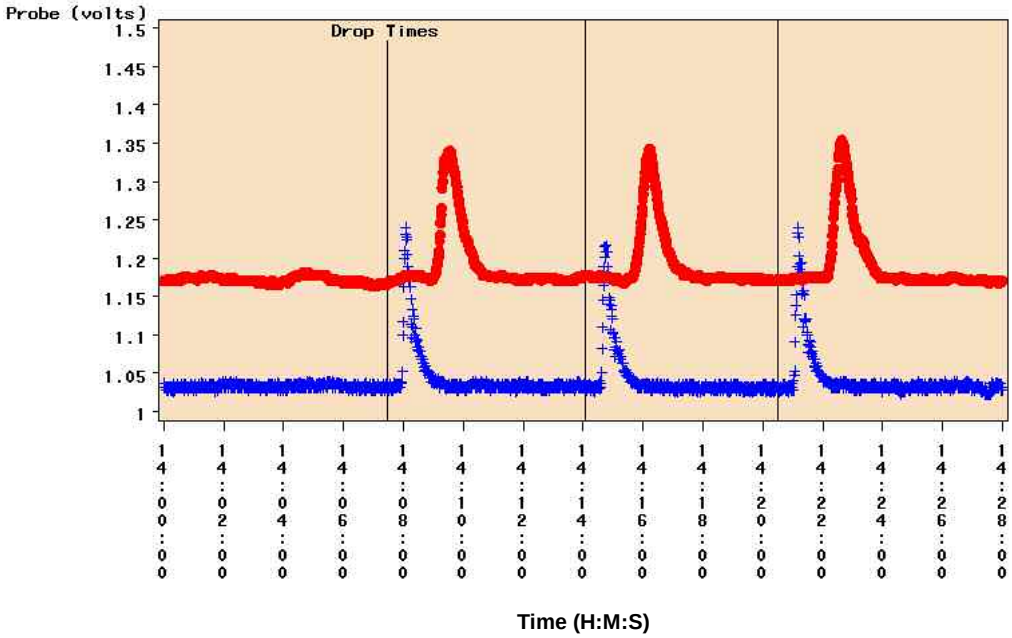

Figure 3-25. Untreated signals from both probes are plotted for a process condition of 30 lbs/hr with a KCl volume concentration of 0.693. The vertical lines are the tracer insertion times. The lower signal is from the probe in the mixing section while the upper signal is from the probe at the die entrance.

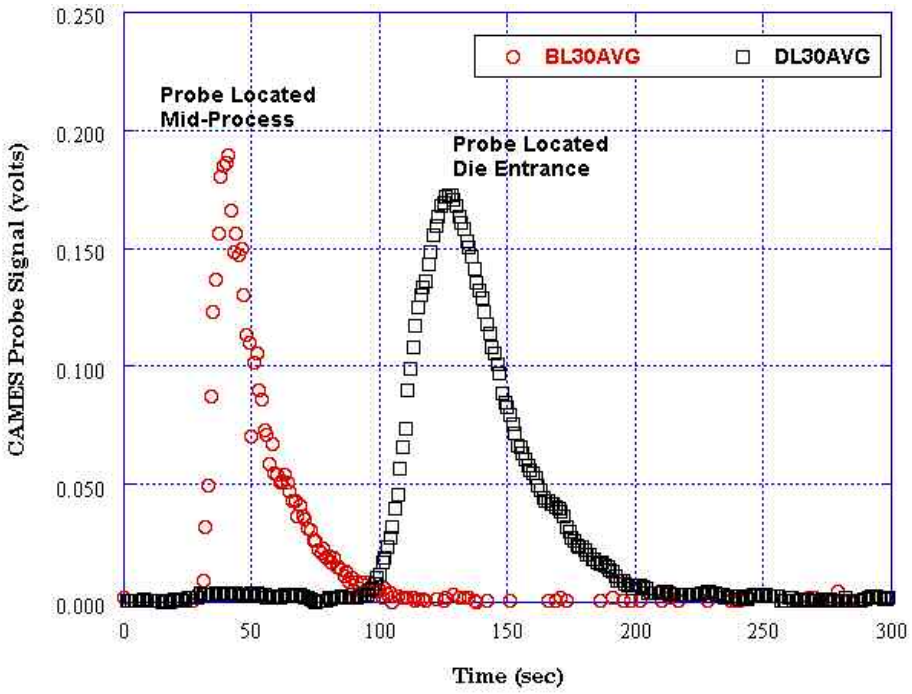

Figure 3-26. This plot illustrates the variation in shape of the RTD at two locations in the process. The curves are averages of three signals each from the barrel and die probe locations for the condition of 30 lbs/hr and KCl volume fraction of 0.693.

3.2.7 Conversion to RVDs

The data used for the conversion of the RTDs to the RVDs is provided in Tables 3-5 and 3-6. The response curves are shown in Figure 3-28. At the same mass throughput, the two 30 lbs/hr conditions have the same delay volume but the tail dissipation reflects a possible concentration effect. The 50 lbs/hr condition in the volume domain still was significantly different. Although *q/n* was higher for that condition, the data for that condition were not replicated due to that the KCl feeder was beginning to starve. This may account for the anomalous result in the RVD.

Table 3-5. Process conditions and residence time distribution characteristics for 40 mm experiments with inert ingredients.

ID	Probe Location	Volume Solids	Through-put (lbs/hr)	Number of Tests Averaged	Delay Time (sec)	Time End (sec)
DL30avg	Die	0.693	30	3	91±1	257±1
DH30avg	Die	0.800	30	4	102	201
DH501	Die	0.800	50	1	73	151

Key to ID: L-low solids and H-high solids.

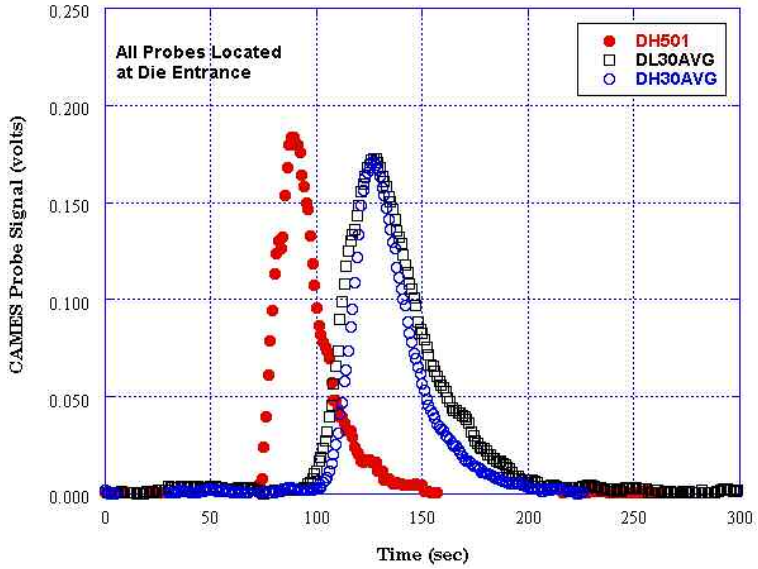

Figure 3-27. RTD responses were experimentally measured for the propellant simulant as functions of total throughput and filler concentration.

Table 3-6. Residence volume distribution characteristics for the propellant simulant.

ID	TMD	Volumetric Throughput (liter/sec)	Volume Start (l)	Volume End (l)
DL30avg	1.73	0.00219	0.199	0.561
DH30avg	1.82	0.00208	0.212	0.418
DH501	1.82	0.00347	0.250	0.524

TMD – theoretical maximum density in g/cm^3

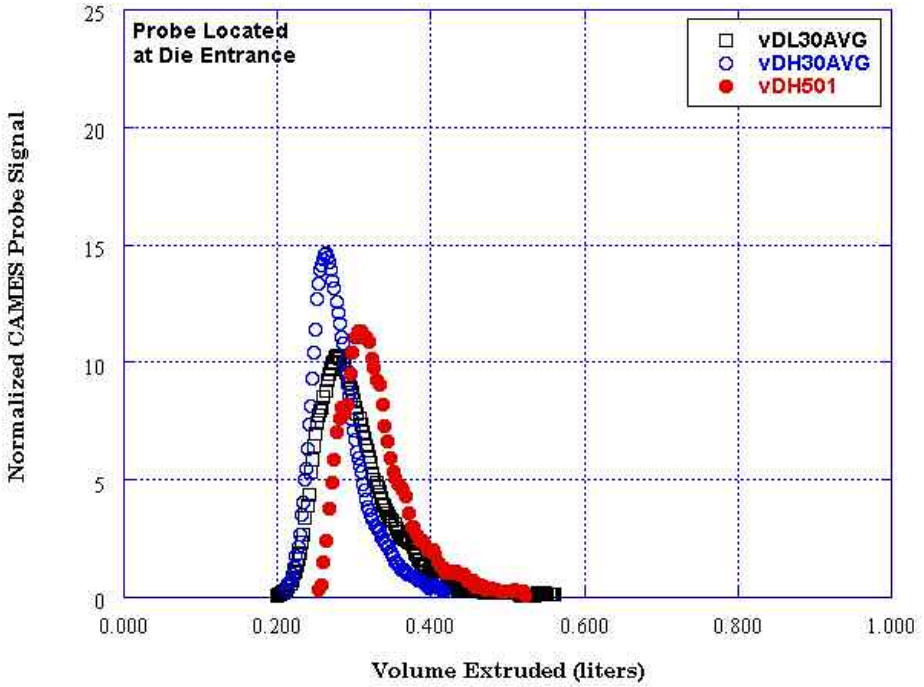

Figure 3-28. The plot illustrates the RVD responses for the inert composite as functions of total throughput and filler concentration. The KCl feeder was beginning to starve during measurements for DH501.

3.2.8 Fitting Filtered Data to Higher Order Process models

The RVD data was fit to process models of various orders to determine the best description. Interestingly the data did not fit a two or three-order process model. Rather, higher order models of fourth and fifth order were used fit the data with the fit parameters given in Table 3-7. The estimates of the best-fit model for each curve indicate good correlation with the experimental data, as seen in Figure 3-29.

The normalized curves revealed the concentration effect on the backmixing, as shown by the longer tail dissipation for the 30 lbs/hr condition with a lower

concentration. The increased solids concentration decreased the visco-elasticity of the mixture resulting in more positive transport. The volume delays for the 30 lbs/hr were not significantly different. At the same mass throughput, the shape factor for the higher concentration curve was significantly higher than that for the lower concentration. This comparison was possible because the two models were of the same order.

Table 3-7. RVD parameters were determined from best fits to higher order process models used to describe the processing of inert composite (test #02I) in the ZSK-40 at NAVSEAIHMD.

ID	Delay Volume, v_d (liters)	Order of Model	Shape Factor, a_v	Error for Shape Factor	Sum Squares Residuals	Best Fit?
DL30avg	0.198	2	17.26	±1.55	498.7	
DL30avg	0.198	3	28.18	1.12	188.0	
DL30avg	0.198	4	39.04	0.67	54.28	
DL30avg	**0.198**	**5**	**49.86**	**0.39**	**15.57**	**YES**
DH30avg	0.211	2	25.64	2.35	637.1	
DH30avg	0.211	3	41.91	1.61	210.5	
DH30avg	0.211	4	58.00	0.92	54.59	
DH30avg	**0.211**	**5**	**74.08**	**0.78**	**33.93**	**YES**
DH501	0.249	2	23.04	1.64	161.2	
DH501	0.249	3	37.31	0.81	27.74	
DH501	**0.249**	**4**	**51.25**	**0.84**	**23.90**	**YES**
DH501	0.249	5	64.95	1.61	76.31	

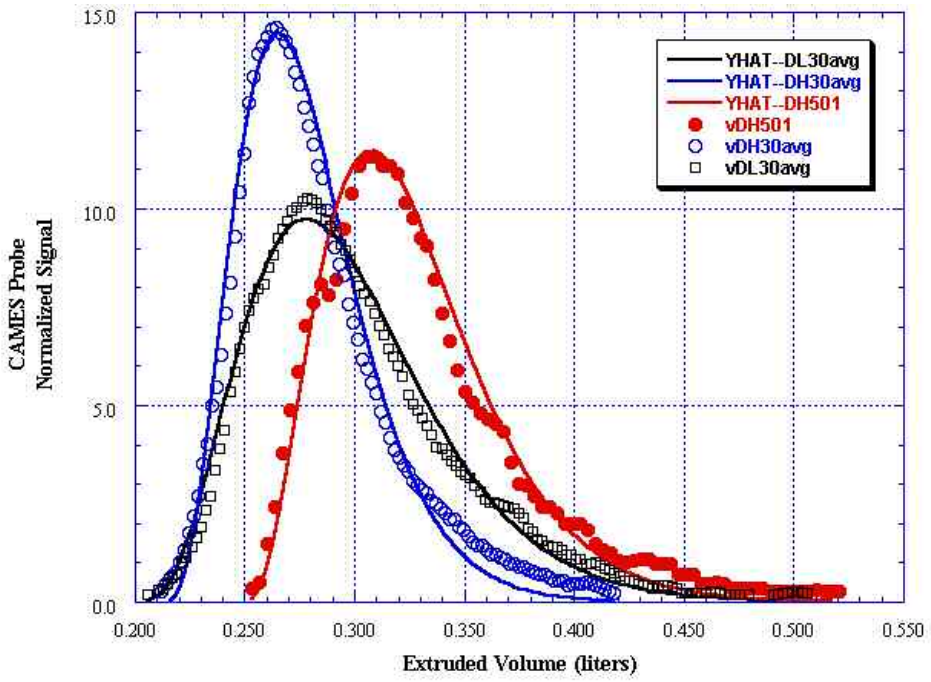

Figure 3-29. RVD data were plotted for inert composite processed in the ZSK-40 TSE with the best fits for higher order process models (02I).

The best-fitting model for the 50 lbs/hr measurement is fourth order. It is incorrect to assume that increasing the order automatically increased the degree of fit. While this is often true for polynomials, it cannot be applied in these analyses. A fifth order fit of the 50 lbs/hr data was worse than the fourth as shown in Table 3-7.

These data were not expected to be similar to the data obtained from the measurements of the KCL-filled elastomeric composite at UMD. Furthermore, any differences can be attributed to a number of factors. Many of them are straightforward. The properties of the polymeric binders were not the same, and the filler particle size distributions were completely different. The screws for the ZDSK-28 were tri-lobed while the ZSK-40 has two-lobed. To identify the differences that are not immediately obvious would be the objective of a scaling analysis for the mixer. Scaling analysis is not appropriate for the systems under consideration due to the obvious differences in formulations that have been described.

3.3 Residence Distribution Experiments of IH-AC3 Rocket Propellant in NSWC 40 mm Twin-Screw Extruder

There were a number of TSE trials with propellant to support this research investigation. These were trials to determine a viable processing window given

numerous feeding performance constraints and processing expertise, and there was a trial to prepare functionally graded grains for characterization. Those trials are discussed in later chapters. There were additional trials to determine the residence distributions characteristics of the propellant with the same screw design and process configuration as conducted for the inert composite (or simulant). This is discussed in the following section.

3.3.1 Ingredient/Formulation Discussion

The nominal formulation for the extruded rocket propellant is given in Table 3-8. It was selected because it was an extruded product and one for which there was a great deal of familiarity with processing in a TSE. It is a material with the greatest number of feed streams that has been continuously processed at NAVSEAIHMD, which increased the complexity of the process but was offset by the advantage that no development time was required for qualifying the formulation in the extrusion facilities. The formulation in Table 3-8 is nominal. For this project the ammonium perchlorate concentration was varied through the range of 0.79 to 0.87 fraction by weight. The nominal coarse-to-fine ratio was 70/30 as shown in the table. However the ratio of the coarse particle fraction to the fine particle fraction ranged from 50/50 to 81/19. The effects of the varying the ratio on the burning rate properties of the energetic formulation are presented in a later chapter to show the relationship of the process to the properties of the continuously graded extruded polymer composite.

Table 3-8. This is the nominal formulation for IH-AC3 rocket propellant.

Ingredient	Weight Percentage	Function
Ammonium perchlorate (90 μm)	58.8	Oxidizer
Ammonium perchlorate (10 μm)	27.2	Oxidizer
Zeon Chemical HyTemp® 4404	7.92	Binder
Dioctyl adipate	5.00	Plasticizer
3M Dynamar® HX-752	0.32	Bonding agent
Isophorone diisocyanate	0.26	Curative
Graphite	0.50	Extrusion aid
Zirconium carbide	0.50	Combustion modifier
Iron oxide	1.50	Ballistic modifier

3.3.2 Discussion of RTD Data

There are a number of research issues for processing energetic materials that have been addressed for the first time in this research project. One is the determination of the residence distribution using an on-line method for an energetic material processed in an extruder in the United States. Worldwide there has been no data published on residence distributions with energetic materials. NAVSEAIHMD has long had an interest in collecting residence time data on its continuous processes using on- and off-line methods (Bur and Gallant 1991). However, the studies have always been conducted with inert simulants, i.e., highly-filled composites with no energetic constituents. Up until now, the greatest constraint to evaluating the energetic process has always been the ability to insert tracers remotely. (When the screws are rotating, no personnel are permitted in the vicinity of the facility.)

The objectives of the second series of energetic runs were to collect RTDs and test the response of the process and material to step changes in the feed rates for the ingredients. An attempt was made to gather data over a range of conditions. In one case the supply of AP was exhausted before collecting the final conditions. In another, the change in screw speed was too extreme and resulted in an aborted run. However, there were plenty of high quality RTD data for characterizing the screw geometry and making comparisons between solids content and coarse/fine ratio.

The averaged residence distribution data from each tested condition are given in Table 3-9; the data were collected during two runs. The range of AP concentration and the particle size ratios were the parameters of interest for the study of ingredient effects on burning rates, which is discussed in Chapter 4. The theoretical maximum densities for 79 and 87 percent by weight AP are 1.710 and 1.791 $\frac{g}{cm^3}$ respectively.

Table 3-9. These were the test conditions for characterizing the RTDs of IH-AC3 propellant. Note that the throughput was 30 lbs/hr.

AP Content (by Weight)	Coarse/Fine Ratio	Extruder Screw Speed (RPM)	Avg. T_d (sec)	Avg. T_{end} (sec)	Avg. V_d (liters)	Avg. V_{end} (liters)
87.0	52.7/47.3	85	112	206	0.236	0.434
79.0	79/21	45	142	251	0.311	0.566
79.0	79/21	85	111	255	0.240	0.564

The experimental data were quite remarkable in consistency and repeatability. The delay times were quite consistent and appeared to be independent of solids fill and the coarse/fine ratio for the ranges that were tested. The screw speed effect demonstrated on the smaller extruder was also apparent in the data from the 40 mm, as was expected. There were some differences in the tail resolutions, but there was not enough data to observe a statistical difference.

The data from one run (#FGM07-0048) is given in Figure 3-30. This plot shows the individual measurements. The data from this day were collected in duplicate to conserve material. (The data for 87 percent were collected in triplicate.) There was one dominant trace in Figure 3-30 resulting from a double dose of tracer. Note how it has the same delay time, but very different height and tail resolution. Normalizing the RTD data yields the results in Figure 3-31.

It is a significant observation that the dose size, even double the dose size, was small enough not to disturb the characteristics of this process. There was some concern that the impulse disturbance represented by the tracer addition disrupted the *natural* dynamics of the RD at steady state. If this were true, the signals would not have scaled as shown in Figure 3-31. It is still possible in theory that a large enough magnitude impulse disturbance could interfere with the true characteristics of the process. However, this was not demonstrated, and was beyond the scope of the investigation.

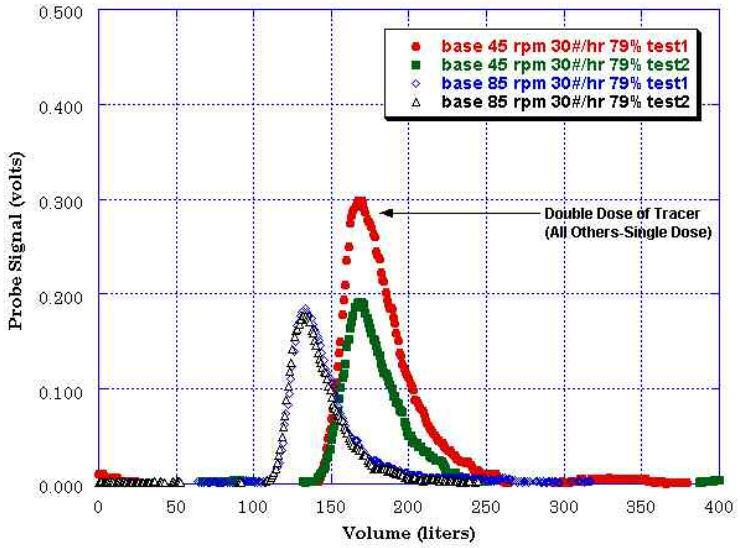

Figure 3-30. These are plots of duplicated experimental RTD measurements for IH-AC3 propellant at 79% AP, 30 lbs/hr, and different extruder screw speeds of 45 and 85 rpm. Note the difference in tracer dose for one case.

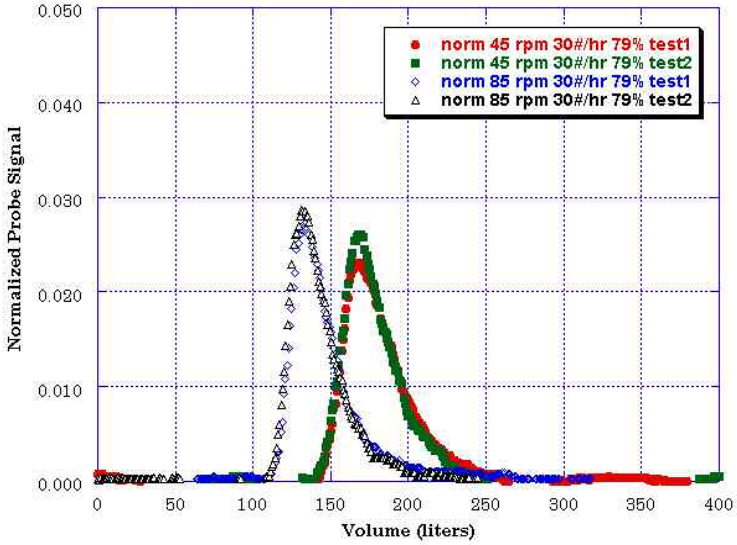

Figure 3-31. These plots are normalized individual RTD measurements for IH-AC3 propellant. Compare to Figure 3-30 and note no difference due to tracer dose.

The RTD data for all three conditions in Table 3-9 are plotted in Figure 3-32. The results of the nonlinear model fitting are presented in Table 3-10. There was no difference in delay time due to the AP concentration or the coarse/fine ratio. There could be a difference in the tail resolution due to either the concentration and/or the ratio, but not enough data were obtained to distinguish which of these effects was responsible.

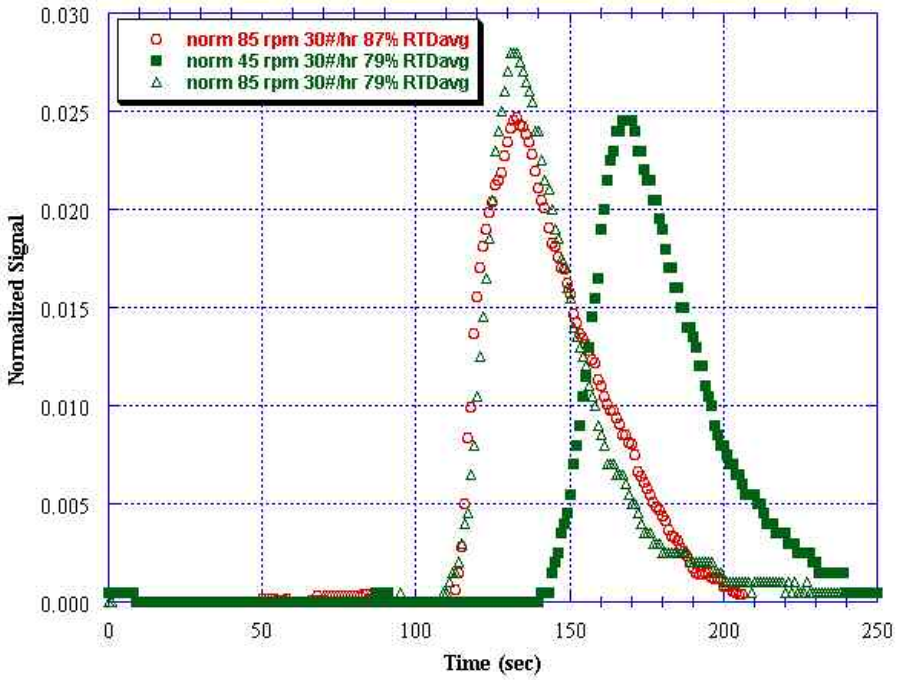

Figure 3-32. The RTDs for IH-AC3 propellant at various processing conditions were averaged, normalized, and plotted.

Table 3-10. RTD parameters were determined from best fits to higher order process models for characterizing the propellant process response to an impulse input using the ZSK-40 at NAVSEAIHMD.

ID rpm/AP	Delay Time, t_d (sec)	Order of Model	Shape Factor, a_t	Error for Shape Factor
85/87	112	2	0.0578	±0.0019
"	"	**3**	**0.0924**	**0.0015**
"	"	4	0.1255	0.0040
85/79	108	2	0.0514	0.0045
"	"	3	0.0847	0.0028
"	"	**4**	**0.1176**	**0.0017**
"	"	5	0.1503	0.0023
45/79	140	2	0.0452	0.0037
"	"	3	0.0740	0.0022
"	"	**4**	**0.1023**	**0.0012**
"	"	5	0.1304	0.0019

3.3.3 Conversion to RVDs

The RTDs were converted to RVDs using the methods presented in earlier sections. As expected the extruder screw speed effect was still apparent as seen in Figure 3-33. In the RVD there was more of a difference due to AP concentration with the lower AP material exhibiting a slight lagging behind the 87 percent material. However they both exhibited the same delay volume.

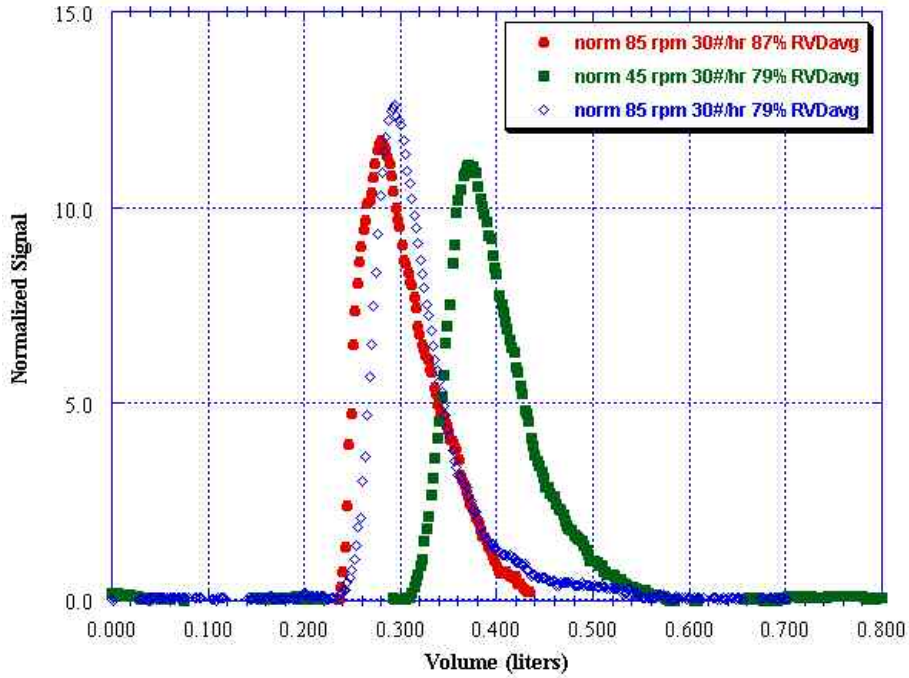

Figure 3-33. The normalized RVDs for IH-AC3 are plotted.

3.3.4 Fitting RVD and RTD Data to Process models

The RVD data for the propellant were fit to process models of various orders. While it was certainly possible to exactly fit an ideal model, it was more likely that the process lies at a non-integer order that could be determined from a mathematical optimization approach to be pursued in a future research effort. Therefore the model fits in Table 3-9 are approximate to the nearest whole order, but still have a high degree of correlation as is evident from the residuals sum squares (RSS). The curves defined by the parameters in Table 3-11 are plotted in Figure 3-34 with the experimental data for each condition.

The shape factors for the 79 percent condition for both screw speeds are similar. In Figure 3-33, the similar shape to the two curves is quite apparent; they only differ by the delay volume that is due to the screw speed effect. Note the independence of the delay volume, v_d, from the concentration. This is important because it implies that the

RVD is independent of the composition of the material—and therefore the gradient architecture. This makes it possible to use the RVD to determine the response at the die to a step change in the feed rates for the addition of an ingredient to the process.

The similarity between the values of RSS in Table 3-11 with the best fits for the propellant simulant in Table 3-7 is evident. Furthermore, the model orders were similar to the simulant. In the case of 79 percent AP, the best model was between the orders of 4^{th} and 5^{th}. The simulant models for 30 lbs/hr were approximately 5^{th} order regardless of the volume loading. Figure 3-33 illustrates the RVDs for IH-AC3 propellant at conditions of two screw speeds (45 and 85 rpm) and two AP concentrations (79 and 87 percent by weight) with the fitted RVD models using parameters from Table 3-11.

Table 3-11. Ideal process model parameters were determined by fitting the RVDs of IH-AC3 propellant collected at various processing conditions.

ID (RPM/%AP)	Delay Volume, v_d (liters)	Order of Model	Shape Factor, a_v	95% C.I. for Shape Factor	Sum Squares Residuals
85/87.0	0.235	3	43.23	±0.59	25.12
85/79.0	0.237	4	51.77	0.55	45.41
45/79.0	0.309	4	46.13	0.39	15.23

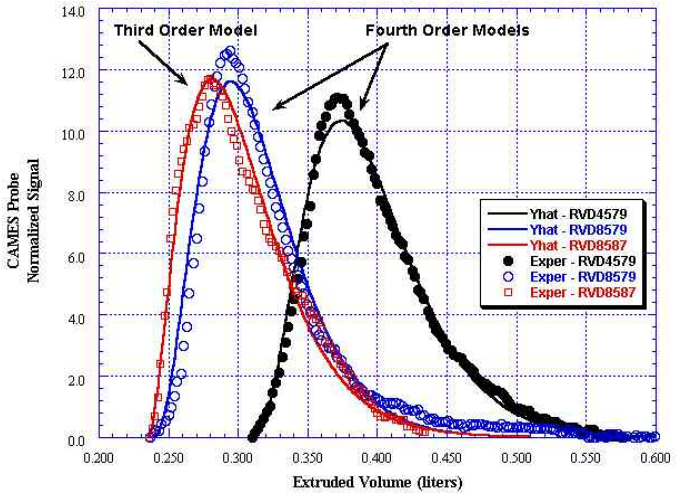

Figure 3-34. The plot illustrates the RVDs for IH-AC3 propellant at conditions of two screw speeds (45 and 85 rpm) and two AP concentrations (79 and 87 percent by weight) with the fitted RVD models using parameters from Table 3-9.

With the RTD and RVD characterization now complete for the inert and energetic formulations, it was possible to proceed to the investigating the effects of transient processing conditions on the evolution of gradient architectures in the TSE process. As mentioned previously, the focus was placed on understanding the physics associated with a step input change to an ingredient in the formulation for the extruded polymer composite. Chapter 5 describes this investigation in relation to the steady-state RTD and RVD process models in this chapter.

4.0 Range of Achievable Burning Rate in Extruded Composite Rocket Propellant IH-AC3

Many factors contribute to the burning rate of a propellant, for example, ingredient types, concentrations and particle sizes (Carvalheira, Campos et al. 1996) (Gocmez, Erisken et al. 1998), method of preparation (Dean 1993) (Muscato, Michienzi et al. 1999), testing conditions (NOS 1968), etc. This project is concerned with the intentional design for the microstructure of a Navy experimental composite propellant, designated IH-AC3. However there was no experimental data to indicate the quantitative effects of the ingredients on the burning rate of twin screw processed material, effects such as oxidizer particle size distribution, filler concentration, rate modifiers, screw geometry, etc.

Thompson & Michienzi had published a well-designed study for many of these effects in IH-AC3 using the batch process to support the development of a near infrared spectroscopy technique to predict burning rate (Thompson and Michienzi 1998). This data was important, but not relevant in light of the unaccounted differences in burning rate observed by Muscato (Muscato, Michienzi et al. 1999) between batch and continuously processed IH-AC3. However this important observation is very relevant to this discussion; its importance in this investigation will be revealed below.

The burning rate characterization testing was conducted at two points in this investigation. The first test set, discussed in this chapter, was to characterize the effects of the process capability space on the burning rate of homogeneous propellant made at various locations within that space. The second point was the characterization of functionally graded propellant using the acoustic strand burning rate test (Chapter 5).

4.1 Design of Mixture Experiments

It was necessary to ascertain the effects of the individual ingredients on the burning rates as produced over the range of feeding and extruding capability for the process. Designed mixture experiment methodology was recognized as the most efficient and

thorough method to achieve this goal. This family of methods can quantify the contribution of individual ingredients and more importantly the combined effects of two or more ingredients using response surface analytical methods. Most mixture designs are based on component proportions and not total quantity of a mixture. This is the situation for the composite propellant; the burning rate is a function of the relative amounts of ingredients and not propellant quantity.

Manufacturing IH-AC3 using the continuous process is more efficient, more environmentally benign, and cost effective compared to the batch process. However, preparing a number of propellant samples remotely at a wide variety of compositions and process conditions is nevertheless an expensive and complex undertaking. While this is the usual route for any propellant development or characterization study, following a designed method will ensure the most viable (and defendable) data and results possible. These facts have been widely recognized, and these methods have been applied to continuous processing at Navy facilities for some years.

4.1.1 Simplex Design

The classical design attributed to H. Scheffe is referred to as a simplex and is evaluated using polynomial models (Cornell 1990). Let q represent the number of individual constituents, where q is two or greater. Note that constituents and ingredients are not the same in this discussion. Then let X_i be the proportion of the i^{th} ingredient that can range from zero to one hundred percent. This is generally represented mathematically as,

$$\sum_{i=1}^{q} X_i = 1.0, \qquad 0 \le X_i \le 1.0 \tag{32}$$

A graphical example is given in Figure 4-1 for a three constituent simplex-centroid design with seven test mixtures. A four constituent simplex-centroid would be a tetrahedron with 15 combinations. The design size has $2^q - 1$ points.

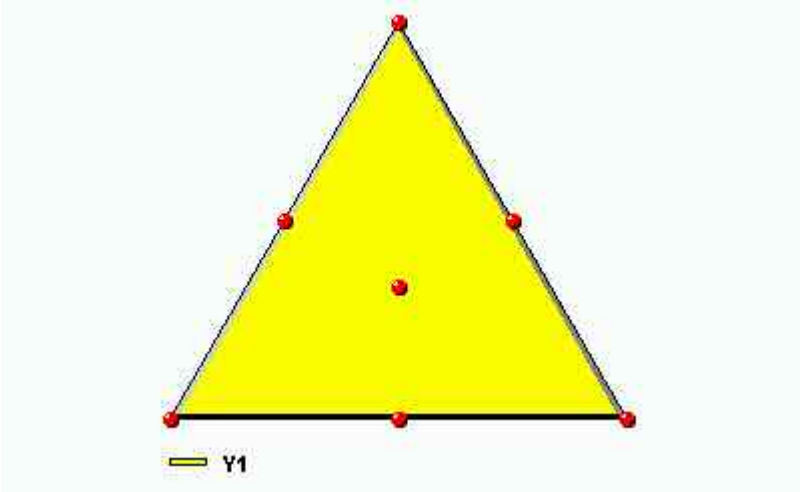

Figure 4-1. Graphical example of three constituent simplex centroid design.

However there are many examples of cases where there are constraints on the combinations that can be allowed due to physical, chemical, economical, safety considerations, or expert knowledge of the system. Experiments with hazardous materials certainly meet these criteria, but most industrial processes can be included as well. For example testing a propellant with low oxidizer or none is a waste of time and money. Furthermore there are levels of oxidizer that are not allowable due to the physical limitations of the process, i.e., a significant safety hazard. Therefore it is desirable to constrain oxidizer to a lower and upper bound. This may hold true for some or all of the other ingredients. Constraining is also advisable in cases where one desires to study the response in a region of interest.

4.1.2 Extreme Vertices Design

The contributions of McLean & Anderson (McLean and Anderson 1966) and Snee & Marquardt (Snee and Marquardt 1974) in the form of extreme vertices designs allow the use of lower and upper bounds on constituents where,

$$\sum_{i=1}^{q} X_i = 1.0, \quad 0 \le a_i \le X_i \le b_i \le 1.0 \tag{33}$$

The sum of the constituents must still equal one, but there are upper and/or lower constraints on the proportions resulting in a design space that is an irregular hyperpolyhedron. However constraints introduce complexities in the mixture combinations to test and the appropriate forms of regression models that the designs can support. Because of physical and safety limitations for propellant mixtures, a

constrained mixture design is imperative. A rather involved formula is used to calculate the number of extreme vertices, edges and two-dimensional faces of the design space (Cornell 1990). The coordinates, which give the mixture proportions, are determined by an algorithm developed by Snee & Marquardt (Snee and Marquardt 1974) and refined further by Snee (Snee 1975) in light of certain complications. The response surface, $\eta(x_i)$, of mixture experiments, regardless of constraints, can be modeled using a Scheffe second-degree polynomial as (Cornell 1990),

$$\eta(x_i) = \sum_{i=1}^{q} \beta_i x_i + \sum \sum_{i<j}^{q} \beta_{ij} x_i x_j \qquad 34)$$

4.2 How the Ingredients and the Twin-Screw Process Influences Burning Rate

One of the observations revealed by Muscato *et al* (Muscato, Michienzi et al. 1999) was an interesting effect of extruder screw speed on the burning rate of IH-AC3. Muscato found that the burning rate decreased an average of 10.6 percent upon increasing the extruder screw speed from 50 to 85 rpm. This effect could not be explained and remained a curiosity ever since it was reported. Since ingredients and process effects influence the burning rate of IH-AC3, it was important to include all possible effects in an experiment design to explore the range of burning rates for the FGM application.

4.2.1 Mixture Designs that Include Process Variables

Therefore it was necessary to use a design methodology for a mixture experiment that incorporated process variables also referred to as process factors. Cornell has contributed the most to the mixture design literature on the inclusion of process factors (Cornell 1990) (Naes, Faergestad et al. 1998) (Piepel and Cornell 1994) (Kowalski and Cornell 2000). The mixture-process design is constructed by combining two types of designs. First a mixture design with *q* constituents is identified, and next a factorial design of *n* process variables is crossed with each point of the mixture design. The result is a design capable of resolving all mixture effects and crossed process effects. It identifies mixture combinations that are more sensitive to process settings than others.

4.2.1.1 Flour Blend Example

One example is the study to determine the effect of flour blends from different sources of flour and the dough preparation conditions to determine sets of conditions

and appropriate blends where loaf volume is insensitive to variations in preparation (Naes, Faergestad et al. 1998). Naes evaluated 10 blends of flours from three sources as defined by a lightly constrained simplex lattice design shown in Figure 4-2(a). Note how the lower bound of the Tjalve flour source is set at 25 percent of the mixture. Two process factors were of interest at three levels resulting in a nine point factorial design as shown in Figure 4-2(b). One traditional model for the process variables is given by (Kowalski and Cornell 2000),

$$\eta_{PV}(z_k) = \alpha_0 + \sum_{k=1}^{n} \alpha_k z_k + \sum \sum_{k<l}^{n} \alpha_{kl} z_k z_l \tag{35}$$

and the combined model, which assumes that $n > 1$, is given as,

$$\begin{aligned} \eta(\vec{x}, \vec{z}) = & \sum_{i=1}^{q} \beta_i x_i + \sum \sum_{i<j}^{q} \beta_{ij} x_i x_j + \sum_{i=1}^{q} \sum_{k=1}^{n} \gamma_{ik} x_i z_k \\ & + \sum_{i=1}^{q} \sum \sum_{k<l}^{n} \gamma_{ikl} x_i z_k z_l + \sum \sum_{i<j}^{q} \sum_{k=1}^{n} \gamma_{ijk} x_i x_j z_k \\ & + \sum \sum_{i<j}^{q} \sum \sum_{k<l}^{n} \gamma_{ijkl} x_i x_j z_k z_l \end{aligned} \tag{36}$$

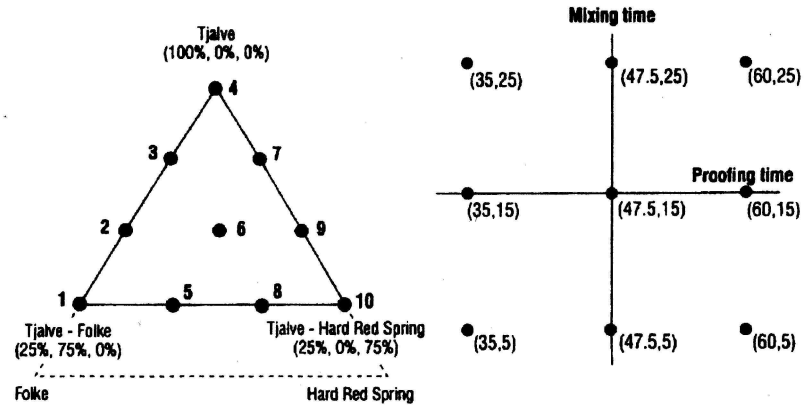

(a) (b)

Figure 4-2.(a) Simplex-lattice mixture design for blending flour from three sources. (b) Two-factor three-level factorial design for the process variables (Naes, Faergestad et al. 1998).

Neas evaluated the complete process design using each of the ten blends in a 90-point experiment. In other words the nine-point factorial design in the process conditions was conducted for each of the ten mixtures. This approach is extremely

thorough, resulting in the maximum amount of estimated effects. These so-called saturated designs are typical in the early literature on mixture-process designs. It is easy to determine that the costs for this type of design could become quite expensive—possibly too expensive to consider for many situations. If one must perform only a limited number of treatment combinations, due to economic or other limited resources, there are various techniques for selecting an optimum fraction of the runs (Cornell 1990). Computer programs can easily perform selections of optimal design matrices according to various mathematical definitions of optimality criteria, but the computer-generated designs should not be used without some consideration given to design balance of the computer output (Cornell 1995) (Kowalski and Cornell 2000).

In the case of producing and testing rocket propellant under a multitude of conditions and constituent combinations, the resource costs of both a batch process or a continuous approach are high. Therefore a reduced experimental design is quite attractive. Kowalski presents a solution that addressed the experiment design needs for this project (Kowalski and Cornell 2000).

4.2.1.2 Kowalski's Algorithm

Kowalski suggests a Taylor series approximation for the process variables which best suits response surface analyses,

$$\eta_{PV}\left(z_k\right) = \alpha_0 + \sum_{k=1}^{n} \alpha_k z_k + \sum_{k=1}^{n} \alpha_{kk} z_k^2 + \sum \sum_{k<l}^{n} \alpha_{kl} z_k z_l \tag{37}$$

Combining (20) and (21) yields a combined second-degree model,

$$\begin{aligned} \eta_{PV}\left(\vec{x},\vec{z}\right) = & \sum_{i=1}^{q} \beta_i x_i + \sum \sum_{i<j}^{q} \beta_{ij} x_i x_j + \sum_{k=1}^{n} \alpha_{kk} z_k^2 + \sum \sum_{k<l}^{n} \alpha_{kl} z_k z_l \\ & + \sum_{i=1}^{q} \sum_{k=1}^{n} \gamma_{ik} x_i z_k \end{aligned} \tag{38}$$

Kowalski asserts that this model includes "the mixture model, plus pure quadratic as well as two-factor interaction effects among the process variables, and two-factor interactions between the linear blending terms in the mixture (constituents) and the main effect terms in the process variables (Kowalski and Cornell 2000)." This model requires a design size of $(q+n)(q+n+1)/2$ points. It requires less design points for fitting than (20), and the quadratic terms can be omitted if not necessary further

reducing the design points. Kowalski describes a process for constructing the new design. However a description of the factors for the IH-AC3 experiment is necessary. The goal of the experiment should dictate the design. To do otherwise is to limit one's success and quite possibly introduce bias.

4.2.2 Mixture/Process Experiment for IH-AC3

There were a number of reasonable process constraints that were identified and incorporated in the design strategy. The ingredients for the propellant were fed to the extruder as blends and mixtures, so the blends were treated as the factors or constituents for the mixture matrix (not the individual ingredients). There were two other constraints to consider. The first was a consideration of the established process methodology for this formulation and the possible strategies for achieving gradient structures in the extrudate within those methods. The other consideration was the ingredient ranges imposed by any particular mixture design. For example some candidate experiment designs required combinations of feeding rates that could not be accommodated economically or safely. These issues were studied exhaustively by the author and concluded satisfactorily.

Suffice to say that gradient control was confined to the two AP feedstreams. While this strategy unfortunately ignored the known influence of the modifiers, there was still enough flexibility with the AP feed streams to yield a significant effect in the burning rate. Given these constraints, the burning rate is influenced by overall concentration of AP as defined by its converse, the concentration of binder. Additionally, it is also influenced by the ratio of coarse to fine AP particles. This was expressed as the individual concentrations of AP grind fractions for the sake of the mixture experiment.

Lastly this experiment represented the best opportunity to settle a longstanding uncertainty, i. e., experiment observations that suggested extruder screw rpm may influence the burning rate. Therefore the mixture and process experiment included three mixture factors and one process factor, the ranges and levels respectively are given in Table 4-1.

Table 4-1. Factors (or Controls) for Burning Rate Experiment on IH-AC3 Propellant.

Ingredient	Type	Range/Levels
AP Coarse Particle Grind (APC)	Mixture	40.3-70.4 % by weight
AP Fine Particle Grind (APF)	Mixture	16.6-41.2
Binder (BIN)	Mixture	13.0-21.0
Extruder Screw Speed (RPM)	Process	45 and 85

An extreme vertice design is shown in Figure 4-3 as a trilinear plot. Each apex of the triangle represents 100 percent by weight of that feed stream. It consists of 5 extreme points, 5 edge centroids and one overall centroid. To include screw speed as a design objective would require at least 22 combinations, i. e., the full eleven points at each rpm. The cost of producing and testing 22 samples of propellant was prohibitive to this project.

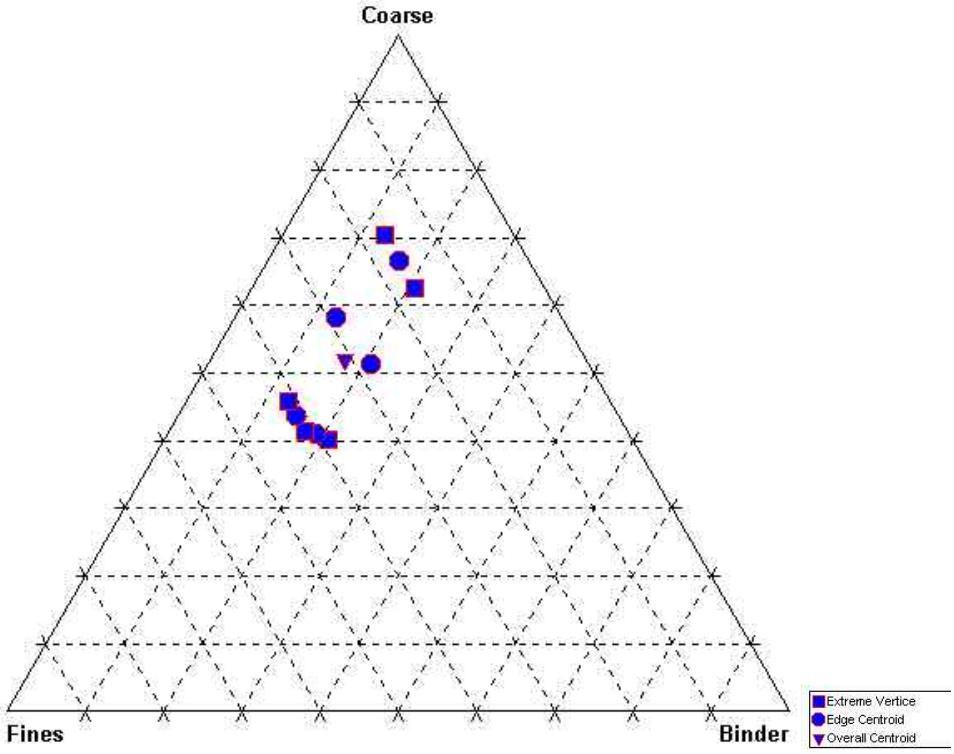

Figure 4-3. Extreme Vertice Design for Three Mixture Factors with Eleven Combinations.

Kowalski's algorithm begins with the full extreme vertice design set of more than twenty-two runs and reduces it to fourteen runs in this particular case. Fourteen

combinations were much more affordable to produce and test. The design implemented for this study is illustrated in Figure 4-4 and listed in Table 4-2. The table of design points gives the proportions in terms of feed streams. Because one feed stream was a blend of fine and coarse particles, the effective amounts of each size fraction is given in Table 4-3 in two ways. The third and fourth columns of Table 4-3 is the weight fraction of coarse and fine particles; the fifth and sixth columns express the AP content as the ratio of each particle size where the total equals 100 percent. Note the nominal formulation for IH-AC3 was within the design space and was added as an additional test combination.

The algorithm generated a balanced design with the five edge centroids and one overall centroid at one RPM, and this was added to the five vertices and one overall centroid at the second level of RPM. One of the overall centroids was repeated for an estimate of the error, and another centroid point was added at the midpoint RPM value. This sums to fifteen test points or runs.

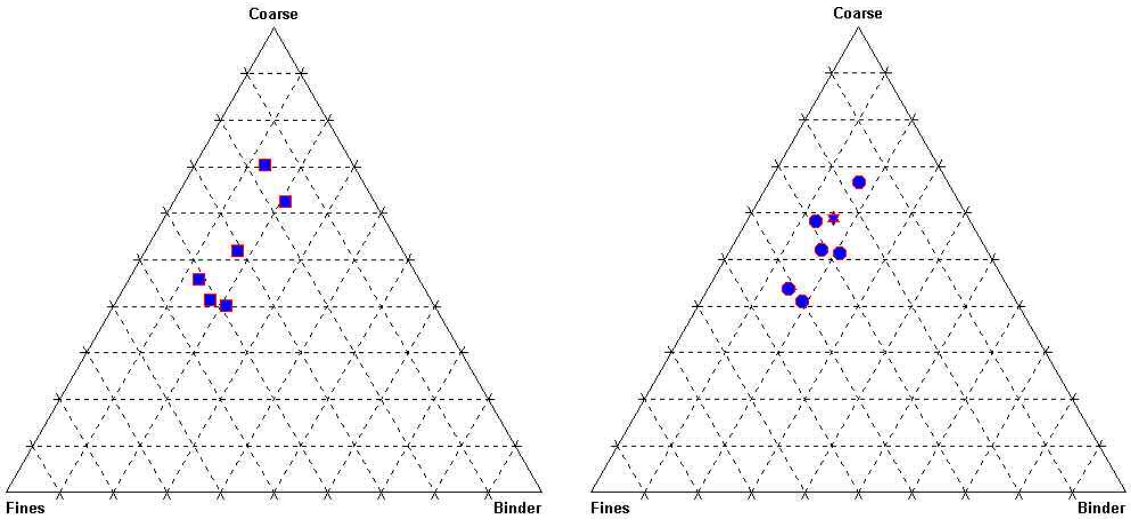

(a) Combinations Made at 45 rpm (b) Combinations Made at 85 rpm

Figure 4-4. Mixture Combinations Extruded for Burning Rate Study:The Star in 4-4(b) Represent the Location of IH-AC3, the Nominal Combination.

4.2.2.1 Results of the Extrusion Trials and Strand Burning Rate Data

All combinations were produced using the 40 mm twin-screw extruder. Small *strands* of propellant measuring ¼ x ¼ x 6 inches were cut for strand burning rate testing (Rampichini, Ruspa et al. 2000). Complete characterization of the burning rate dictates

that the strand testing be conducted over a range of temperatures and operating pressures, since the burning rate is dependent upon the test conditions. However this was a technology program and not a propellant development program, so testing was conducted at one temperature—ambient. This is a typical approach by propellant formulators for screening large sets of strands. Since the graded motors were to be designed with a relatively low operating pressure, the strands were tested at 500, 1000, and 1500 psig chamber pressures. The average burning rate for each mixture and process combination is presented in Table 4-4. The design space yielded a satisfactory range of burning rates. The range approximately doubled at the higher test pressures despite the conservative processing and feeding constraints.

Table 4-2. Mixing Design Points for Burning Rate Variability Study with a Process Variable.

ID	Design Point	Coarse AP Feedstream	Fine/Coarse Blend AP Feedstream	Binder	Extruder RPM
A	Vertex	0.237	0.553	0.21	45
B	Edge centroid	0.237	0.5705	0.1925	85
C	Vertex	0.237	0.588	0.175	45
D	Edge centroid	0.2595	0.588	0.1525	85
E	Vertex	0.282	0.588	0.13	45
F	Overall centroid	0.3884	0.4406	0.171	45
G	Overall centroid	0.3884	0.4406	0.171	85
H	Overall centroid	0.3884	0.4406	0.171	85
I	Overall centroid	0.3884	0.4406	0.171	65
J	Edge centroid	0.395	0.395	0.21	85
K	Edge centroid	0.4575	0.4125	0.13	85
L	Vertex	0.553	0.237	0.21	45
P	Test for Fitness	0.588	0.252	0.16	85
M	Edge centroid	0.593	0.237	0.17	85
N	Vertex	0.633	0.237	0.13	45

Table 4-3. Actual Factions and Common Ratios of Coarse and Fine Ammonium Perchlorate Taking into Account Contribution of Fine/Coarse Blend Feed Stream.

ID	Design Point	Effective Yield		Coarse/Fine Ratio (C + F = 1)	
		Coarse AP	Fine AP	Coarse AP	Fine AP
A	Vertex	0.4029	0.3871	0.5100	0.4900
B	Edge centroid	0.4082	0.3994	0.5054	0.4946
C	Vertex	0.4134	0.4116	0.5011	0.4989
D	Edge centroid	0.4359	0.4116	0.5143	0.4857
E	Vertex	0.4584	0.4116	0.5269	0.4731
F	Overall centroid	0.5206	0.3084	0.6280	0.3720
G	Overall centroid	0.5206	0.3084	0.6280	0.3720
H	Overall centroid	0.5206	0.3084	0.6280	0.3720
I	Overall centroid	0.5206	0.3084	0.6280	0.3720
J	Edge centroid	0.5135	0.2765	0.6500	0.3500
K	Edge centroid	0.5813	0.2888	0.6681	0.3319
L	Vertex	0.6241	0.1659	0.7900	0.2100
P	Test for Fitness	0.6636	0.1764	0.7900	0.2100
M	Edge centroid	0.6641	0.1659	0.8001	0.1999
N	Vertex	0.7041	0.1659	0.8093	0.1907

The data in Table 4-4 were plotted as independent functions of the experiment's design parameters to determine any obvious trends. Figure 4-5 was typical for this type of plot. In the figure the average burning rate data were plotted as functions of the binder content and chamber test pressure. As expected, the average burning rates decreased with increasing inert binder. Also expected was the response of the average burning rates to test chamber pressure. There is a positive relationship between the average burning rate and test pressure. Note that there is also relationship between the slope of the burning rate response to the fraction of binder is different and the chamber pressure. This too was typical of the simple trend plots; the responses were less dramatic for the 500 psig than the 1,500 psig chamber pressure.

Table 4-4. The Individual Test Combinations and Average Burning Rates (Sorted by Fines) of the Homogeneous Propellant Strands.

			Effective Yields			Avg. Burning Rate for Test Pressure (psig)		
ID	Point Type	RPM	Coarse	Fines	Binder	500	1,000	1,500
L	Vertex	45	0.624	0.166	0.210	0.443	0.580	0.625
N	Vertex	45	0.704	0.166	0.130	0.630	1.085	1.460
P	Test Fitness	85	0.664	0.176	0.160	0.536	0.802	0.975
J	Edge centroid	85	0.514	0.277	0.210	0.526	0.735	0.773
K	Edge centroid	85	0.581	0.289	0.130	0.620	1.061	1.276
M	Edge centroid	85	0.664	0.289	0.170	0.513	0.731	0.834
F	Overall centroid	45	0.521	0.308	0.171	0.604	0.943	1.145
G	Overall centroid	85	0.521	0.308	0.171	0.546	0.799	0.915
H	Overall centroid	85	0.521	0.308	0.171	0.550	0.784	0.939
I	Overall centroid	65	0.521	0.308	0.171	0.601	0.899	1.072
A	Vertex	45	0.403	0.387	0.210	0.571	0.884	0.988
B	Edge centroid	85	0.408	0.399	0.193	0.609	0.854	1.001
C	Vertex	45	0.413	0.412	0.175	0.664	0.997	1.156
D	Edge centroid	85	0.436	0.412	0.153	0.666	1.006	1.272
E	Vertex	45	0.458	0.412	0.130	0.701	1.116	1.528

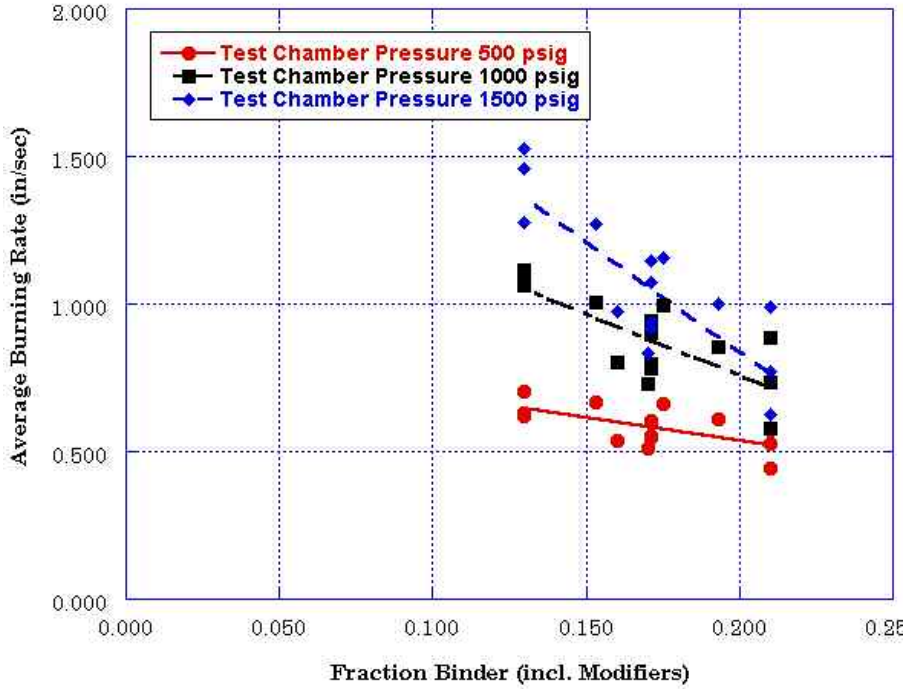

Figure 4-5. The Relationships between Average Burning Rate, the Fraction of Binder, and the Chamber Test Pressure.

Likewise similar plots were prepared for the concentrations of the two particle size fractions of ammonium perchlorate in Figures 4-6(a) and 4-6(b). The data for 1,000 psig were omitted for clarity. Trends were present in the data and can be reasonably interpreted. Overall there is a downward effect on burning rate as the amount of coarse AP was increased. Conversely increasing the fraction of fine particle AP resulted in a corresponding increase in burning rate.

These data could be two sides of the same coin. As the fraction of coarse increases, i.e., the fines were thus decreasing, the average burning rate decreases. The converse is true as shown in Figure 4-6(b). There is the appearance of scatter in the 1,500 psig data that is misleading. The data are scattered because there are other effects due to screw rpm, total solids loading, and the coarse/fine ratio. Furthermore there is a tendency for the effects to be more pronounced at the higher test pressures.

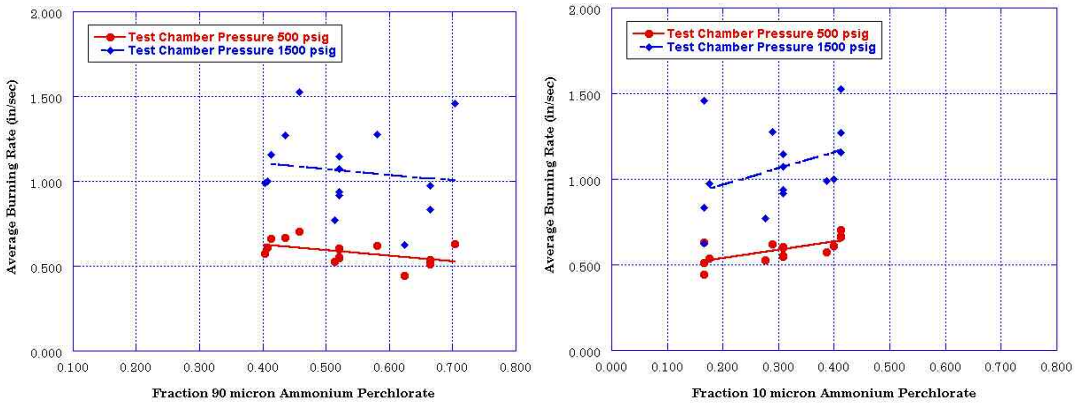

(a) (b)

Figure 4-6. The Effects of Particle Size and Fraction Concentrations on the Average Burning Rate.

One of the powerful effects on average burning rate was the extruder screw rpm. This effect had been observed by Muscato (Muscato, Michienzi et al. 1999), but not systematically documented or studied in conjunction with the ingredient effects until this research. There indeed was an influence of the screw rpm on the burning rate as indicated in Figure 4-7. The possible explanations lie in the important effects of $\frac{Q}{n}$, i.e., the combined influence of throughput and rpm together on the degree of fill in the mixing zone. At the lower rpm the degree of fill is higher in the machine and vice versa. There is a difference in the mixing history between the extruder screw speeds. What is unknown is if the changes are due to different particle dispersion efficiencies or other changes on the microstructural scale.

These results indicate some directions for future research into gradient manufacturing. Instead of creating the gradient with the ingredients, one would study the dynamic influence of the screw rpm. It is possible to even consider deliberate and subtle changes in the screw rpm to impart particular nuances in the burning of the grains.

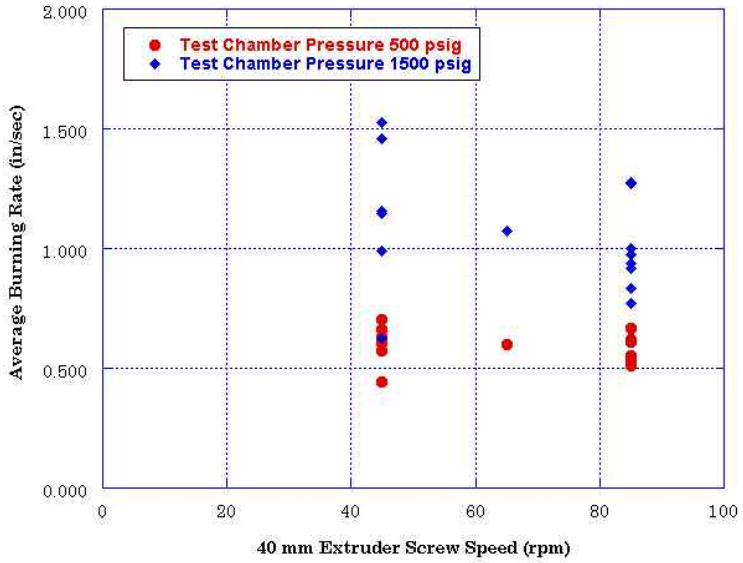

Figure 4-7. There was an observed overall decrease in burning rate at extruder screw speed was increased.

4.2.2.2 Analysis and Interpretation of the Burning Rate Data

A rigorous response surface analysis was conducted for the burning rate data according to methods proposed by Kowalski & Cornell (Kowalski and Cornell 2000) and Piepel & Cornell (Piepel and Cornell 1994). The mixture points were expressed in terms of the actual yields of coarse and fine particles as in Table 4-4 where,

x_1 = fraction of coarse 90 µm Ammonium Perchlorate

x_2 = fraction of fine 10 µm Ammonium Perchlorate

x_3 = fraction of binder including modifiers

Because upper (and lower by implication) bounds were used to constrain the mixtures, the constituents were converted to *u*-pseudocomponents (Crosier 1986). Therefore the u-pseudo-components were,

$$u_i = \frac{U_i - x_i}{\sum_{i=1}^{q} U_i - 1} \tag{39}$$

where,

U_i = the upper limit of the i^{th} component

then, for the number of mixture components, $q = 3$,

$$u_1 = \frac{0.7041 - x_1}{0.3257} \tag{40}$$

$$u_2 = \frac{0.4116 - x_2}{0.3257} \tag{41}$$

$$u_3 = \frac{0.2100 - x_3}{0.3257} \tag{42}$$

The model (43) was tested against the u -pseudocomponents for each chamber pressure using step-wise regression and analysis of variance. Conditions *I* (the centroid point at 65 rpm) and *P* (an extra point to check the fit of the model) were excluded from the model analysis. The analysis of variance was conducted step-wise using a significance of $\alpha = 0.10$; however the results were down-selected to alpha values of much less. The results are summarized in Tables 4-5 through 4-7. The correlation coefficient, r^2, is increasing as one moves down the table. This is because as each significant term is stepwise added into the probabilistic model, the correlation coefficient improves. The variables are listed in order of significance.

$$\eta_{PV}(\bar{u},\bar{z}) = \eta_{PV}(3,1) = \beta_1 u_1 + \beta_2 u_2 + \beta_3 u_3 + \beta_{12} u_1 u_2 + \beta_{13} u_1 u_3 + \beta_{23} u_2 u_3 + \alpha_{11} z_1^2 + \gamma_{11} u_1 z_1 + \gamma_{21} u_2 z_1 + \gamma_{31} u_3 z_1 + \varepsilon \tag{43}$$

Table 4-5. Estimates for the Coefficients in the Regression Model where Chamber Pressure = 1,500 psig. Level of Significance, $\alpha \leq 0.025$.

Model Term	Variable (Effect)	Estimate (β_i)	Standard Error	Model r^2
z^2	$(rpm)^2$	0.989	0.043	0.9458
u_3	Binder	3.046	0.277	0.9848
u_2	10 μm AP	-0.558	0.090	0.9913
$z \bullet u_3$	rpm – Binder interaction	-0.360	0.127	0.9965
$u_1 \bullet u_3$	90 μm AP – Binder interaction	-1.689	0.557	0.9982

Table 4-6. Estimates for the Coefficients in the Regression Model where Chamber Pressure = 1,000 psig. Level of Significance, $\alpha \leq 0.035$.

Model Term	Variable (Effect)	Estimate (β_i)	Standard Error	Model r^2
z^2	$(rpm)^2$	0.893	0.038	0.9706
u_3	Binder	2.068	0.239	0.9888
u_2	10 μm AP	-0.453	0.078	0.9944
$u_1 \bullet u_3$	90 μm AP – Binder interaction	-1.729	0.485	0.9971
$z \bullet u_1$	90 μm AP – rpm interaction	-0.052	0.020	0.9984

Table 4-7. Estimates for the Coefficients in the Regression Model where Chamber Pressure = 500 psig. Level of Significance, $\alpha \leq 0.011$.

Model Term	Variable (Effect)	Estimate (β_i)	Standard Error	Model r^2
z^2	$(rpm)^2$	0.591	0.024	0.9863
$u_1 \bullet u_3$	90 μm AP – Binder interaction	-1.729	0.485	0.9939
$u_1 \bullet u_2$	90 μm – 10 μm AP interaction	-0.052	0.020	0.9969

Across all test pressures, the quadratic term for the rpm was the dominant factor. Figure 4-8, comprising of experimental data, shows that this effect is indeed real and is nonlinear. The data were restricted to the centroid design points, i.e., conditions *F*, *G*, *H*, and *I* in Table 4-4. The compositions were identical at the centroid of the design; only the rpm was different. This is the reason that a midpoint rpm value was included in the design to check for this effect. Note in Figure 4-9 the excellent repeatability of average burning rate for the 85 rpm condition.

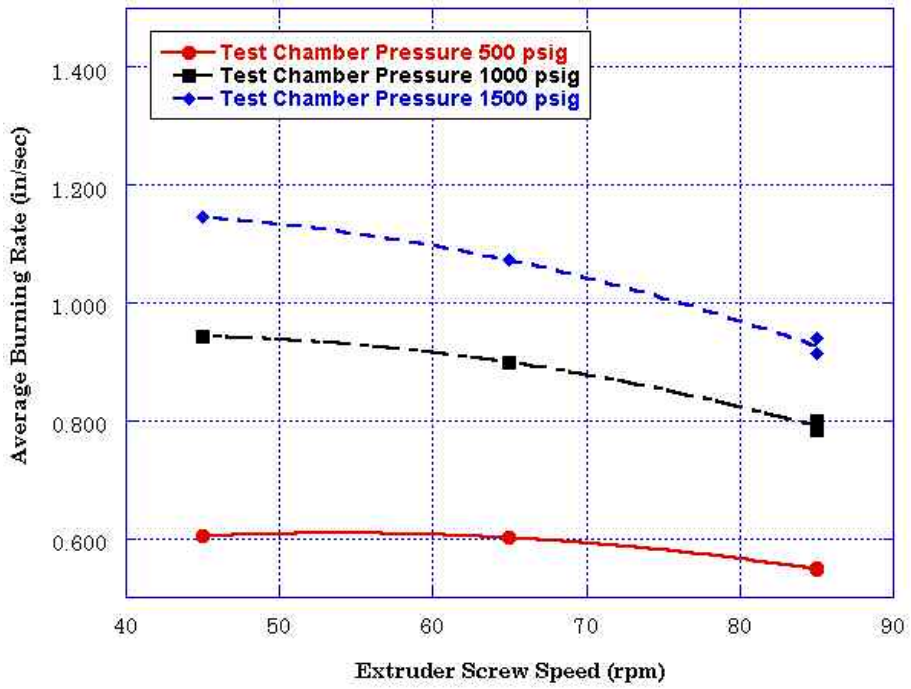

Figure 4-8. Given the same filler concentration and ratio, there was a quadratic effect of extruder screw speed on the average burning rate.

4.2.2.3 Response Surface Analysis Burning Rate Data

The corresponding models given by the parameters in Tables 4-5 through 4-7 were used to generate the response surface curves for 500, 1000 and 1500 test pressures illustrated in Figures 4-9 through 4-11. The predictions for an extruder speed of 85 rpm were of most interest because that speed was to be used to make the graded propellant. The contours indicate the predicted burning rate for that screw speed and many ingredient combinations. The plotted points are the experimental burning rates for that combination and screw speed. The comparisons for each test pressure are given in Tables 4-8 through 4-10. Considering the complex relationships between the mixture constraints and process factor, the agreement with the predicted and experimental was excellent.

Because of the way that the three-axis triplot (Figure 4-4) was translated for plotting as two-axis contour plots, only the solids fraction is readily identifiable in the Figures 4-9 to 4-11. The top line in each diagram represents 13 percent binder or the highest level of AP tested. The AP fractions were best interpreted as the ratio of coarse to fine. As one moves from left to right across the figures the coarse to fine ratio is decreasing, i. e., the relative amount of fine particles is increasing. The dotted line in the

left hand side of each figure represents a coarse to fine ratio of 79/21. At the opposite side, the ratio is 50/50 for the rightmost vertex. The ratio passing through the centroid is approximately 63/37.

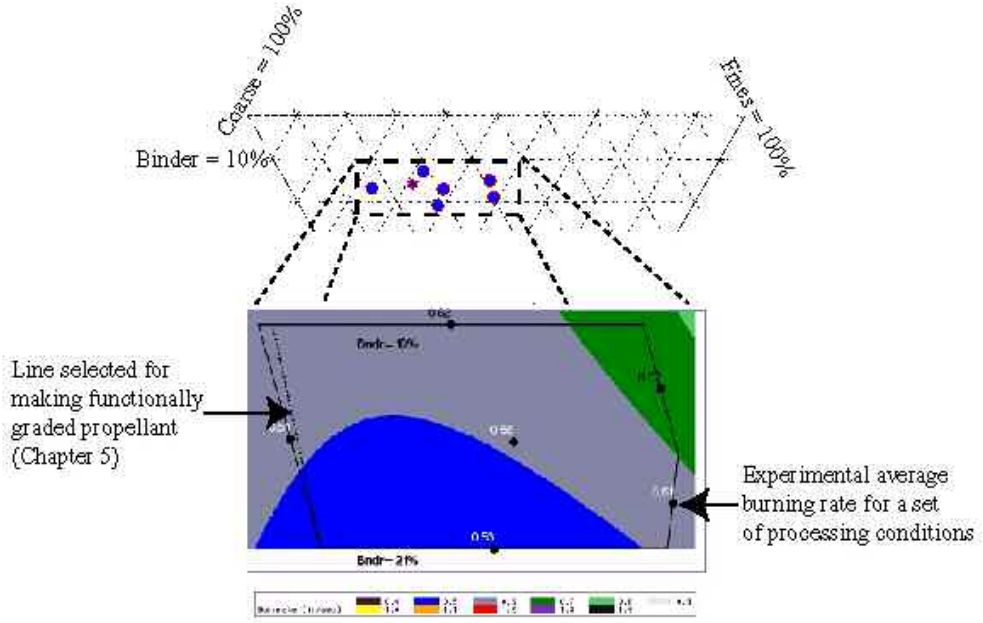

Figure 4-9. The results of the response surface analysis were plotted as a two-dimensional contour for a 500 psig condition and extruder speed of 85 rpm. The numbers are the experimental results.

Table 4-8. A comparison between the experimental data and the predicted burning rate for test pressure of 500 psig and extruder screw speed of 85 rpm. The entries in the table start at the top of the diagram and precede clockwise ending in the center.

ID	Average Experimental Burning Rate (in/sec)	Standard Deviation, *s*, (in/sec)	90% C.I. for Experimental (in/sec)	Predicted Burning Rate (in/sec)
K	0.620	0.006	±0.007	0.591
D	0.666	0.007	±0.007	0.685
B	0.609	0.002	±0.003	0.609
J	0.526	0.042	±0.041	0.489
M	0.513	0.007	±0.009	0.562
G	0.546	0.007	±0.009	0.559

As one moves from bottom to top in each diagram the solids are increasing and the predicted burning rate increases. The magnitude of course is dependent upon the test chamber pressure. The particle size ratio effect was expected as well, but it has never been experimentally determined in this way. These results clearly define the possibilities for creating a gradient within the extruder's process window as defined for this research.

Table 4-9. A comparison between the experimental data and the predicted burning rate for test pressure of 1,000 psig and extruder screw speed of 85 rpm. The entries in the table start at the top of the diagram and precede clockwise ending in the center.

ID	Average Experimental Burning Rate (in/sec)	Standard Deviation, *s*, (in/sec)	90% C.I. for Experimental (in/sec)	Predicted Burning Rate (in/sec)
K2	1.061	0.024	±0.023	1.050
D7	1.006	0.018	±0.022	0.964
B8	0.854	0.027	±0.025	0.855
J12	0.735	0.125	±0.092	0.675
M10	0.731	0.008	±0.008	0.773
G6	0.799	0.006	±0.007	0.851

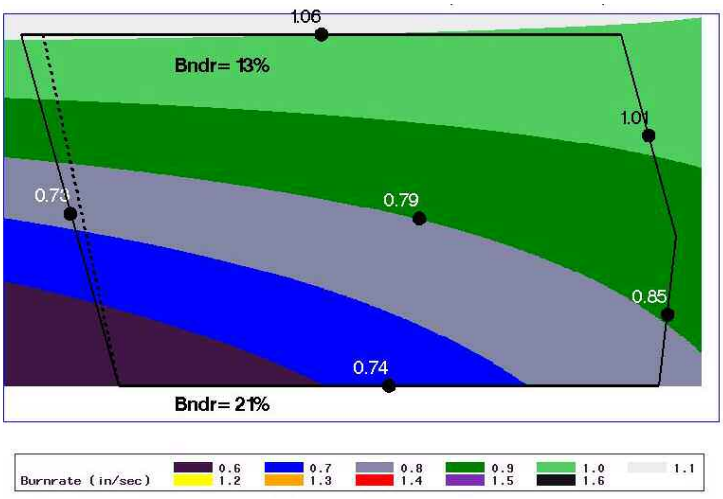

Figure 4-10. The results of the response surface analysis were plotted as a two-dimensional contour for a 1,000 psig condition and extruder speed of 85 rpm. The numbers are the experimental results.

Table 4-10. A comparison between the experimental data and the predicted burning rate for test pressure of 1,500 psig and extruder screw speed of 85 rpm. The entries in the table start at the top of the diagram and precede clockwise ending in the center.

ID	Average Experimental Burning Rate (in/sec)	Standard Deviation, *s*, (in/sec)	90% C.I. for Experimental (in/sec)	Predicted Burning Rate (in/sec)
K2	1.276	0.005	±0.006	1.245
D7	1.272	0.018	±0.017	1.184
B8	1.00	0.019	±0.016	1.019
J12	0.773	0.174	±0.166	0.763
M10	0.834	0.006	±0.007	0.864
G6	0.915	0.018	±0.021	1.003

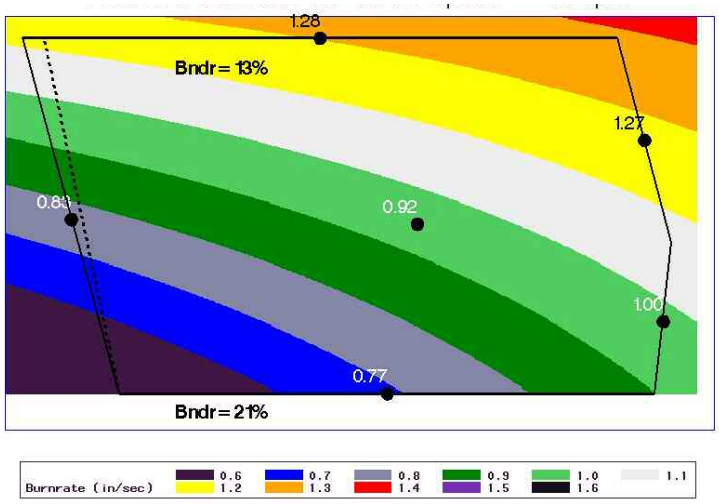

Figure 4-11. The results of the response surface analysis were plotted as a two-dimensional contour for a 1,500 psig condition and extruder speed of 85 rpm. The numbers are the experimental results.

4.3 Design of Functionally Graded Rocket Propellant

4.3.1 Selection of Gradient Architecture

The next step in the research was to prepare functionally graded propellant for characterizing in acoustic strand burning tests. (These burning rate data for graded propellant are described in a later section.) Aside from the obvious benefit of revealing

the full range of burning rates within the process and formulation constraints chosen, the response surface analysis provided invaluable insight in choosing directions in which to construct functional gradients. In that these propellants had never before been produced or tested, a strategy to select the proper gradient was followed.

The most palpable choice was to maximize the magnitude of the gradient; this would have had the benefit of being the least ambiguous to characterize. Not too surprising was the fact that the predicted extremes in burning rate lie at the vertices. Referring to Figure 4-11, the maximum burning rate was predicted at the upper right-hand vertex where the concentration of inert binder was lowest and the relative amount of fine particle AP was highest. Likewise the lowest predicted burning rate was located at the bottom left-hand vertex. At this location, the binder content was highest and the fine AP content was lowest. This strategy could have been achieved using the same process configuration used for producing the homogeneous samples—two AP solids feeders.

However there was an additional constraint added. It was necessary to be able to visually detect the onset of the gradient in an extruded grain; otherwise, there would have been no indication that the correct graded segment was chosen for characterization until the material was actually fired. That approach would have been unwise.

The introduction of a dye into the extruder at the initial time of the solids step change was a method that had been developed and tested at UMD in the gradient research using the smaller extruder. The same material and hardware that was used to conduct studies at NAVSEAIHMD could be used to mark the start of the gradient. This came at the expense of one solids feeding port thus limiting the gradient production to one AP feeder. In other words, maximum gradient production and introduction of a tracer were incompatible goals.

Therefore being limited to one solids feeder dictated a limitation to a single coarse-to-fine (C/F) ratio during the gradient manufacture. A blend AP particle sizes feeds well, and a sufficient supply of it was blended in advance and stored in a room-sized oven for preservation. The dotted line in Figures 4-9 through 4-11 indicates the direction of a constant ratio. Specifically that ratio was 79/21. This was chosen as the gradient for producing the first functionally graded rocket propellant for testing and characteriza-

tion. The gradient strategy was to use a step change in the concentration input of AP to produce a gradient response in the extrudate.

4.3.2 Prediction of Burning Rates Along Gradient

Predictions of the burning rates for the extremes of the chosen gradient and some intermediate points were made possible using the response surface empirical models. From these an estimate of the burning rate exponent could be calculated. Three models were used—one for each of the test chamber pressures. The predictive expressions are as follow using the coefficient estimates from Tables 4-5 to 4-7.

$$\dot{r}_{1500\,\text{psig}} = 0.5417u_1 + 3.5684u_3 - 1.7211u_1u_3 + 0.4462z_1^2 - 0.4972u_3z_1 \qquad r^2 = 0.9982 \qquad (44)$$

$$\dot{r}_{1000\,\text{psig}} = -0.4531u_2 + 2.0684u_3 - 1.7289u_1u_3 + 0.8930z_1^2 - 0.0521u_3z_1 \qquad r^2 = 0.9984 \qquad (45)$$

$$\dot{r}_{500\,\text{psig}} = 0.5911z_1^2 - 0.4209u_2z_1 + 0.6451u_3z_1 \qquad r^2 = 0.9969 \qquad (46)$$

These new predictions use the exact same coarse/fine ratio (79/21) and an extruder screw speed of 85 rpm. Instead of only approximating the extremes, exponents for some intermediate binder concentrations were calculated. The ingredient parameters are given in Table 4-11 along with the transformations to *u*-pseudocomponents using (40) through (42). The models were retained in the pseudocomponent form for convenience. The effective yields can be interpreted as the resultant amounts of 90 μm and 10 μm AP in the target compositions. In other words, it takes into account that the AP was fed as a blend. The resulting burning rates predicted by (44) to (46) are given in Table 4-12.

Table 4-11. The ingredient combinations used to make the gradient in extruded rocket propellant and their transform to *u*-pseudocomponents.

	Effective Yields			***u*-pseudocomponents**		
RPM	**Coarse**	**Fines**	**Binder**	u_1	u_2	u_3
85	0.624	0.166	0.210	0.246	0.754	0.000
85	0.656	0.174	0.170	0.149	0.729	0.123
85	0.672	0.179	0.150	0.100	0.716	0.184
85	0.687	0.183	0.130	0.052	0.703	0.246

Table 4-12. Predicted burning rates (inch/sec) for 85 rpm are given as a function of binder concentrations and chamber pressures.

Binder Fraction	0.21	0.19	0.17	0.15	0.13
For 1500 psig:	0.579	0.721	0.872	1.034	1.207
For 1000 psig:	0.538	0.653	0.778	0.913	1.058
For 500 psig:	0.513	0.537	0.557	0.573	0.584

The log of the predicted burning rates was plotted as a function of the log of test pressures to estimate the predicted burning rate exponents in Figure 4-12. The exponents calculated from the above predictions are given in Table 4-13 using the following relationship (ignoring the effects of temperature—a factor that was treated as a control). The relationship between burning rate and operating pressure can be modeled as a power law (47). The exponent is very significant to rocket motor designers and propellant formulators.

$$\dot{r} = AP^n \tag{47}$$

As the exponent approaches one, the sensitivity of the burning rate to pressure disturbances increases. It is possible for the burning reaction to escalate to a deflagration resulting in a catastrophic failure of the rocket motor. Typically more pressures are tested to get a better estimate of the exponent. In this case, the minimum number of test pressures, three, was requested due to resource constraints.

Table 4-13. The exponents in the table were estimated using burning rates predicted by the response surface models.

Binder	*A*	*n*
0.21	-2.06	0.107
0.17	-1.37	0.416
0.13	-0.578	0.682

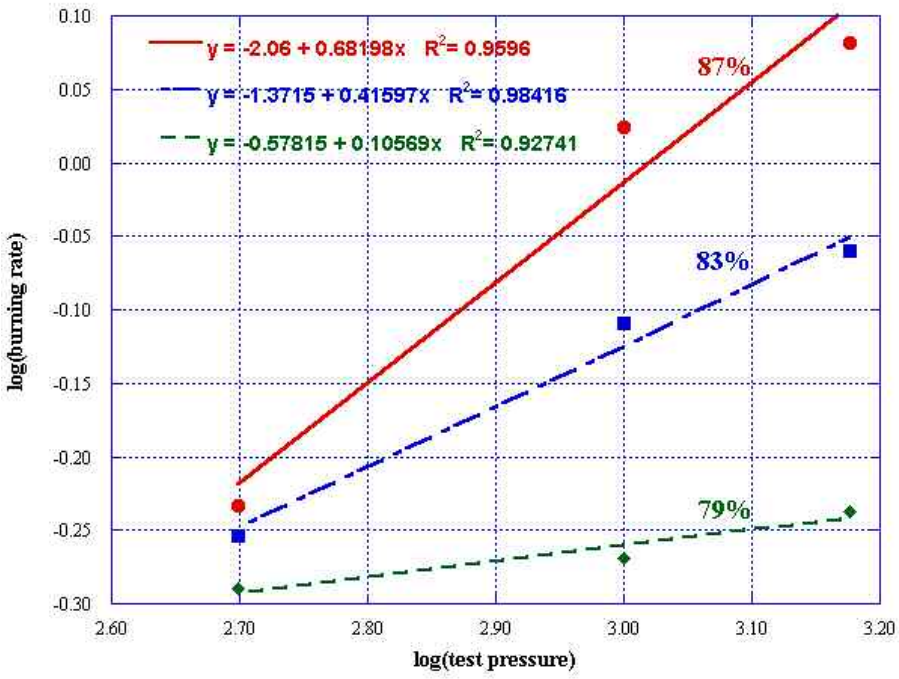

Figure 4-12. The log of the burning rates predicted by the response surface models were plotted as a function of the log of test pressures to estimate the burning rate estimates given by the linear slopes.

Some confidence can be given to these predictions. An extra test point was included in the homogeneous burning rate series (point *P* in Tables 4-2 to 4-4) to check the fit of the response surface model. It was intended to represent the nominal formulation for IH-AC3. However an error in translating the intended mixture setpoints to feed rates resulted in a unique combination of AP far from the nominal. In spite of the error, the point still served as a check of the response.

The measured experimental burning rates for the model checkpoint were compared with the variance from the lack of fit test to validate the response surface model (Beauregard, Mikulak et al. 1992) in Table 4-14. For each pressure the fit test indicated a high level of significance in the predictive model (much better than $\alpha = 0.1$). It can be argued that this significance only applies to the region in the vicinity of point *P*. In a circumstance of good fortune, the error in translating the feed rates resulted in placing the new point along the line that was chosen for the gradient. So the models do a good job of predicting the burning rate behavior in that region of the design space.

Table 4-14. A lack of fit test of the variance indicated that the model is highly significant in predicting burning rates in the vicinity of point *P*.

Test Pressure	Predicted (in/sec)	Measured (in/sec)
1500 psig:	0.953	0.975
1000 psig:	0.845	0.802
500 psig:	0.566	0.536

A rigorous check of the response surface should involve more than one point strategically placed in centroids of subsets of the design region. The combination and loading of AP in the nominal formulation was close to one of these extra points. More is always better in conducting experiments of any nature, but this is especially true in statistical analysis. However, it was very important to keep the total of experiment combinations to a minimum, so more test points were not included.

Later in the research during the functionally graded strands test series, strands made at the terminal homogeneous compositions were tested in the acoustic strand burner, 79 and 87 percent by weight with a coarse/fine ratio of 79/21. The data are presented in Table 4-15. Note that these test pressures are different than those used to model the response surface; however, an accurate prediction for the two homogeneous compositions were easily made by the following.

The burning rates predicted from the three models for the pressures of 1,500, 1,000 and 500 psi were fit to equation (48) compared with the experimental results in Table 4-15. The linear least squares of the log transformation were conducted.

$$\log_{10} \dot{r} = \log_{10} A + n \log_{10} P \tag{48}$$

The burning rate exponent, *n*, and coefficient, *A*, were easily determined, and the following equations were used to predict the burning rate response for the pressures tested using the acoustic strand burner. The values used in (49) and (50) were given in Table 4-13.

$$\text{For } 79\%: \ \dot{r} = 0.264 P^{0.106} \tag{49}$$

$$\text{For } 87\%: \ \dot{r} = 0.00872 P^{0.682} \tag{50}$$

These equations based on the response surface models predicted the experimental results quite accurately with only one exception.

Table 4-15. The experimental burning rates were measured using the acoustic strand burner of the two homogeneous compositions representing the homogeneous beginning and ending conditions of the functional gradient. The predicted rates are presented for each composition and pressure.

Test Pressure:	**400 psi**		**800 psi**		**1,200 psi**	
Wt. Percent AP	**Measured (in/sec)**	***Predicted (in/sec)***	**Measured (in/sec))**	***Predicted (in/sec)***	**Measured (in/sec)**	***Predicted (in/sec)***
87.00	0.688	***0.519***	0.865	***0.833***	1.074	***1.098***
87.00 (replicate)	NA		0.889		1.014	
79.00	0.463	***0.498***	0.518	***0.536***	0.602	***0.559***
79.00 (replicate)	0.453		0.583		0.622	

Another concern with producing a large gradient in the solids loading between fractions of 0.79 and 0.87 by weight was the relatively high burning rate exponent of the higher loaded composition—a predicted exponent of 0.68. A high exponent can amplify chamber pressure fluctuations into an upward cycle that can lead to catastrophic failure of the test motor. An upward pressure fluctuation increases the burning rate according to the exponent, the higher burning rate results in a higher pressure.

5.0 Characterizing the Evolution of Gradient Architectures in Response to Step Inputs

This project is concerned with the transient state for operating the extruder in order to understand how the response of the process can be used to control the evolution of gradient architectures. In this sense, a change in ingredient feeding is an intentional disturbance, and the flow through the various zones in the extruder is unbalanced. There has not been much research in quantifying and predicting the transient nature of the degree of fill/mass flow. An as yet unpublished work by Mudalamane & Bigio (Mudalamane 2002) at UMD has investigated applying the principles of conservation of mass to individual sections in the process and iteratively solving for a solution. The results of that research investigation can be used to provide first-order principles for modeling the effects of operating conditions investigated in this research effort, explaining the measured shape function factors and possible effects of transience on the response of the extruder. However, for this research, the steady state RTD and RVD process models were sufficient to predict the evolution of the gradient architecture.

The step response experiments were conducted at both UMD and NAVSEAIHMD using inert and energetic material respectively. In either case, a steady state process was disturbed by a step change (positive or negative) in the feeding rate of the filler. In both machines the response of the material transport was measured at the entrance to the die using fiber optic probe sensors. In the UMD experiments a black colored concentrate was added concurrently with the KCl at the time that the step change was initiated. At NAVSEAIHMD, a one-time pulse of dye marked the beginning of the gradient. Furthermore the probe used at NAVSEAIHMD was sensitive enough to detect the shift in propellant color due to the change in solids loading without doping with a dye.

Conducting various material property measurements on samples of the extrudate allowed further measurements of the responses. The techniques were different depending upon inert of energetic and efficacy of the test. Initially there was an

emphasis on nondestructive techniques such as Shore hardness and deformation due to ball indentation. As these methods proved to be insensitive or prone to scatter, destructive testing methods were employed with better success ranging from density and burning to cutting resistance and optical analysis of serially sectioned extrudate.

5.1 Inert Composite at UMD

5.1.1 Sample Quality Strategy

The development of a viable process to produce the KCl-filled inert composite using the ZDSK-28 twin-screw extruder was focused on finding a range of solids fill that would allow viable sampling over a range of conditions and die geometries. Experimentation with measurements and sample collection methods was being conducted concurrently. Sample collection alone was challenging because the composite had to be processed at a high temperature to minimize accumulation in the KCl feed port that in turn necessitated a higher degree of fill to increase the stiffness of the extrudate such that it maintained some physical integrity. Yet the minimum fill level had to be low enough to allow a reasonable jump for the ingredient step experiments. A step input of 40 to 60 percent solids by weight and vice versa was quickly determined as a reasonable parameter.

A *low budget* conveyor was built and refined over a period of weeks that would allow the collection of long strands of extrudate and yet minimizing kinking and stretching of the strand. The result was the establishment of a viable process window (throughput, filler concentration, temperature zone set-points, and screw rpm), tracer addition methods, and a suitable collection technique.

The selection of die geometry was progressive during this process, and the geometry needs were dictated by the optimization exercises and material characterization needs and results. The first choice was the round geometry. With a diameter of 12.4 mm, it had the largest diameter possible given the design of the adapter. It offered the largest cross-sectional area; and therefore, the least die pressure, the most simple die flow, and the slowest linear extrusion rate. However it was prone to losing its round geometry by *slumping* before cooling sufficiently that resulted in a non-uniform surface and cross-sectional shape as seen at far right in Figure 15. Upon collection the strand would deform to a broad oval shape with a flattened bottom. Also

the quality of the collected strands suffered due to that fact that it was used with the earliest incarnation of the conveyor.

Figure 5-1. These are representatives of the best samples collected using the slit, square, and round-shaped dies.

Table 5-1. Die geometries and cross-sectional areas fabricated to use with UMD's TSE.

Die Shape	Dimensions	Cross-Sectional Area
Round	12.4 mm	153.8 mm^2
Slit	10.9 x 4.1 mm	44.7 mm^2
Square	8.4 mm	70.6 mm^2

Initially it was thought that a more flat and thin geometry would be easier to characterize physical properties using methods such as Shore A hardness, the round die was dropped in favor of the rectangular or *slit* die. Given a height of 4.1 mm, the 10.9 mm width of the slit was the maximum allowed by the design of the adapter. The slit die did have some of the same problems such as stretching and kinking as the round die; however, this was reduced as improvements to the conveyor were made. Furthermore, it had a higher linear velocity resulting in a strand with a much greater length compared to the round shape for the same volume extended. The bottom of the extrudate was relatively flat due to the conveyor collection method, and the top had a convex surface as seen in Figure 5-1 far left. The most serious detriment to using the slit die was the resulting complex three-dimensional die effects introduced into the evolving gradient. The complex flow field was attributed to die entrance effects resulting from the compromised design of that die. (There were machining demands in the original design that could not be met within the dimensional constraints.)

The slit die was in turn dropped in favor of the 8.4 mm square die that had a higher cross-sectional area than the slit die. Because of the low aspect of the geometry, the EDM constraints did not compromise its design. Also it was used with the latest incarnation of conveyor design. The two combined to yield a high quality strand that did still have some necking problems if the operators were not completely steady in their collection. However it had the most consistent surface quality compared to the other two dies, and most importantly there were no three-dimensional die flow effects.

It was expected that any die would have some measurable effect of material distribution within the evolving gradient structure due to shear-induced flow. This was seen with each die in that the gradient would first appear in the center of the extrudate and spread outward as a function of time until the transition was complete—a two dimensional gradient. The idea gradient would be one-dimensional. The slit die resulted in three-dimensional effects that likely contributed to difficulties in characterizing the physical properties of the graded slit-shaped specimens.

The focus of the characterization methods gradually progressed from non-destructive (NDE) to destructive methods. These are described below and in a subsequent chapter. It was desirable to have one or more NDE methods to fully characterize the development of the graded microstructure in an extruded material. Attempts were made with Shore A hardness and ball indentation methods without any conclusive and quantitative results. The methods of characterization progressed to techniques that required serially sectioning the strand. These were a force of cutting determination, grayscale image analysis of thin cross-sections, density measurements of short length (1-2 cm) sections, and microscopic analysis using scanning electron microscopy and energy dispersive x-ray (EDX or EDS) spectroscopy. A completely destructive test of pyrolosis was performed on selected sections to quantitatively determine the content of solids that proved to correlate well with the density.

5.1.2 Experimental Conditions and Responses for the Step Experiments

The graded strands of the KCl composite were produced by positive and negative step inputs of solids fill from 40 to 60 percent by weight and vice versa. Smaller steps of 50 to 60 percent filler were collected as well. Two screw designs using two dies were

evaluated though not independently. The screw designs were designated #0722 and #0814 as given in Figure 3-10.

The step changes were affected by the KCl feeding rate alone. Recall that the twin-screw compounding operating had two stages—polymer addition and melting in the first stage and solids addition and mixing in the second stage. The twin-screw extrusion operation for IH-AC3 propellant was a two-stage system; therefore, it was intended to reproduce the process similarity for the UMD studies.

If a polymer feed rate change were to be made upstream of the KCl addition, the mean residence time of the upstream section would have to be taken into account. Furthermore the measured response to any solids step change would be inextricably coupled with the polymer change. To keep the research at a fundamental level of understanding, the step change was studied uncoupled from any changes in the polymer transport. In other words, the polymer feeding rates were not changed during the measurements.

Simultaneous with the KCl step change, a step change in tracer was initiated. The tracer was Reed Omnicolor black color concentrate which was added at rate of one pellet every 4 seconds for at least three minutes and often much longer. The tracer was added to the top of the KCl feed chute. It represented a visible leading front of the gradient and was useful to determine when the gradient was approximately completely developed in the collected strands.

At the same time at the KCl feeding rate change and the initiation of the tracer, an operator would cut the extrudate stream at the die and begin collecting the long strand of extrudate. The reason the strand was cut at that time is to give a point of reference on the collected strand as to when the change was made. In other words, it was a ready reference for t_0 on the collected strand. At the end of sample collection, the strand was cut and the tracer addition was halted. The KCl was maintained at its current rate. As the tracer was flushed from the processing section, it more than allowed enough time for the process to reach a steady state at the new KCl feeding rate. The next step change was not initiated until the color of the extrudate had returned to a brilliant white.

5.1.3 Characterization of Gradient Architecture Evolution of the Inert Composite

Two of the research objectives were:

1. How to characterize the gradient produced by disturbances to the twin-screw extrusion process?

2. Can the description of the gradient be related to some process characteristic?

A variety of methods were employed to ascertain the nature of the gradient induced by the step input. On-line real time measurements were made as well as off-line characterization techniques were investigated. The first objective was to determine a non-destructive method. On-line analysis of color using a light reflectance measurement was one technique that proved successful. Other non-destructive evaluation (NDE) methods were Shore A hardness and force measurements by a ball indenter. These methods were not sensitive enough to detect the change in solids content in the POE.

A number of off-line destructive techniques were employed to quantify the microstructure of the gradient. Several employed microscopic analysis to characterize the morphology of the filler, SEM, EDX, and optical for example, and image analysis techniques to quantify the development of the gradient. Samples were taken to NAVSEAIHMD for density analysis using a helium pycnometer. Two other techniques were force measurements during razor sectioning and gravimetric ash residue. These are discussed in the following.

5.1.3.1 Gradient Characterization by On-line Light Probe

The on-line response of the extruder's processing section to a step input was measured using the same instrumentation as for the residence time. The technique for delivering the tracer was described in the preceding section. Measurements were taken for both gradient directions—positive (solids increasing) and negative (solids decreasing) directions. The filtered, but otherwise untreated, data are plotted in Figures 5-2 and 5-3. Note that as a matter of convention, the signal response data is plotted such that the final state is always *high*. This is consistent with the step input; the step is always from low to high regardless of actual solids concentration. (The convention does not carry over to the physical characterization measurements presented later in the chapter however.)

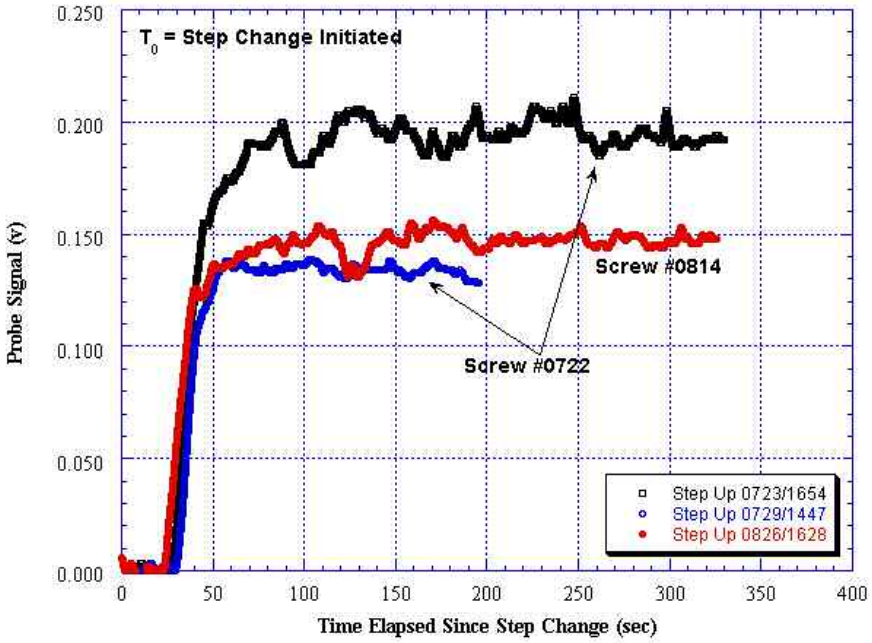

Figure 5-2. The filtered, but otherwise untreated, online reflected light probe response to a step input of solids filler is shown for a positive step change in the concentration of KCl. The delay time, t_d, was dependent upon screw geometry. The differences in signal magnitude represent a day effect in instrument sensitivity.

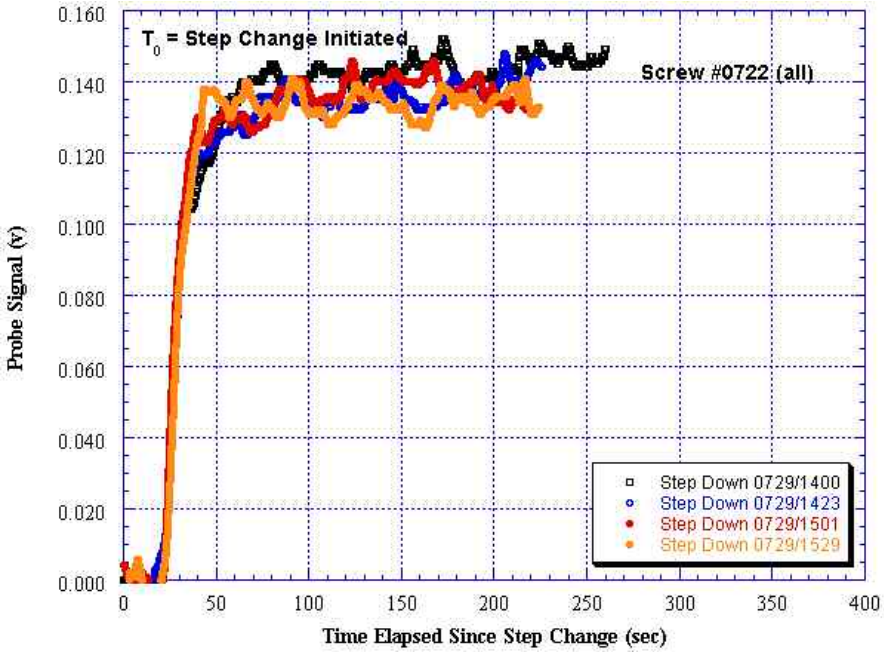

Figure 5-3. The filtered, but otherwise untreated, online response to a step input of solids filler is plotted for a positive change of 40 to 60 percent by weight KCl. The response was consistent and repeatable for a given screw design (#722).

The signals were scaled such that the average maximum of $F(t)$ = 1 and fitted to various convolution functions of different order. The first order was the best fit (Figure 5-4a) for one sample, but the second order was the best fit (Figure 5-4b) for another sample run on a different day. The fit quality was determined by the values for mean of residuals squared (RMS) as given in Table 5-2. This suggests that one function can be used to approximate the other and that the order of the system is most likely between first and second order.

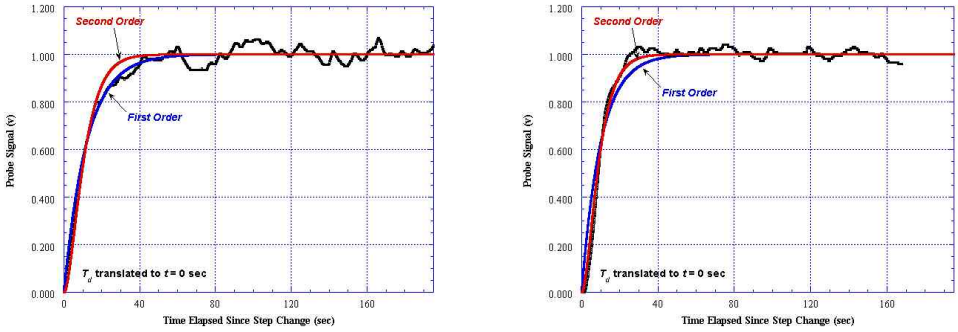

(a) (b)

Figure 5-4. Step changes were scaled so that the average maximum signal was equal to one, and the signals were then fitted with first and second order convoluted functions.

Recall that the RTD and RVD responses were fit to models of one and multiple ideal mixers in series with a delay time (Tables 3-1 and 3-3 respectively). The issue was to determine if the shape factors of the RTD or RVD can be related to the response of the on -line light intensity sensor as the gradients evolved. The shape factor for a second order fit of (14) to a normalized RTD was evaluated as a prediction term for the gradient evolution response at the diehead (where the light sensor was located). The experimental data for the UMD TSE were mixed for reasons due to how the tracer was introduced and the accumulation of material in the KCl feed port. There was a difference between filled and unfilled POE. For example, the step response for conditions of 180 rpm screw speed, 3.60 lb/hr total throughput of unfilled polymer, such as test 0723/1547 from Table 3-1.

Table 5-2. Shape factors for first and second order models fits to responses in on-line color analysis for step changes in KCl feeding rate.

Step Direction	Screw Design	Sample ID	System Order	Shape Factor, a_t	95% C.I. for Shape Factor	Sum Squares Residuals
Positive	#722	1654	first	0.0829	±0.0002	0.0011
"	"	"	second	0.1777	0.0005	0.0018
"	"	1447	first	0.0991	0.0004	0.0022
"	"	"	second	0.2027	not available	0.0005
"	#826	1628	first	0.0823	0.0002	0.0013
"	"	"	second	0.1776	0.0004	0.0014
Negative	#729	1400	first	0.0837	0.0002	0.0008
"	"	"	second	0.1847	0.0005	0.0017
"	"	1501	first	0.1132	0.0004	0.0012
"	"	"	second	0.2442	0.0006	0.0015
"	"	1529	first	0.1059	0.0007	0.0014
"	"	"	second	0.2168	0.0004	0.0007
"	"	1423	first	0.0922	0.0003	0.0013
"	"	"	second	0.2035	0.0005	0.0015

In the unfilled case, the step response due to a change in filler concentration was simulated by a step change in color introduced at the second open feed port (where KCl was fed for filled conditions). Characterization of extruded graded strands show that the dispersed color concentrate was transported at the same rate as particles of KCl in the ZDSK-28 and AP in the ZSK-40 extruders. Data supporting that conclusion are presented later in this chapter. The method of effecting the step was to begin feeding pellets of Reed Omnicolor black concentrate at a rate of one pellet every four seconds. The filtered response of the light intensity sensor is shown in Figure 5-5 along with an RTD measurement at the same conditions.

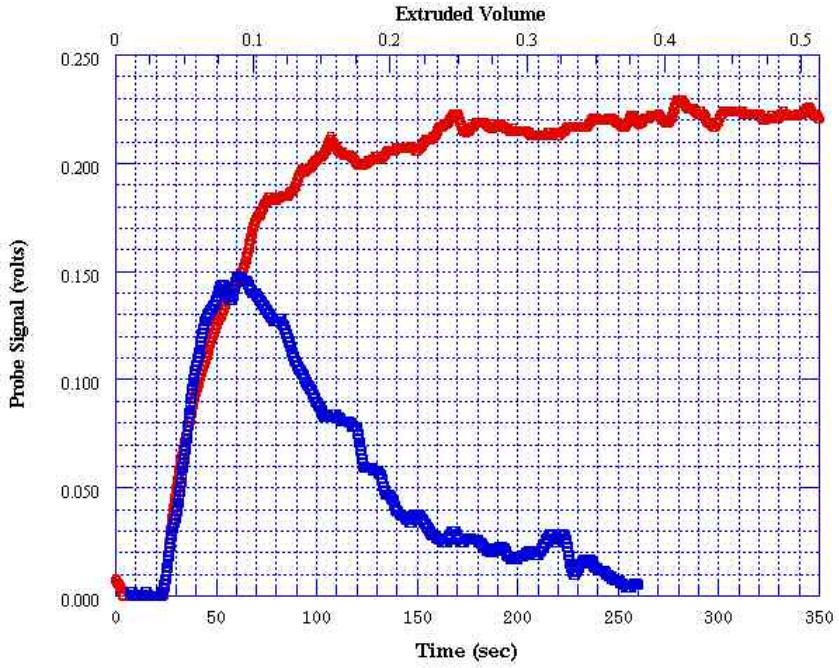

Figure 5-5. The responses for a step and impulse input of tracer are shown for processing conditions of 3.60 lb/hr POE (no filler), 180 rpm screw speed, and screw design #0723.

The step response data were scaled such that they ranged from 0 to 1, and the RTD data were scaled such that the mean residence time, t_m = 75.3 sec, coincided with 0.5 on the ordinate. The mean residence time (for a second order RTD) was calculated using,

$$t_{mean}(t) = \int_{t_d}^{t_{end}} a_t^2 \left(t - t_d\right) e^{-a_t\left(t-t_d\right)} t \, dt \qquad (51)$$

The scaled data were plotted as shown in Figure 5-6 along with predictions for the gradient response using the convolution functions for a first order mixer with a delay time. (The second order convolution model was not appropriate for any shape factor.) The simple convolution function for this type of system, Table 2-1, was given by,

$$F(t) = 1 - e^{-a_t\left(t-t_d\right)} \qquad (52)$$

The values for the parameters were based on the RTD for these conditions. The RTD parameters, Table 3-1, were used instead of the RVD because the step response was measured in the time domain. Unsubstantiated assumptions regarding the instantaneous flow rate would be necessary for the step response to be translated to the volume domain. However with instrumentation to determine flow rate at the die (or elsewhere internal to the extruder); the more general and preferential treatment of the on-line

probe data in the volume domain could be performed. This approach will be pursued in future studies.

RTD for 0% KCl and 3.60 lb/hr
Best First Order Nonlinear Fit:

$$f(t) = 0.00910\, e^{-0.00910(t-20.756)}$$

Best Second Order Nonlinear Fit:

$$f(t) = 0.0265^2 (t - 20.756)\, e^{-0.0265(t-20.756)}$$

Predictive Convolutions of *f(t)* to
Predict First Order Step Response
Poorly Predicts Step Input Response

$$\boxed{F(t) = 1 - e^{0.00910(20.756-t)}}$$

Accurately Predicts Step Input Response

$$\boxed{F(t) = 1 - e^{0.0265(20.756-t)}}$$

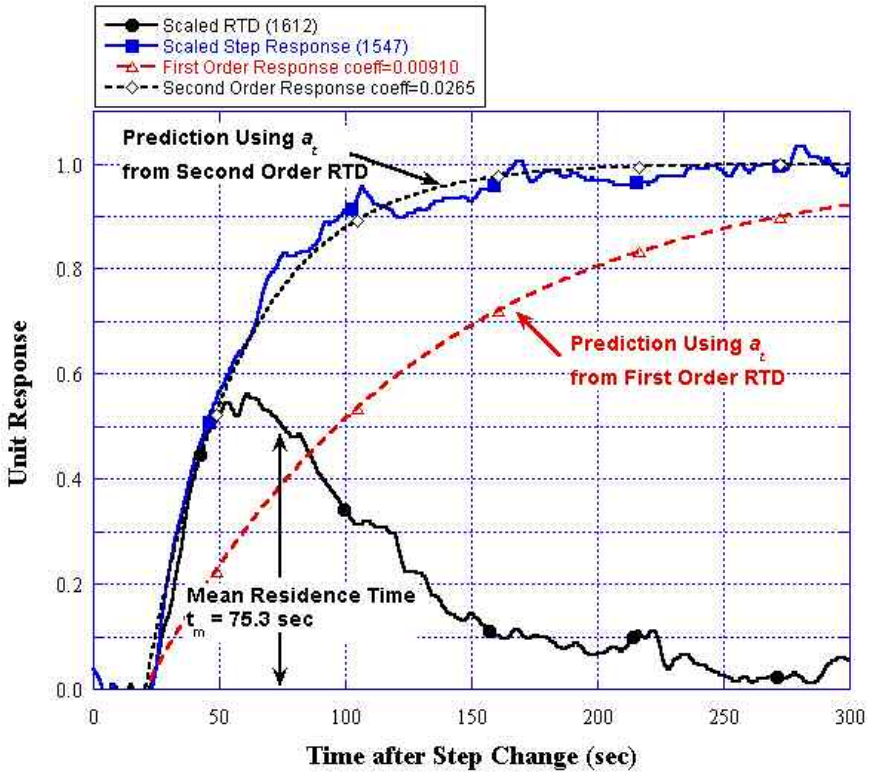

Figure 5-6. The optical probe data from Figure 5-5 were scaled for the unit response to impulse (RTD) and step inputs of tracer. The shape factor, a_t, from the first and second order RTD models were compared in their efficacy for predicting the first order step response at the same set of processing conditions.

A similar treatment of the response with the KCl-filled inert composite was not as fruitful for a number of possible reasons. The scaled data for an impulse and step response are plotted in Figure 5-7 with predictions for the step response. There were two apparent anomalies that were inconsistent with the unfilled case. The first was the longer delay in the light intensity probe response: t_d for the RTD was 17.180, and t_d times for the positive step responses were 28.564 sec and 26.828 sec (data not shown in

Figure 5-7). Experimental error was unlikely because the response was approximately repeatable according to data from an experiment conducted on another day. Note also that the t_d (21.508 and 20.776 sec) for the negative step response was closer to the experimental RTD with only a slight delay.

One explanation is that there was a rheological effect at the site of the probe tip. The tip was slightly recessed in the barrel nip creating at small pocket. At steady state conditions the refresh rates for material transport at the probe tip were very high and reproducible. A step disturbance in solids loading certainly affected the rheological properties, and the probe response data indicate that the recovery was dependent upon gradient direction. For a positive step the more viscous material (60 percent filler) was less efficient in clearing the less viscous material (40 percent) than the case for a negative step. The less viscous material in the *nip pocket* acted similarly to a slip layer, so the rate of removal was small. Once enough material had been exchanged, the gradient evolution was well developed. The probe was then exposed to a process stream in which the color change was advanced. This was evident in the rapid response rate shown in Figure 5-7.

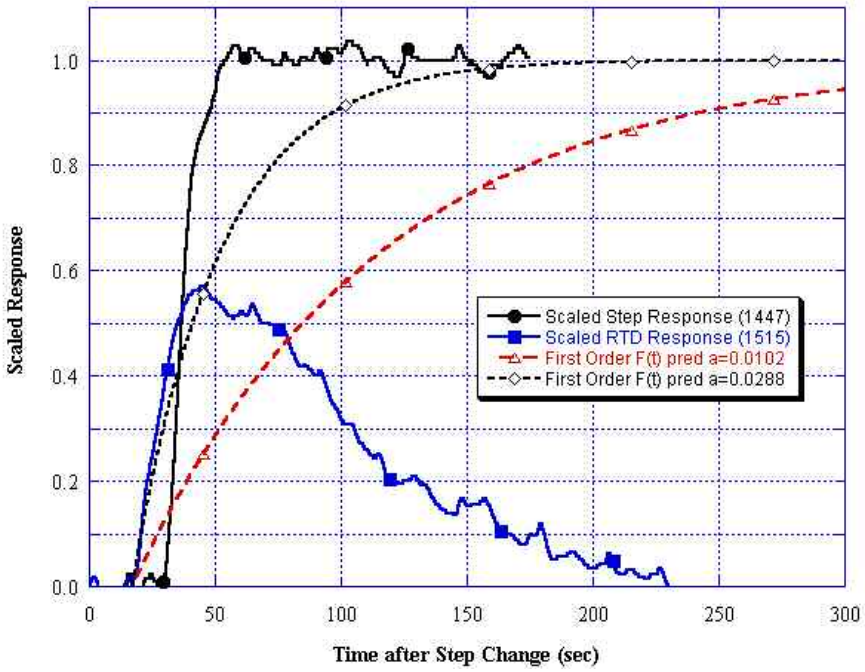

Figure 5-7. Experimental responses for the impulse addition (RTD) and step inputs were scaled and plotted for the case of KCl-filled thermoplastic elastomer. Shape factors for the first and second order RTD models poorly predicted the step response for the same set of processing conditions.

5.1.3.2 Shore A Hardness Measurements

The hardness of a polymer matrix composite is a function of many factors, such as, polymer composition and degree of crosslinking, filler type and concentration, size distribution of the polymer, temperature, etc. The method for determining the surface hardness is empirically measured by the resistance of the surface to a penetrating spindle using a durometer (ASTM 2002). The Shore Instrument and Manufacturing Company makes the most common durometers. Their devices are referred to as a Shore A or Shore D durometer for soft or relatively firm materials respectively. The hardness is attributed to a complex combination of physical effects and is thus considered an empirical measurement only. However it is useful to track the progress of the crosslinking reaction for thermoset polymer matrix composites. It was hypothesized that the hardness of the KCl-filled composite would vary as a function of filler content.

In addition to the composite properties, there are many other factors that influence the Shore A measurement. The sophistication of the durometer is important, e.g., damped release, electronic vs. mechanical gauge, surface characteristics of the sample, time of reading after penetration, etc.(ASTM 2002). Under the best of conditions, the readings are generally given as ± 5 according to the ASTM. Surface condition was a strong negative factor in this study.

For this project, the efficacy of the Shore A instrument was studied to determine its sensitivity to two-dimensional changes in filler concentration for the graded extruded strands. Two types were used. The first was manually operated with no damper and was obtained on loan from NAVSEAIHMD. It was no surprise that operator dependence strongly influenced the data especially the maximum reading. Furthermore, the mechanical gauge incorporated a second needle that would remain at the maximum reading; this feature had a tendency to retard the readings was well. It is the nature of elastomeric composites to relax after penetration, so a fixed arbitrary time was allowed before taking the second reading—thirty seconds in this case. Regardless of operator, the data from the manual device were highly variable and no objective trend was observed along the length of a graded sample.

A second device was obtained from within the Mechanical Engineering Department at UMD. It was more modern than the manual device and featured an

automated descent and penetration measurement with an electronic display. Samples from a strand of graded composite were measured for surface hardness using a. The samples represented the best surface collected to date in terms of flatness and geometrical consistency, although there were instances of slight and severe kinking of the strand during collection. Measurements were taken from the top of the strand, characterized by a convex cross-sectional shape, and the bottom which had a flatter cross-section shown in Figure 5-8. Samples were chosen from the *beginning* of the strand with the higher KCl content of 60 percent by weight, the *end* with the lower concentration of 40 percent by weight, and many locations in the graded transition region.

(a) (b)

Figure 5-8. Cross-sections of KCl-filled strands extruded through square (a) and slit (b) dies illustrating the flatness of the surfaces. Both samples were saturated with black-colored tracer.

The results are presented graphically in Figures 5-9 and 5-10; only the rectangular shaped sample was hardness tested. In Figure 5-9, the hardness was tested at three locations each along the top and bottom external surfaces. Note that there is little or no apparent difference between the two filler concentrations. To eliminate the possibility that external surface imperfections were negatively influencing the accuracy of the results, further testing was conducted on strand cross-sections where the gradient was present. The results, plotted in Figure 5-10, show that the surface was having a adverse effect, but the hardness was not strongly influenced by the filler content over the range studied. Further statistical testing, such as Scheffe's means testing (Hicks 1993) could be used to quantify or disqualify the data, but the insensitivity of the test seems to be graphically apparent.

5.1.3.3 Color Analysis of the Gradient Evolution in Extruded Strands

The extruded strands were labeled and sectioned into 5 cm segments as in Figure 5-11. The die effects on material flow were quite apparent. While a one-dimensional gradient was expected in theory, the manifested gradient in the thin strands was more complex. The white material is the initial composition—60 percent KCl by weight. The dark material is the second phase—40 percent KCl. These effects were attributed to variations in the fluid velocity field within the eight-to-round transition piece and the die entrance especially. This was one of the reasons for abandoning the slit die in favor of the square die. A second strand made with the square die was subject to this method of analysis. Cross-sections of this strand are shown in Figure 5-12.

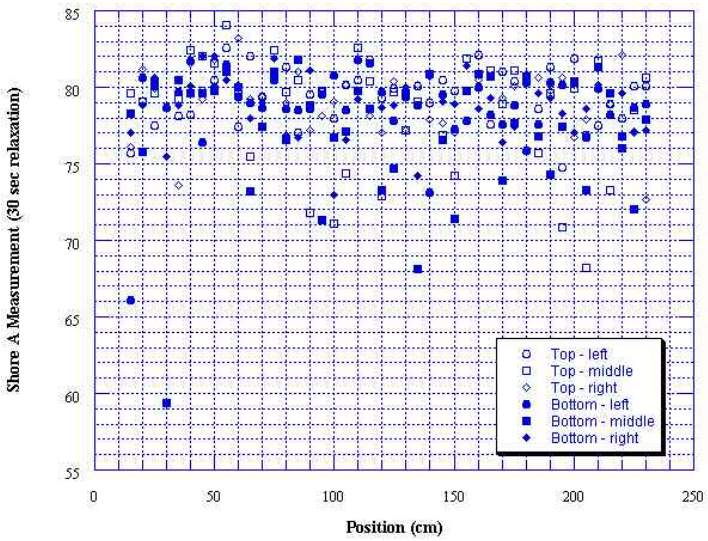

Figure 5-9. Shore A measurements after a 30 second relaxation period for graded strand using automated instrument on top and bottom surfaces of extruded strand.

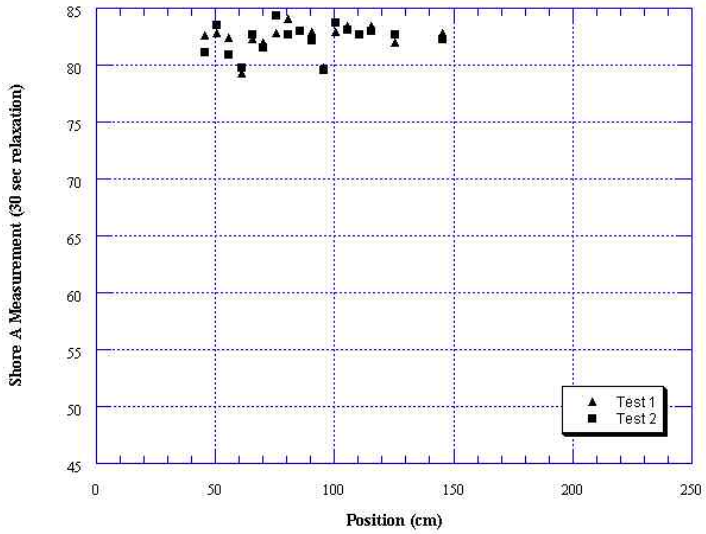

Figure 5-10. Shore A measurements after a 30 second relaxation period measured on strand cross-sections. High KCl concentration is on the left hand side and low concentration is on the right hand side of the plot.

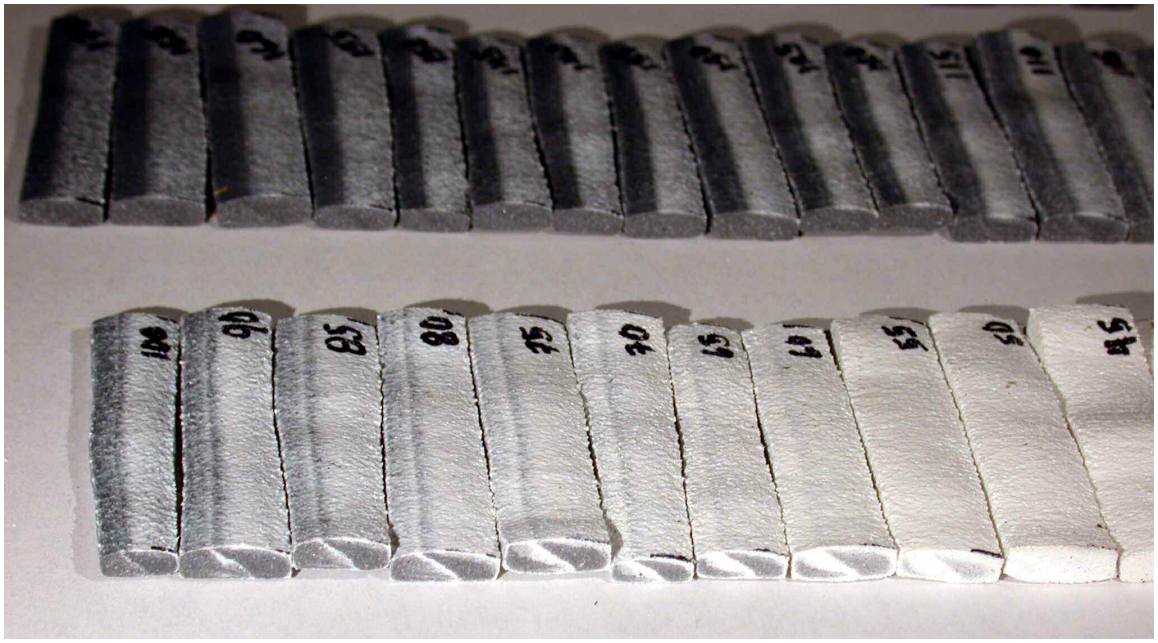

Figure 5-11. These sequentially dissected samples from an extruded strand representing the internal onset of the step change (set #1501) from an initial high concentration of KCl (white) to a lower concentration (dark).

Figure 5-12. A strand extruded through a square die was dissected in the same manner as Figure 5-11. The strand was formed by a step change (set #1628) from an initial low concentration of KCl (white) to a higher concentration (dark).

A cross-sectional slice of approximately 2 mm thickness was taken from a free end of each segment, and characterized by image analysis at a magnification of 10x. Two typical cross sections are shown in Figure 5-13. Using Adobe PhotoShop software, each a rectangular selection box was drawn to maximize the internal area of each sample. A histogram of grayscale values for all the thousands of pixels within that selection area was computed. There was no significant difference in the mean and median values, so only the mean values were recorded and plotted as a function of location in Figure 5-14 for the case of negative gradient and Figure 5-15 for the positive gradient example.

As shown in the Figures, the RVD was a good predictor of gradient onset in the extruded strand. Note that it was more difficult to maintain dimensional integrity for the rectangular strand introducing more error in the volumetric estimation. Also note that once the gradient is apparent, the volumetric flow rate is also changing thus rendering the volumetric estimate less and less accurate as distance increases.

(a) (b)

Figure 5-13. Cross-Section of Graded Strand at 10x Magnification for Gray Scale Analysis. (a) Sample at 50.3 cm Near Beginning of Gradient. (b) Sample at 110.2 cm Showing Full Development.

5.1.3.4 Density of the KCl/Engage Composite

Samples of approximately 1 cm in length from the same extruded strands were taken to NAVSEAIHMD and were subjected to density analysis using a helium pycnometer. Only a limited number of strands were submitted due to the labor costs of the analysis. However density proved to be a reliable measure of the filler content and overall was a revealing and important property for gradient characterization. The test method consisted of one measurement per sample. Higher accuracy could have been achieved with measurements in triplicate but at higher costs also. The precision of the results was reported to four decimal places. Without multiple measurements, the accuracy can only be roughly estimated. In practice the density is reported to two decimal places.

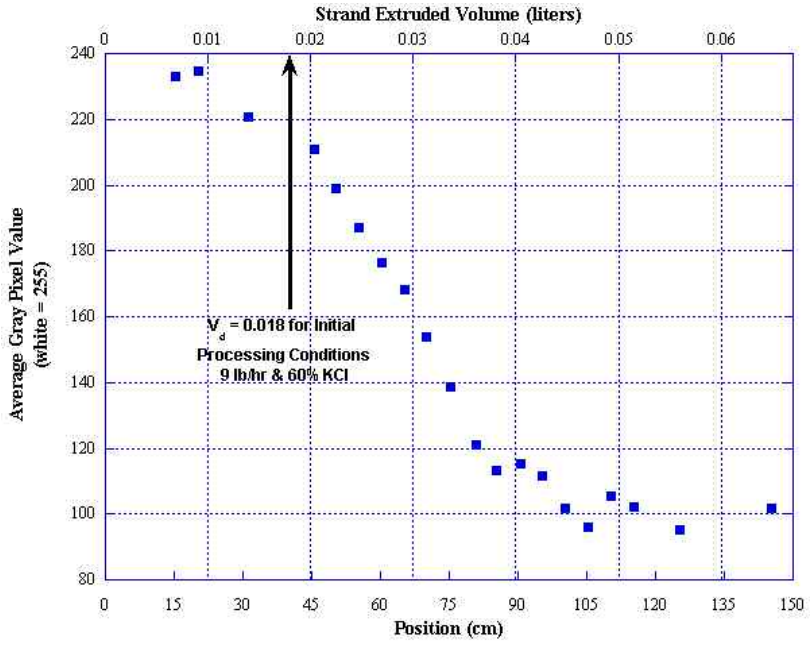

Figure 5-14. The average grayscale values for the internal surface of cross-sections in sample #1501 were plotted as a function of position and volume. Volumes greater than V_d on the abcissa are not accurate.

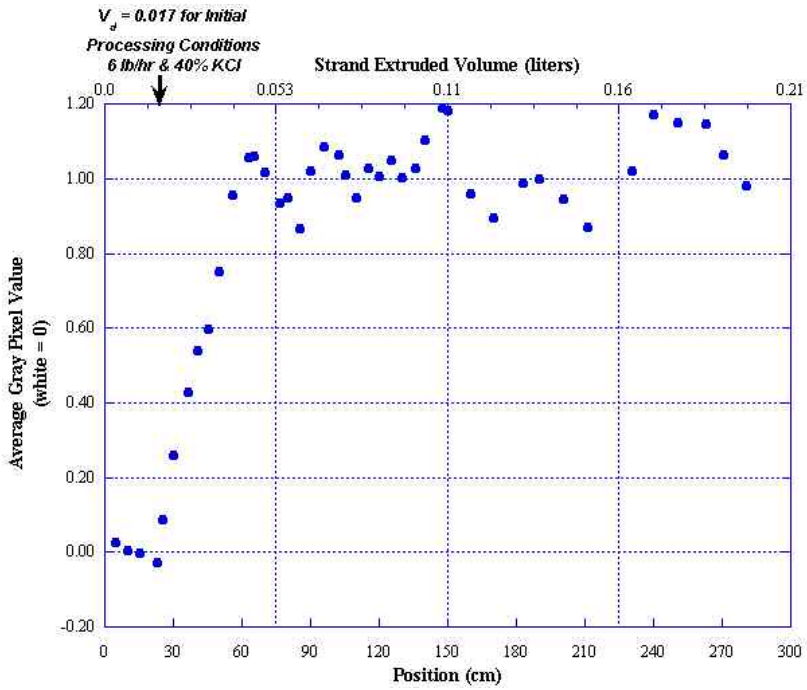

Figure 5-15. The average grayscale values for the internal surface of cross-sections in sample #1628 were plotted as a function of position and volume. Volumes greater than V_d on the abcissa are not accurate.

The density data for the two graded strands is plotted in Figures 5-16 for the case of the negative gradient and Figure 5-17 for the positive step. The tests revealed that there was porosity in the samples. This was not unexpected because a vacuum was not applied to the extruder barrel after the KCl mixing zone. At the time of these studies, the ZDSK-28 at UMD was not equipped for vacuum processing. The degree of porosity was between 90 and 95 percent theoretical maximum density and was later witnessed by scanning electron microscopy (SEM) discussed in the next Chapter.

In the case of the responses to the positive step change, the gradient is observed in the data where it would have been expected as predicted by the RVD. Also the density data reinforce the observed image response. This was not true in the case of the negative step. The image analysis indicated the start of the gradient approximately where it would have been expected. However the density data of the negatively graded samples

indicate the solids change is detectable approximately 0.1 liter after the color change is first detected. In that the microstructure of the rectangular sample was complex and far short of ideal, the ability to make predictions of the gradient characteristics was quite handicapped. The square extrudate was closer to ideal, and its microstructure was related to the RVD.

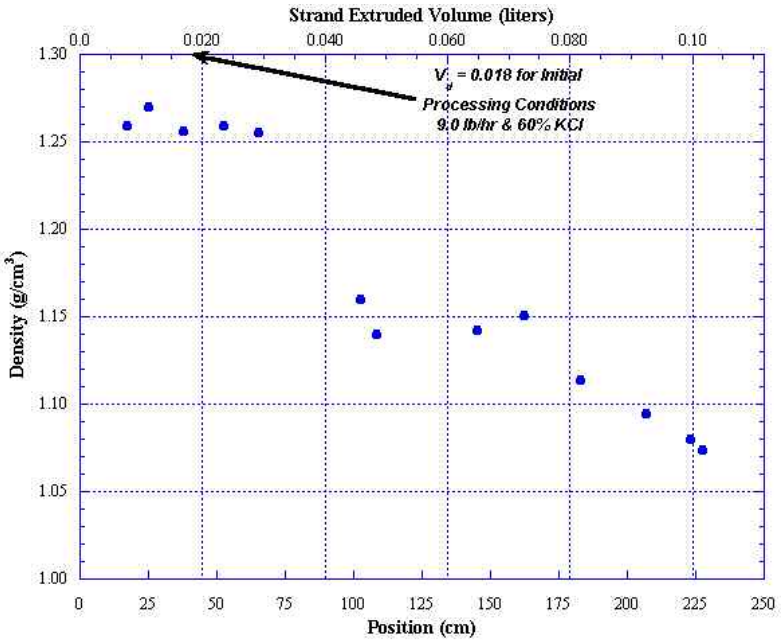

Figure 5-16. The density values for approximately 1 cm length sections of sample #1515 were plotted as a function of position and volume. Volumes greater than V_d on the abcissa are not accurate.

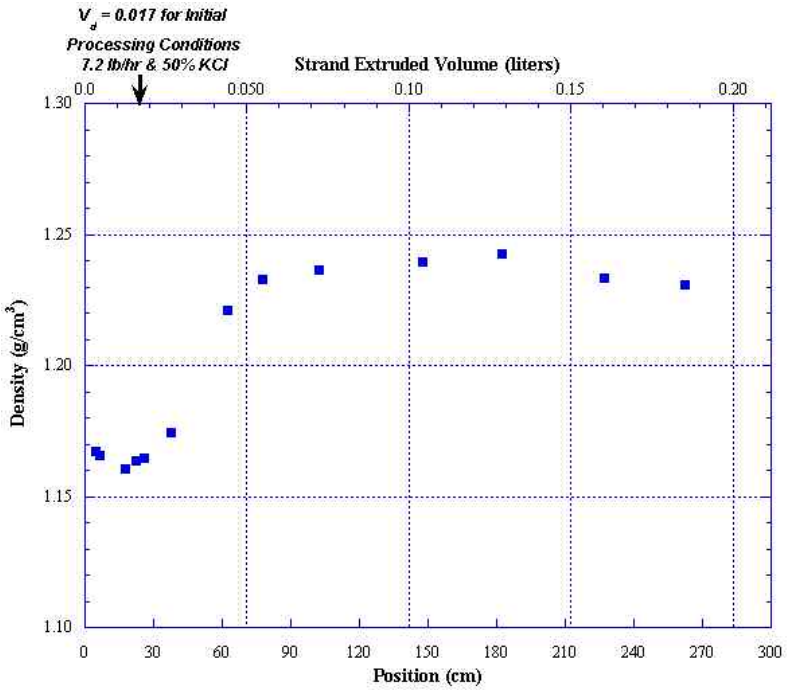

Figure 5-17. The density values for approximately 1 cm length sections of sample #1628 were plotted as a function of position and volume. Volumes greater than V_d on the abcissa are not accurate.

5.1.3.5 Pyrolysis of KCl/Engage Composite

The technique of pyrolysis for quantitative solids determination was pursued to validate the density measurements. It was especially important to validate the continued decrease in solids concentration for positions beyond 175 cm in the rectangular sample. The method was simple in that the mass of the sample was determined before and after consumption in a furnace set at 1250 F. The binder was completely consumed by the fire. Date for extruded samples was compared with a standard that consisted of an admixture of the starting ingredients. The accuracy of the measurements was better than 0.7 percent. The results for the negative and positive gradients are plotted with the density values in Figures 5-18 and Figure 5-19 respectively.

Although the method was destructive, it did validate the density measurements and eliminated any uncertainty caused by the porosity. The long and unsteady decrease in solids concentration for the rectangular strand, #1501, was attributed to the effects of die geometry. However the pyrolysis does show that the solids content was approaching 40 percent for that negative gradient. The results also show that the positive gradient begins at 50 percent and gradually increases to 60 percent in strand #1628. A review of

process notes for that test indicated that there were perturbation alarms for the KCl feeder that day. That would have contributed to the initial concentration being closer to 52 percent rather than the setpoint of 50 percent by weight.

5.1.3.6 Force Measurements for Sectioning KCl/Engage Composite

The force required to section the strands was measured as a function cutting time and position along the graded strands. An Instron load measuring test device was fitted with a razor blade and measurements of the force to cut the strands perpendicular to the direction of extrusion were made. The data were treated several ways such as maximum force and force divided by strand width (which was not a constant). There was wide variation in the measurements but it could not attributed to filler content or position. The technique was not pursued any further, but mechanical testing should be considered in future studies. It will likely be necessary to adapt methods and hardware to accommodate small samples although.

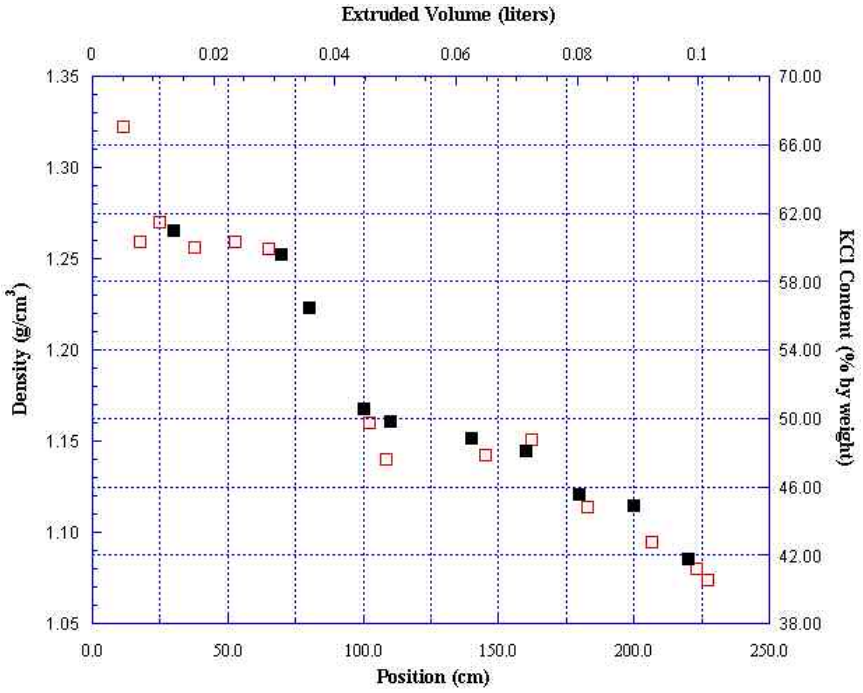

Figure 5-18. The KCl content as determined by pyrolysis and density values for strand #1501 were plotted as a function of position and volume. The two characterization techniques were equally sensitive in detecting the gradient.

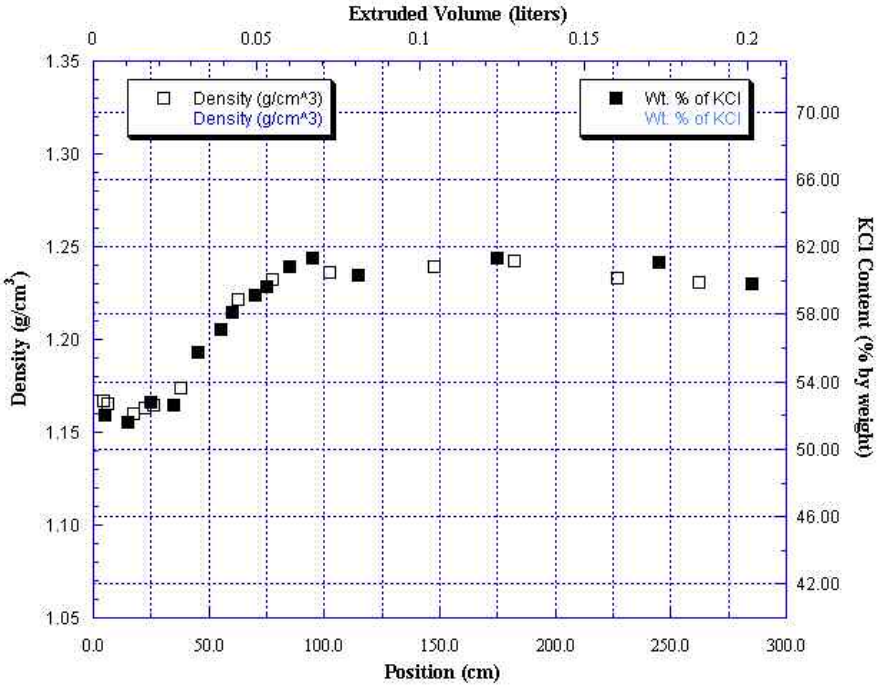

Figure 5-19. The KCl content as determined by pyrolysis and density values for strand #1628 were plotted as a function of position and volume.

5.1.3.7 Prediction of Gradient Response in Inert Composite Physical Properties

The efficacy of RVD models to predict the architecture of the gradient in extruded material was explored in this research. Three material responses for the inert polymer composite processed on the ZDSK-28 TSE were determined and found to exhibit similar characteristics. Figure 5-20 shows the physical properties, density, color, and filler content, of the graded composite as functions of position normalized to the unit step response. Note that they were similar in response rate indicating that a single predictive expression will suit all three.

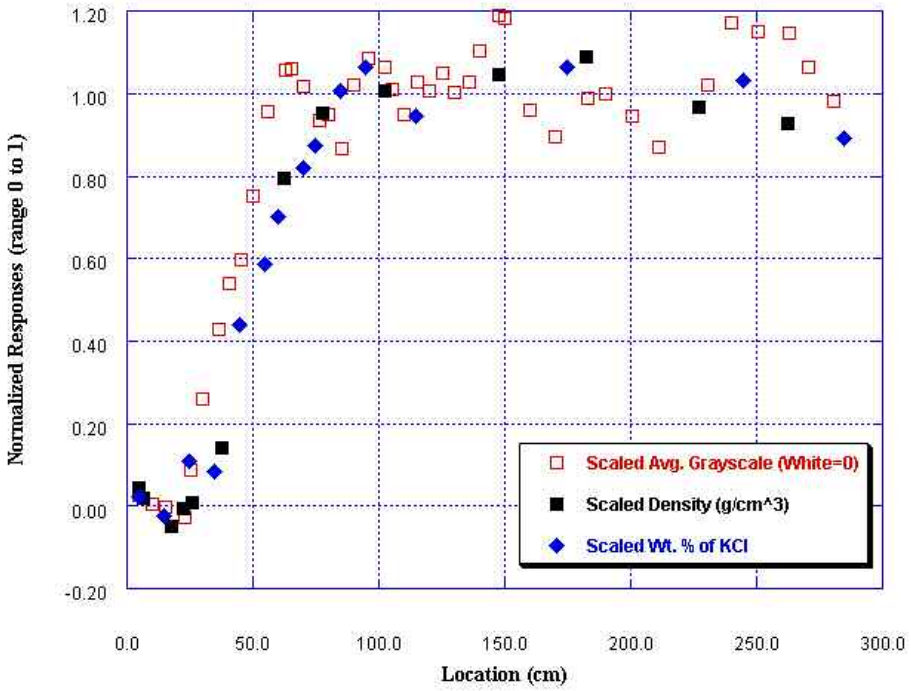

Figure 5-20. The material property responses for a step change from 50 to 60 percent filler.

In this particular case several models were appropriate to describe the responses. Due to the relatively short gradient, higher values of the RVD shape parameter, a_v, were favored. With $a_v = 80$, there was not much distinction between a first or second order response. This suggests that the response may lie in between the two ideal cases and that more data within the area of the gradient would be warranted. Figure 5-21 shows the excellent fit of the first and second order responses. While RVD models were shown to describe the characteristics of gradient architecture, the next section discusses how RTD models were convenient to characterize process responses, e.g., on-line probes, die pressure, extrusion torque.

An important point regarding Figure 5-21 is that a shape factor from a third set of processing conditions was used to illustrate the robustness of the method to predict the material process responses for an extruded graded composite. The initial conditions in Figure 5-21 were 50 percent KCl and total throughput of 7.20 lb/hr, and the final conditions were 60 percent at 9.00 lb/hr throughput. The RVD shape factor was from a fit of a third order RD model at conditions of 40 percent filler at 6.00 lb/hr. This would not have been possible using the RTD parameter.

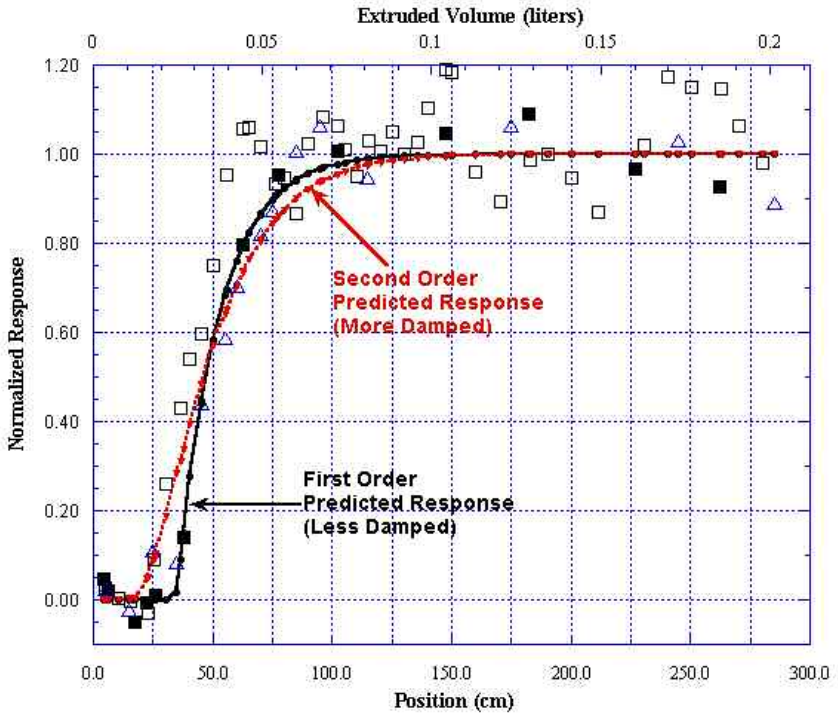

Figure 5-21. Using the RVD shape factor for processing conditions different from the initial or final states, a prediction in material property responses was still possible. The same shape factor predicted first and second order responses.

5.2 Processing and Characterization of Functionally Graded Rocket Propellant

5.2.1 Processing Functionally Graded Propellant in a Twin Screw Extruder and On-line Gradient Characterization

The justification for selecting a gradient of 79 to 87 percent solids at a constant 79/21 coarse/fine particle ratio is given in great detail in Section 4.3. The process approach for gradient formation in the propellant was first studied at the UMD facility with inert material and discussed in the preceding section. The inert process at UMD was staged into zones because of the methods used at NAVSEAIHMD for the solid propellant.

In the propellant continuous process, the first stage was the feeding, mixing, and plasticization of the binder ingredients. The throughput through the first stage was unchanged during the manufacture. The second stage was the feeding and mixing of the AP and a cross-linking compound. A step-change in the feeding rate of the AP intiated the formation of a gradient. The step change propagated through the second mixing section and continued through the die. There was a fiber optic probe at the diehead of

the extruder that could detect a color change in the propellant as the gradient developed; the probe was also used to detect a blue tracer that was dropped at the same time as the step change was made. This enabled a plainly visible demarcation of the beginning of the gradient in the extruded grain.

The propellant was a deep red color with enough structural integrity to easily maintain its geometry during handling and a five-day cure in an oven at 55 C without slump. Because of die flow effects, traces of blue die on the outside surface of the extrudate are not accurately indicative of the beginning of the gradient. Being able to find the gradient in the extruded strands of propellant was of greatest concern during the planning for this stage of the research. Therefore significant planning and process estimation based on the UMD results were necessary before any process work was started.

The objective was to make graded propellant for strand burning rate testing and small rocket motor testing. A meeting of the project's participants and stakeholders was held to determine how much graded material to produce to adequately meet the test plan. A liberal number of nine rocket motors were determined as necessary for testing using slab motor testing hardware with certain significant modifications.

Four of the motors were planned to consist of homogeneous propellant—two each at the low and high solids content. The remaining five were to consist of graded material, a mix of positively and negatively graded propellant with length and specific orientation to be determined after analysis of the strand burning rate results. Additionally enough material was needed to satisfy the requirements for strand burning rate testing at three pressures and only ambient temperature.

5.2.1.1 Method of Manufacture and Remote Grain Collection

The following questions were addressed to plan a successful extrusion trial.

1. What length of extrudate to collect?
2. How to find the beginning of the gradient?
3. How long after the step disturbance would the gradient emerge?
4. How to distinguish composition and direction among various grains on the collection table?

The throughput of 30 lb/hr and screw speed of 85 rpm were selected as the nominal conditions for this research. This formulation has been processed in excess of 50 lb/hr on the 40 mm TSE; however, the lower rate was chosen due to material conservation and especially die pressure minimization over a previously unexplored range of solid fills and coarse/fine ratios (details in Chapter 4). For the gradient condition selected, a change from 79 to 87 percent by only changing the AP feeding rate resulted in a throughput change from 30.00 to 48.48 lb/hr respectively. This influenced the dynamics of the volumetric throughput. The volumetric throughput and the linear extrusion rates are given in Table 5-3.

Table 5-3. The volumetric throughputs and linear extrusion rates for the steady state over the range of gradient starting conditions.

Weight Throughput (lb/hr)	Percent AP	Theoretical Max. Density (g/cm^3)	Volumetric Throughput (cm^3/sec)	Linear Extrusion Rate (cm/sec)
30.00	87	1.794	2.107	0.27
30.00	79	1.710	2.211	0.28
48.48	87	1.794	3.405	0.43
48.48	79	1.710	3.572	0.45

The RDs in Figure 5-22 for the composite in the 40 mm TSE were used to estimate the length and time necessary to collect the extruded grains. It was straightforward to establish the length to collect for the homogeneous specimens. Since the maximum motor length was 19.7 cm (7 ¾ in.), a total of fifteen inches was collected of the two homogeneous compositions.

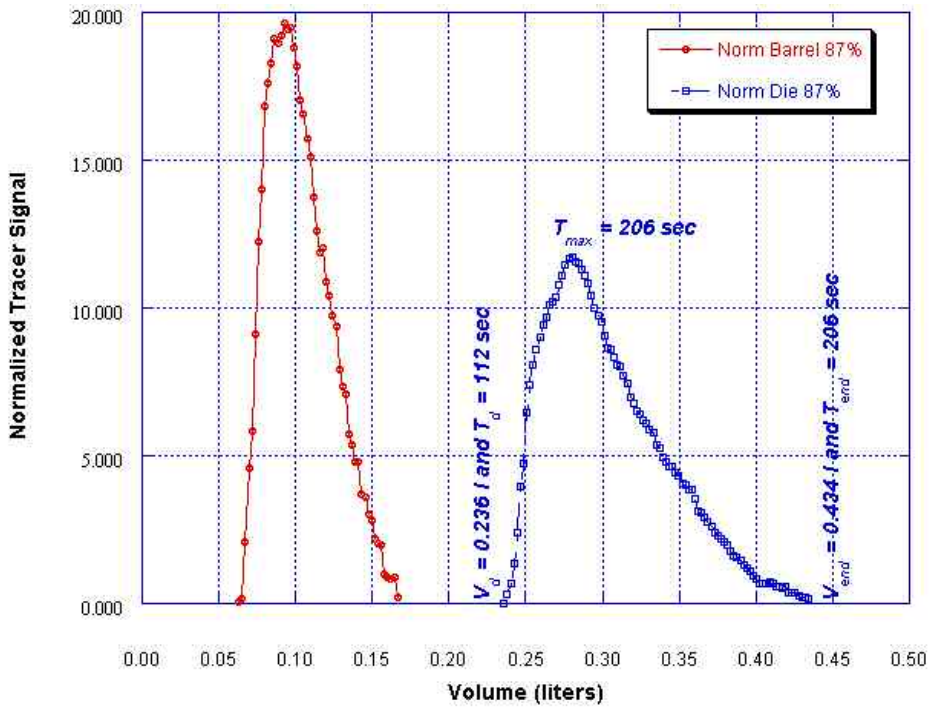

Figure 5-22. The plot shows the RVDs for IH-AC3 processed in the 40 mm TSE—the first for the probe in the AP mix zone and the other at the die entrance.

The length of graded specimen was determined as follows. Using time as the metric, the lowest velocity extrudate was selected as the baseline. Let time zero represent the time of the step change. Therefore the gradient will be reaching the entrance to the die and the fiber optic probe at the delay time of 112 sec (29.8 cm extruded so far). The gradient will begin to emerge from the die exit at 112 sec plus the die residence time, t_{die}, which was unknown beforehand. Results from experiments at UMD suggested that the gradient was nearly fully developed at t_{max}. At that point more than 35 cm have been extruded. At t_{end} the full gradient development is certainly complete (>55 cm total length extruded).

The t_{die} was still unknown but assumed to be less than the time to extrude an additional 20 cm, the length of a motor. In other words, the gradient was thought to occur over a length between 6 to 25 cm (2.5 to 10 inches) based on reasonable and conservative interpretations of the RVD. Therefore a total grain length of 55 plus 20 cm (29.5 in. rounded up to 30 in.) was planned to be collected.

The time to extrude and collect 75 cm was estimated using the following rationale based on the RVD in Figure 5-22.

$$\frac{\text{Volume initially extruded}}{\text{Initial volumetric throughput}} + \frac{\text{Max. volume to complete gradient}}{\text{Final volumetric throughput}} + \frac{\text{Volume of one test motor}}{\text{Final volumetric throughput}} = \text{total seconds} \tag{53}$$

For the positive gradient the total time was,

$$\frac{236\,\text{ml}}{3.41\,\frac{\text{ml}}{\text{sec}}} + \frac{434-236\,\text{ml}}{2.21\,\frac{\text{ml}}{\text{sec}}} + \frac{156\,\text{ml}}{2.21\,\frac{\text{ml}}{\text{sec}}} = 229\,\text{sec} \tag{54}$$

and for the negative gradient,

$$\frac{236\,\text{ml}}{2.21\,\frac{\text{ml}}{\text{sec}}} + \frac{434-236\,\text{ml}}{3.41\,\frac{\text{ml}}{\text{sec}}} + \frac{156\,\text{ml}}{3.41\,\frac{\text{ml}}{\text{sec}}} = 211\,\text{sec} \tag{55}$$

The volume extruded in each case was the same, 590 ml. Dividing by the cross-sectional area of the die, 7.92 cm^2, yields 74.5 cm (29.3 in.). Therefore extruded grain sizes of 30 in. were collected.

Knowing the number, kinds, and lengths of grains to collect, the execution of the extrusion trial was planned. A flawless execution of this plan with no process upsets enabled all the grains to be produced in one day's work without having to conduct a refill of the AP hopper. This was the most complicated extrusion run performed to date at NAVSEAIHMD in the 13 plus years of the 40 mm facility because of the control room operations required to remotely execute the gradient formations and collections. It required four people at four stations in the control room:

1. Someone to drop the dye and paint identification marks.
2. A lead operating engineer to monitor the overall process and keep track of time.
3. An AP feeder operator in change the feeding rate.
4. Someone to operate the guillotine cutter and collection conveyor.

A chart with 24 run objectives was given to each operator. The chart included the number of spots to paint for identification, the AP feeder setpoint, percentage solids, and the estimated time required for the task.

A typical process stage was conducted as follows.

1. During the *ready* stage, the feeder operator would enter the new setpoint but not the *Send* key.
2. The timekeeper would announce *go*, and simultaneously, the painter would actuate the *Newtomatic* thus dropping a tracer pellet, the cutter would cut the extrudate at the die face with a guillotine cutter, and the AP feeder operator would press the send new rate button.
3. After several inches had extruded, the painter would paint a series of dots using black ink and an air brush. There were four varieties of grains corresponding to AP solids fill, thus each grain was painted with one to four dots. The ink was applied to the leading end of the extrudate so that the correct direction of extrusion would be preserved.
4. The feeder operator would get ready with a new set point.
5. After the required length had been extruded, 15 or 30 inches, the cutter would actuate the guillotine. Most instances this cut corresponded with the beginning of the next task and the procedure would be repeated.

5.2.1.2 Process Response to Gradient Formation

Without going into great detail, a number of process responses were recorded using the facility's data acquisition system. These included material temperature in the process section, fiber optic sensor response, extruder torque response, material pressure in the processing sections and the die, etc. The probe data is presented and analyzed in the next section. The pressure at the die and the extruder torque are of paramount concern in any extrusion process. There was a concern beforehand that the viscosity of the 79 percent fill was too low to clear the die of the higher viscosity 87 percent fill during a positive gradient step. If this happened, the die would have become blocked terminating the experiment for the day. This fortunately did not happen, nor was it close to happening.

The pressure and torque were however quite responsive to the presence of the gradient. Figure 5-23 is a plot of the motor speed of the AP feeder and the material pressure at the die entrance—the same location as the optic sensor. The abrupt jumps in the feeder's motor speed on the right hand side mark the initiation of the positive and nega-

tive step changes in AP feeding rates. How those changes affected the die pressure is shown in Figure 5-24. A close examination reveals that the pressure response due to the arrival of the gradient is consistent with the volume delay, v_d, as shown in Figure 5-24.

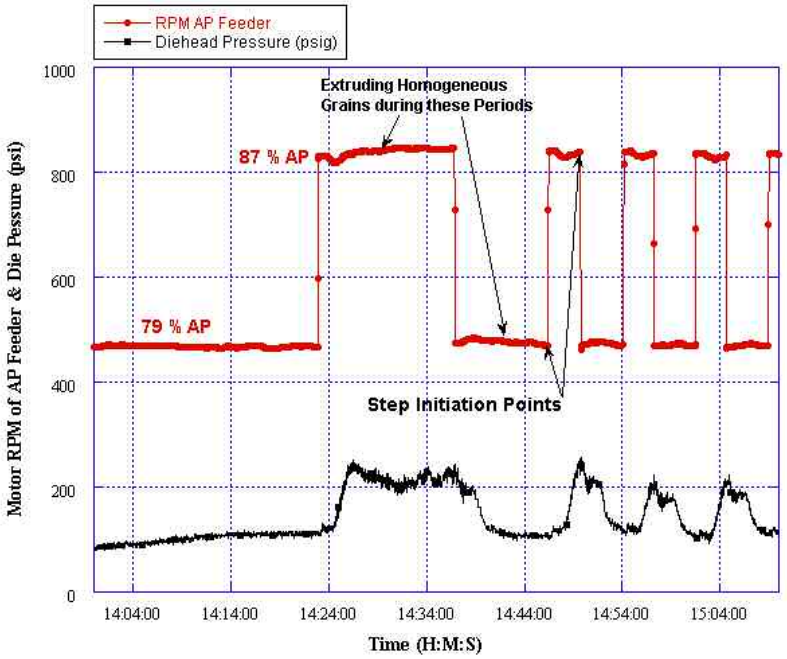

Figure 5-23. The plot taken from data collected during the twin-screw extrusion of the rocket motors shows the response of the AP feeder to step changes of the setpoint and the delayed response of the die pressure.

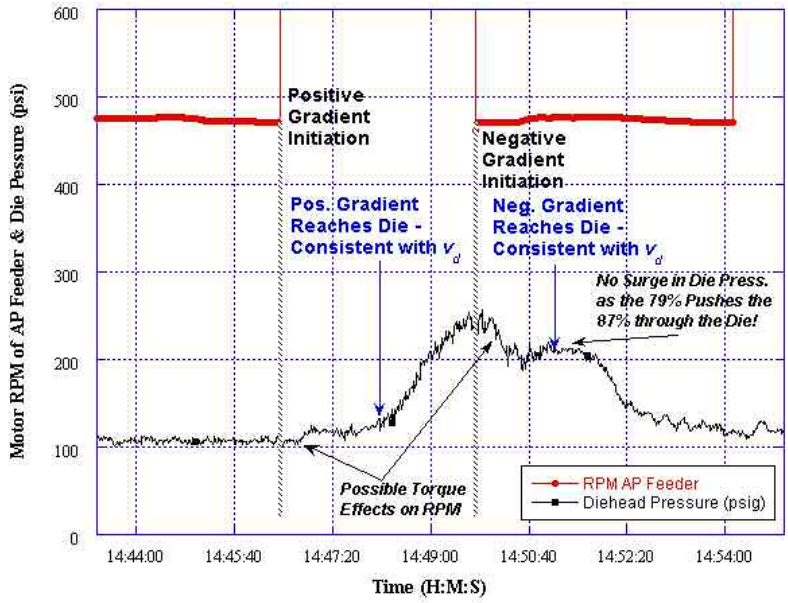

Figure 5-24. Interpretation of the volume delay accounts for the pressure increase at the die due to the arrival of the gradient.

Preceding the gradient pressure response was a slight (10 psi) increase in die pressure that was consistent with the volume delay in the AP mixing section, i.e., the volume processed from the point of step change until the tracer was detected at the left-handed element in the AP mixing zone. The pressure increased at the die due to a likely torque increase due to the higher viscosity material in the mixing zone that was over compen-sated by a slight increase in the extruder screw speed.

The measured extrusion torque can be treated similarly. One difference from a pressure response is that the torque responds immediately to a disturbance. Material pressure did not respond until the disturbance had propagated to that particular location. Figure 5-25 illustrates the torque response.

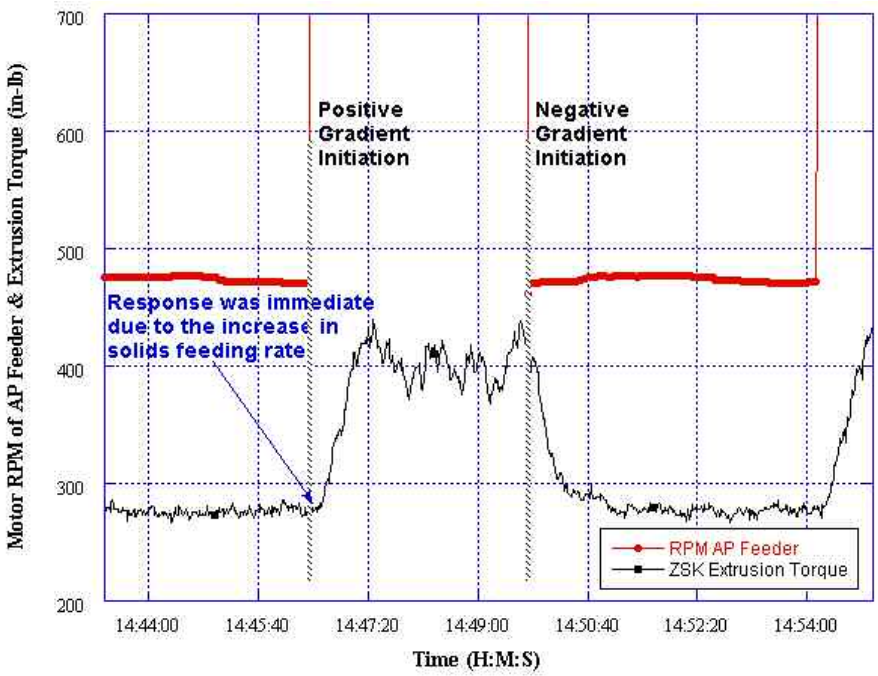

Figure 5-25. Plot of the ZSK-40 extrusion torque in relation to step *disturbances* in the AP feeding rate.

There are some measurements missing that would complete the understanding of the die pressure response. The first is an accurate and continuous measurement of the extrusion velocity. The second is more pressure transducers located slightly upstream of the die along the axis of the extruder screws to determine the degree of *backfill* at the die. Experience with other products has indicated that backfill is typically very low—two or three flights at steady state. But that is the key term. The gradient formation process does not happen in the steady state rather the dynamic or *disturbed* state.

There was also a concern with making a relatively large change in the solids fill in one step due to perceived differences in viscosity. In conducting the reverse gradient from high solids, ergo high viscosity, to a lower viscosity flow, it was unknown if the pressure gradient generated by the screws would have been high enough to overcome the inertia due to a die full of high viscosity material. In other words, could the lower viscosity flow push out a die full of high viscosity propellant? It was shown experimentally that this was not a concern. In the pressure response data for the die pressure in Figure 5-24, there is not even a surge in the die pressure as the lower filled material enters the die.

5.2.1.3 Optical Sensor Response to Step Inputs

The CAMES probe was used during the production of the graded grains to monitor the progress of the dye. A tracer containing a blue dye was inserted in the AP feed stream at the same time as the step changes; the dye served as a means to identify the gradients' starting location. However upon analysis of the probe an important observation was made that had previously gone unrecognized. The color of the propellant changed in response to the gradient even in the absence of the blue tracer as shown in Figure 5-26. The optical probe had the sensitivity to detect the evolution of the gradient without tracer.

The step changes between 79 and 87 percent solids in the feeding rate are quite apparent in Figure 5-26. Note that the feeder established a new feeding rate in 3 to 4 seconds. The probe response showed shifts due to the alternating changes in the propellant's color intensity and spikes resulting from tracer addition.

5.2.1.4 Prediction of the Gradient Responses using RD Functions

The color change in response to a positive gradient, Figure 5-27, was subjected to further analysis to relate it to a residence distribution (RD) function. The shapes of the RDs for 79 and 87 percent AP were very similar as shown in Figures 3-25 through 3-28 (live RTDs and RVDs). The coefficients of the RTD functions that best describe these data are given in Table 3-9 according to function order: first, second, third etc. At issue is if a RD function can be used to predict the gradient response as shown in Figure 5-27. The CAMES probe proved to be sensitive not only to blue colored tracer but also to changes in AP concentration. The concentration in Figure 5-27 is shown changing from 79 to 87 percent by weight.

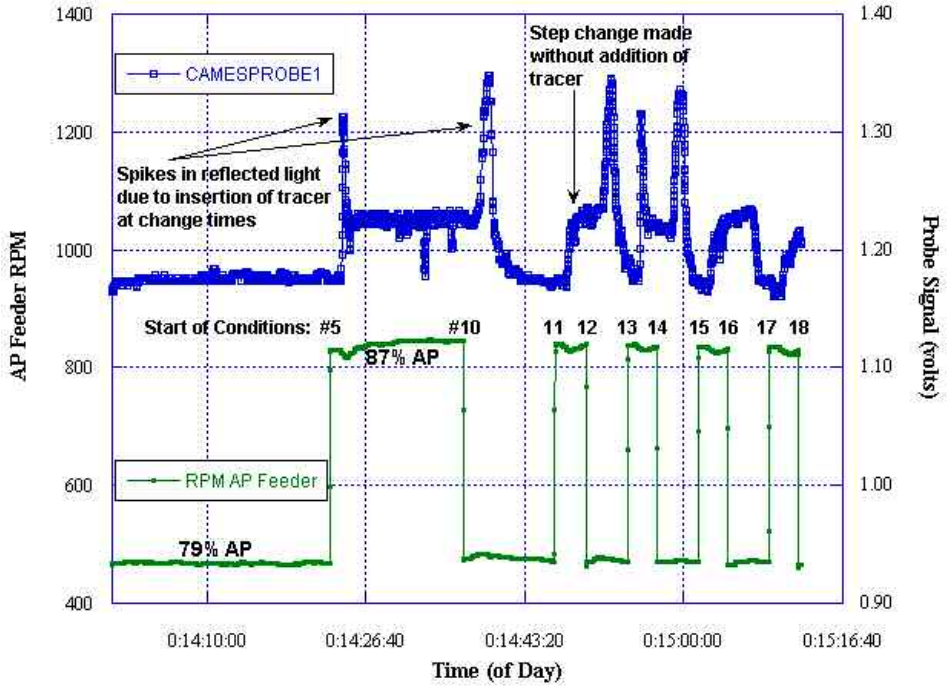

Figure 5-26. The trace of the AP feeder screw speed was plotted with the response of the CAMES probe. Step changes were readily apparent in both signals.

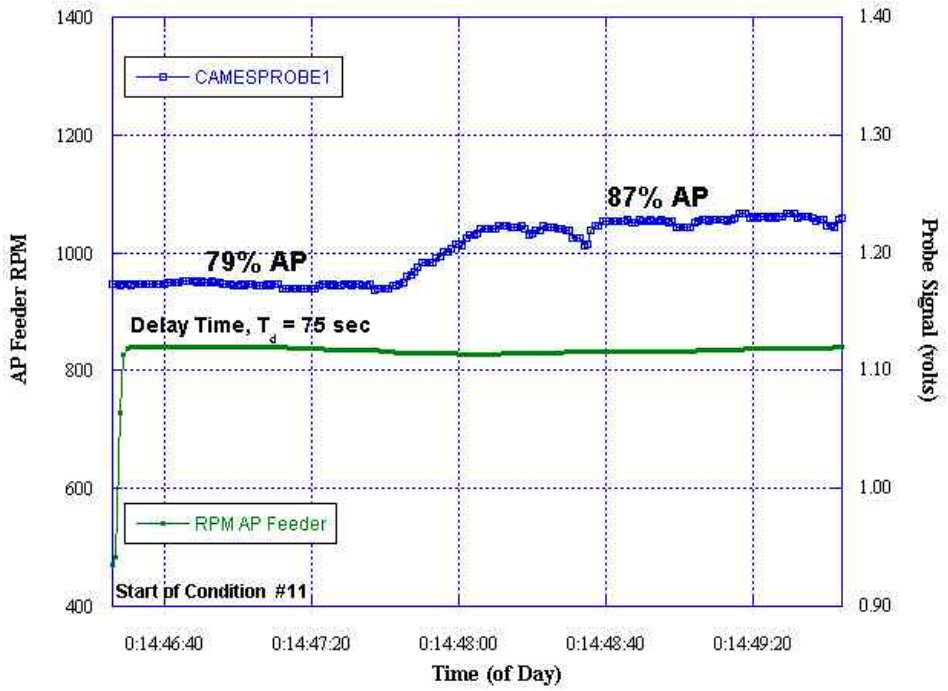

Figure 5-27. The response of the CAMES probe as a gradient evolves from 79 to 87 percent AP.

In Section 2.2.4, the convolutions of the RD functions were developed to predict the responses of the RD functions to a step input. These were applied to the measured responses from the extrusion studies conducted on inert composite at UMD as described in Section 5.1.3.1. The CAMES probe response was used to demonstrate that this was possible for a different material, i.e., IH-AC3 propellant, processed in a different TSE.

The signal responses for the CAMES probe, extrsion torque, and die pressure transducer were isolated and unit normalized as shown in Figure 5-28. The die pressure and torque exhibited a slight over-shoot as the die was cleared of lower viscosity propellant during the gradient extrusion. The pressure transducers used at NAVSEAIHMD operated at 7 Hz; the signal was acquired at 1 Hz. The hardware was only capable of that one acquisition rate. Higher rates would have been desirable.

The CAMES probe measured the light reflectivity of the propellant at a single fixed location, i.e., the die entrance or the screw tips. The torque and color response can be described using the model for a first order response. The model parameters were the shape factors from the second order RTD process models. Note the robustness in that the parameters for either 79 or 87 percent filler were satisfactory. The second order RTD shape factors were powerful in that they were able to characterize color response, extrusion torque response, and die pressure.

Although the die pressure transducer was located at the same position in the die entrance as the light reflectivity sensor, it measured an aggregated response representing effects of the die itself, the eight-to-round die approach, and the backfill on the rotating screws, in other words, a much larger volume than the sensor. The die pressure response was characterized by a second order response as shown in Figure 5-29. The response is not sensitive to using parameters from 79 or 87 percent AP systems.

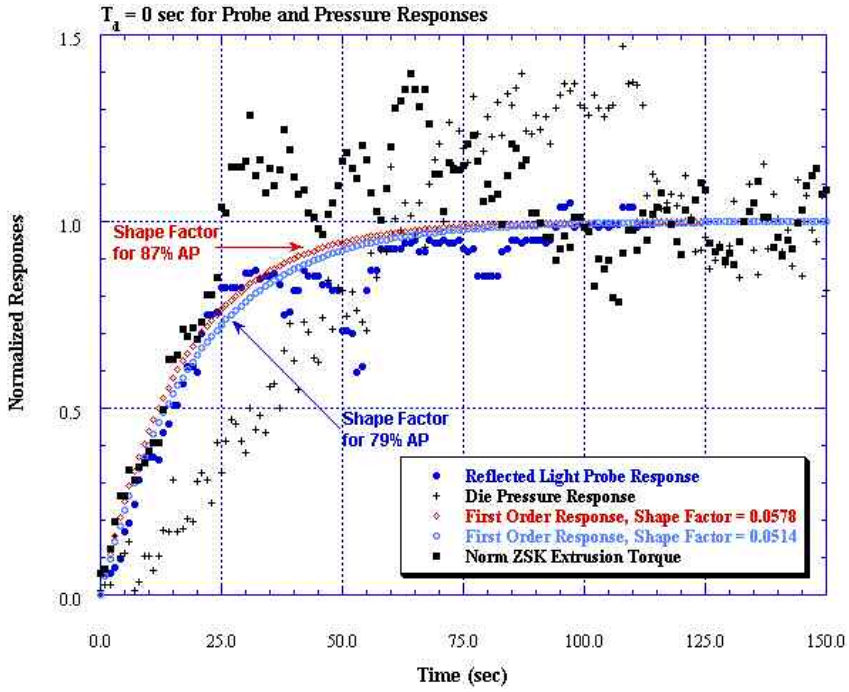

Figure 5-28. Plot illustrates how shape factors for RTDs can be used to predict the development of the gradient in the TSE. Extrusion torque and probe response are first order responses and can be predicted using RTD shape factors for second order systems.

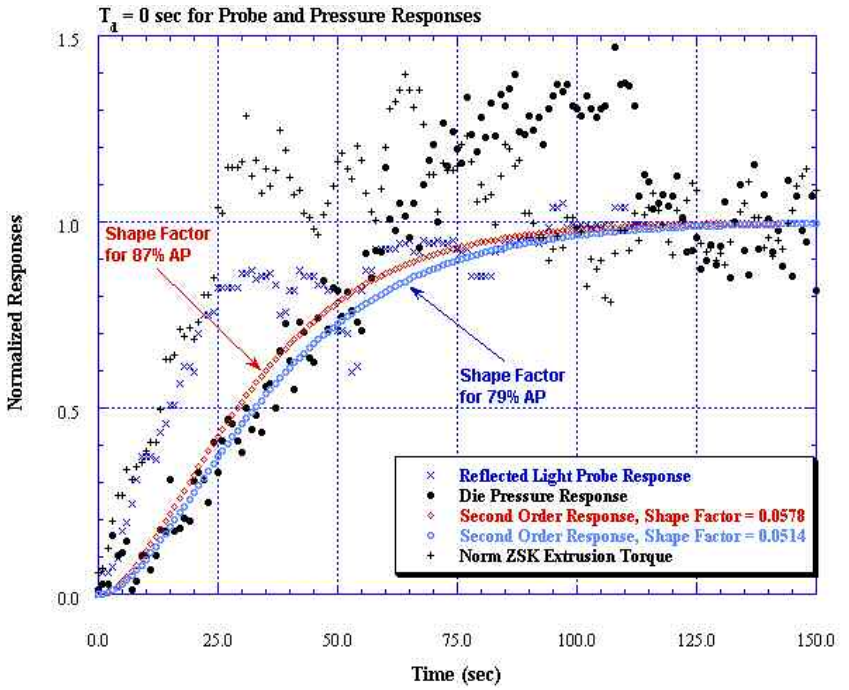

Figure 5-29. Plot illustrates how the response in die pressure to the processing of a gradient in rocket propellant can be predicted using shape factors from second order process models for the RTDs. The pressure response was second order.

5.2.2 Combustion Rate Characteristics of Functionally Graded Propellant and Performance Profiles for Functionally Graded Rocket Motors

5.2.2.1 Acoustic Strand Burner Test Description

The best measure of a propellant's combustion properties is of course to test it in a motor; however, this is costly and inefficient during development. Instead a good alternative is to conduct strand burning tests under a range of conditions, for example, chamber pressure and temperature. Testing at different pressures allows determination of the burning rate exponent. The common method of strand burning is to test six-inch long strands ¼-inch in thickness and report the average burning rate for approximately six strands. Two thin tin bridge wires are inserted through the strand after the ignition point and before the end. The distance and time between wire failure is used to estimate the burning rate. The accuracy of the method is >> 1 percent.

The dynamic burning rate of functionally graded propellant was characterized using an acoustic strand burner (Rampichini, Ruspa et al. 2000). Employing a microphone in the combustion chamber, it is much more accurate, approximately 0.7 percent, than using wires. The technique also allows a more local measurement of burning rate by putting a series of *notches* at regular intervals along the length. As the combustion front passing through a notched area, the acoustic signature will be affected. Post-processing the data through filters theoretically yields the time of occurrence for burning through each notch. Knowing the distance between them allows a local characterization of the burning rate.

This technique is uncommon at NAVSEAIHMD, and there is not a lot of experience using it. Before the graded strands were tested, an excess of homogeneous samples were submitted to determine the efficacy of technique with IH-AC3. For reasons not completely understood, the acoustic signature from notched specimens was not yielding results that could be analyzed objectively. One reason may be due to the signal processing filters available in the analysis software for the unit. Another reason may be due to the fact that the notches excessively disturbed the combustion front affecting the burn through subsequent notches.

Due to these reasons, it was necessary to reformulate a test plan for the graded strands. The test unit was still the most accurate way to measure the burning rate over

the terminal length of a sample using the acoustic signature. Furthermore the test unit accommodated one pair of bridge wires to measure the *mechanical* burning rate. A new technique and some modification of the test system were quickly implemented to allow testing of smaller lengths. Eventually it was found that strands as short as two and three-inch segments could be tested. The distance required between bridge wires limited their use to the three-inch specimens. The general sectioning scheme and bridge wire placement strategy for a typical set of four graded strands is shown in Figure 5-30. The plan allowed for the fourth strand to be used in case of a misfire. A photograph of a set of test specimens with igniters and bridge wires in place is shown in Figure 5-31.

5.2.2.2 Sample Preparation for Acoustic Strand Burning

One of the most important questions was the location of the gradient relative to some external reference. The external reference was the end of the grain that had been cut as the step change was implemented. Two of the grains, one for each step direction, were split axially to determine the starting location and internal structure of the gradients. Since the blade was approximately 6.5 inches wide, each of the two 30-inch grains was first cut into 6.5-inch lengths before being sectioned lengthwise. A photograph of the split grains is shown in Figure 5-31.

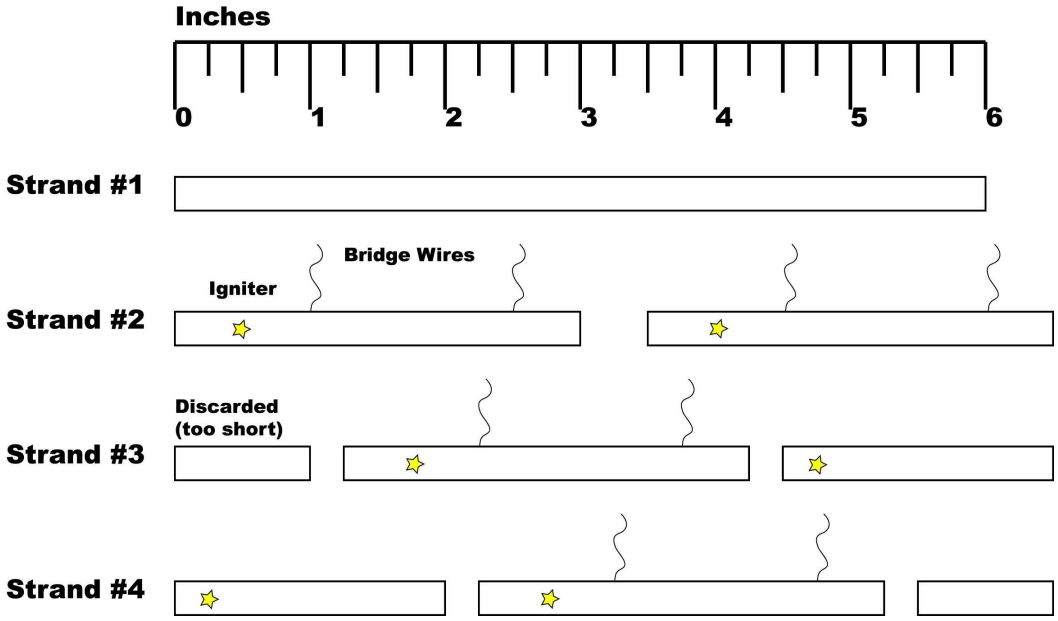

Figure 5-30. This was the plan for burning rate tests in the acoustic strand burner.

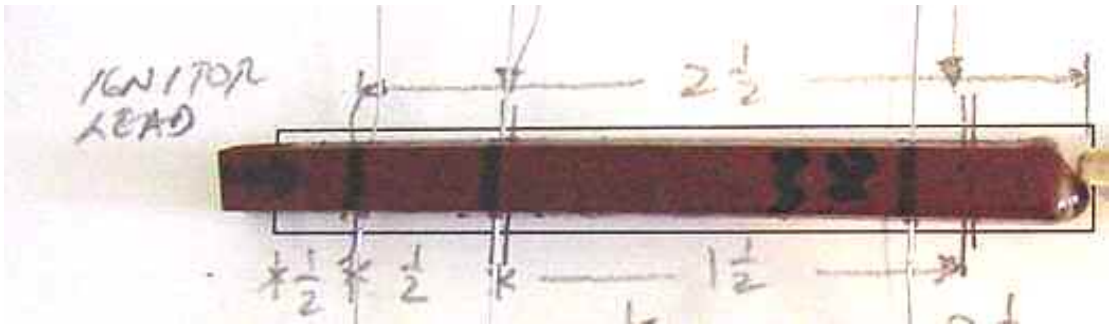

Figure 5-31. Typical 3-inch strand shown with igniter leads and bridge wires.

A number of important observations can be made from Figure 5-32. The deep red color is due to the iron oxide burning rate modifier present in the binder. However the intensity of the red appeared to be dependent upon the binder concentration. Looking at for example, the gradient within the topmost grain in Figure 5-32 was made by stepping down from 87 to 79 percent AP. The end with the higher solids loading, i.e., the left-hand side, is lighter in color intensity. Contrast the left-hand side with the right hand side that consisted of 79 percent AP.

The most interesting feature is the onset of the gradient as indicated by the blue dye. Recall that the dye was introduced simultaneously with the change in AP feeding rate. Since the dye was added as an impulse and not a step, only the onset of the grade can be readily seen. More definitive characterization using burning rate was conducted and described below. Judging by the contrast in red color to the left and right of the blue dye, there is a strong indication that the dye is transported at the same rate as solids in this process.

The color in Figure 5-32 was falsified to enhance the contrast between the blue tracer and the red binder. The result of this process is shown in Figure 5-33. Another especially interesting observation was that the dye dispersion was a fascinating witness to the flow velocities and deformation rates during die flow. The onset location was expected to be different in that there were different volumetric flow rates in the initial states. For example in the topmost grain, the AP concentration was 87 percent by weight and weight throughput was 48.48 lb/hr. This explains why more material was extruded before the gradient formed.

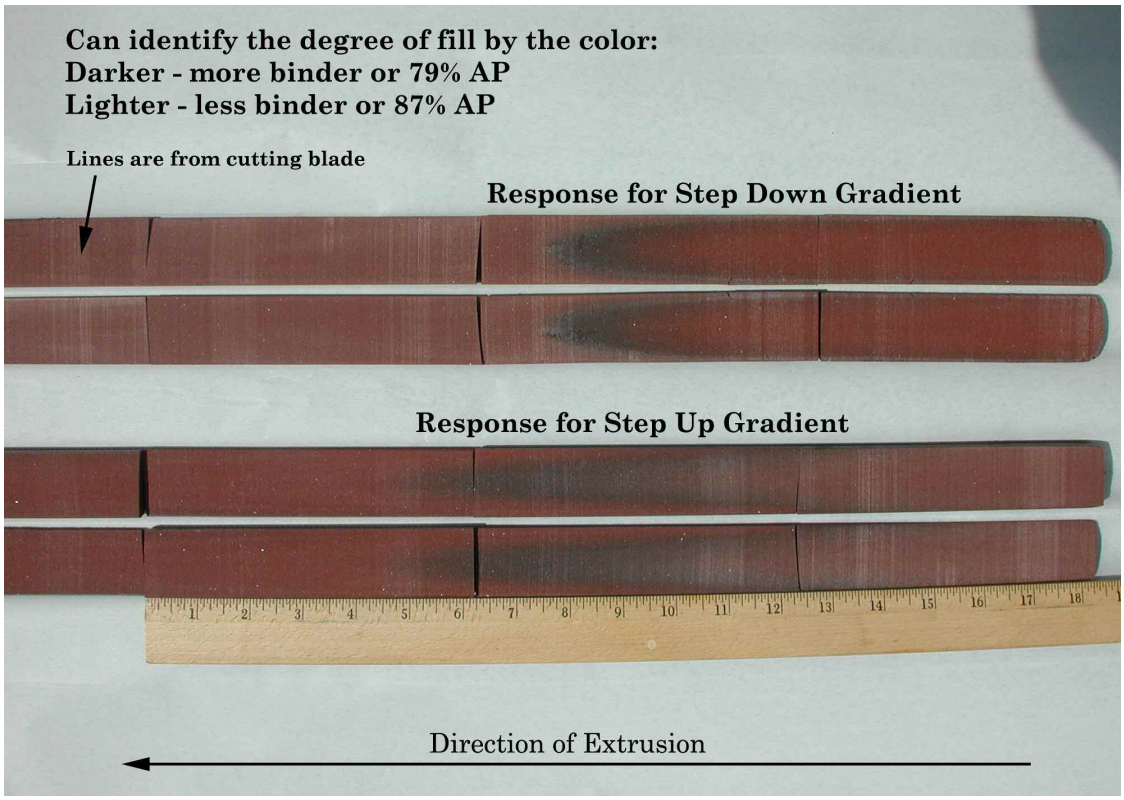

Figure 5-32. A photograph of the axially split grains for each gradient direction shows the distinct difference in the die flow effects and internal structure of the grains.

The onset location was estimated from the process RTD, but this estimate also relies upon the RTD of the die. The die RDs were not known *a priori*. It was determined that the RD for the die was equal or greater than that of the processing section.

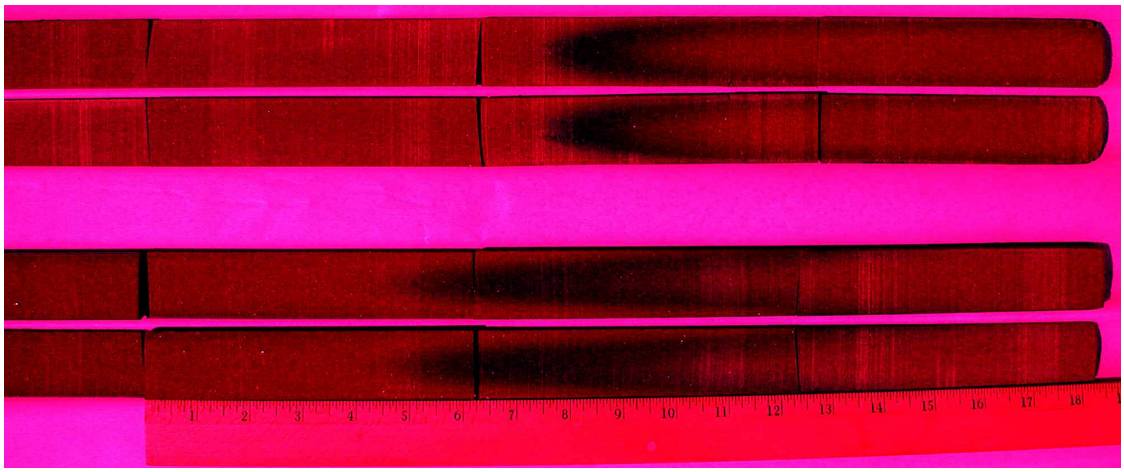

Figure 5-33. The contrast between the blue tracer and red binder was enhanced in this false-color image of Figure 5-32.

Since the acoustic burning rate strand length was limited to a maximum of 6 inches, it was necessary to take samples at two starting locations to achieve a longer range of measurements. Since the internal gradient was different depending upon the direction, a separate strategy was needed for each. Using the *step down* grain in Figure 5-32 as an example, the first set of four strands was taken from a point two inches before the apparent beginning of the gradient. These points were based on the original knowledge that resolution of the local burning rate was possible to one half inch using notched samples. Two inches prior to the gradient would have been enough length to characterize the homogeneous material from the initial conditions. The first half-inch was reserved for the placement of the igniter leaving three measurements of the burning rate before the combustion front entered the gradient. Likewise the second sampling location was chosen based on the expectation of some measurements in the homogeneous region behind the gradient. To capture the full length, the second set was taken from a complete second extruded grain at point two inches *downstream* of the first set. A similar reasoning was followed for the *step up* grains except the second set was sampled further down from the first, because the gradient appeared more dispersed than the other direction.

The strand cutting and sampling locations was quite complex. In a typical homogeneous propellant characterization study, the control over sampling location is not nearly as critical. This basic research effort had the goal of treating the graded propellant as a one-dimensional structure. For this reason only strands sharing the center axis were submitted for acoustic burning rate testing. These were identified as strands 1 through 4 as shown in Figure 5-35. The center strands are also shown to scale superimposed over a photo of the grains in Figure 5-34. A set of four strands representing the outer (closer to the external surface) were collected as well shown as strands 5 through 8. There was not a plan or adequate funding to test these outer strands. However they will be retained for a short time, because interest in characterizing the two dimension gradient effect may grow in the near future.

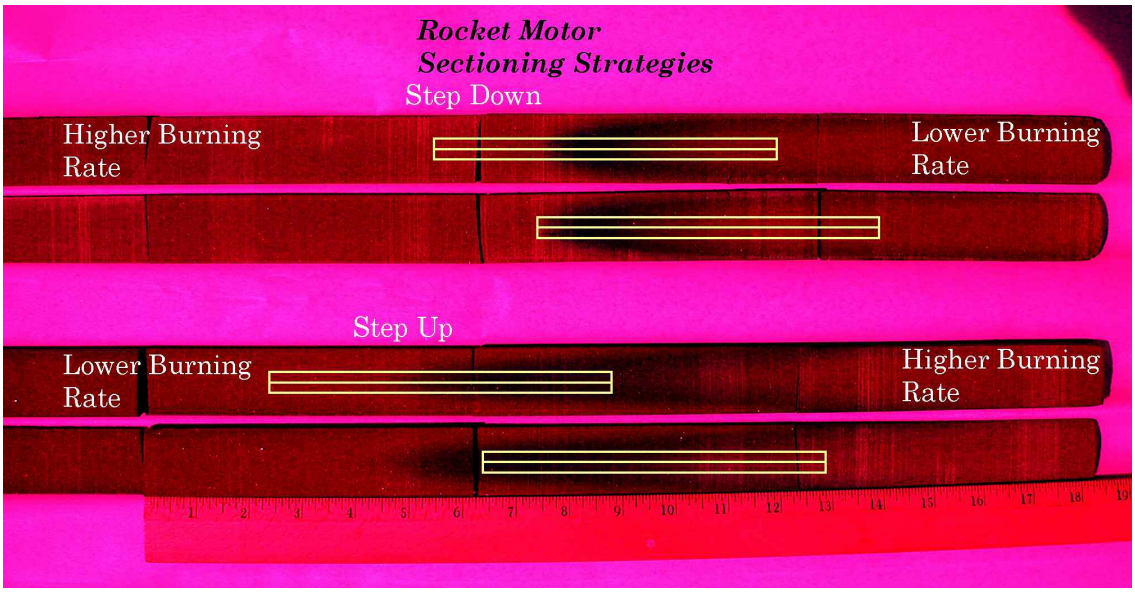

Figure 5-34. This is the plan for sampling the acoustic burning rate test strands. There was a different plan depending upon the direction of the step change. The grains were extruded from left to right. Only the internal strands that are closest to the central axis are outlined in yellow.

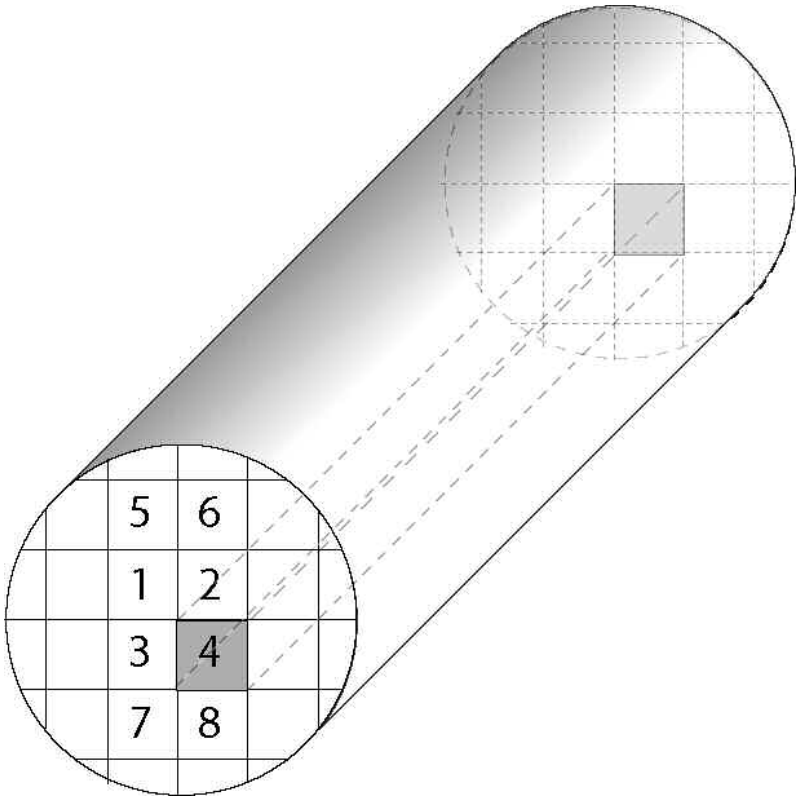

Figure 5-35. Eight strands were gleaned from each segment according to the above scheme. Numbers 1-4 were the internal strands along the axial center of the grain; these were of primary interest. Numbers 5-8 were taken 0.25 inches away from the centers; these were not tested.

5.2.2.3 Acoustic Strand Burning Test Results and Interpretation

Once the capabilities of the acoustic test unit and the strand test strategy were settled, testing proceeded smoothly with minimal failures of the mechanical bridge wire measurements. The measured burning rate data for one set of four strands sectioned into six test specimens, as illustrated in Figure 5-30, are plotted in Figure 5-36. In that particular test series, there were two failures of the bridge wire measurement. Therefore only two *mechanical* points were plotted in Figure 5-36 instead of four. Because the test method of notching the strands at close intervals was changed after they had been cut, there was not enough length before the gradient to verify the initial homogeneous composition. These data will be sought in the future. For reference, the ranges of experimental burning rate measurements for the 87 and 79 percent homogenous compositions are shown in Figure 5-36.

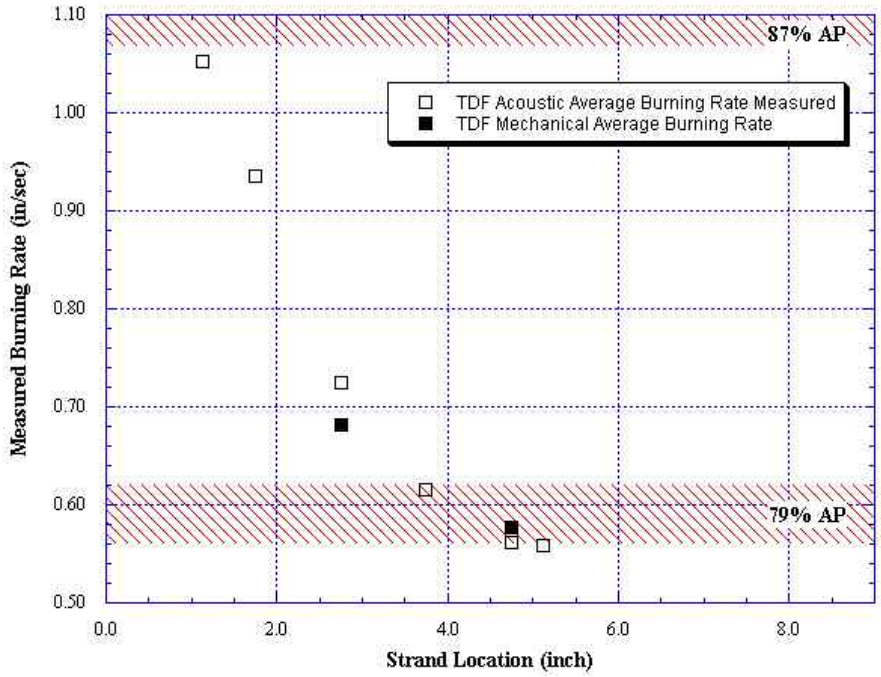

Figure 5-36. The measured strand burning rates for the six short strands taken from the center of a single functionally graded rocket grain were plotted. Burning rates were determined acoustically and electrically. The reference burning rate ranges for 87 and 79 percent AP are shown.

Figure 5-37 illustrates clearly how the sectioning strategy was used to characterize the gradient; only data from a single grain is shown for clarity. The best approach to interpret the data is to consider the measurements as moving averages. For example in Figure 5-37, the bars are not any uncertainty but rather represent the length over which

the average was taken. The mechanical burning rates (from the tin bridge wires) were treated as a moving average over a slightly shorter distance, though the technique not was as accurate as the acoustic measurements and were subject to higher variance.

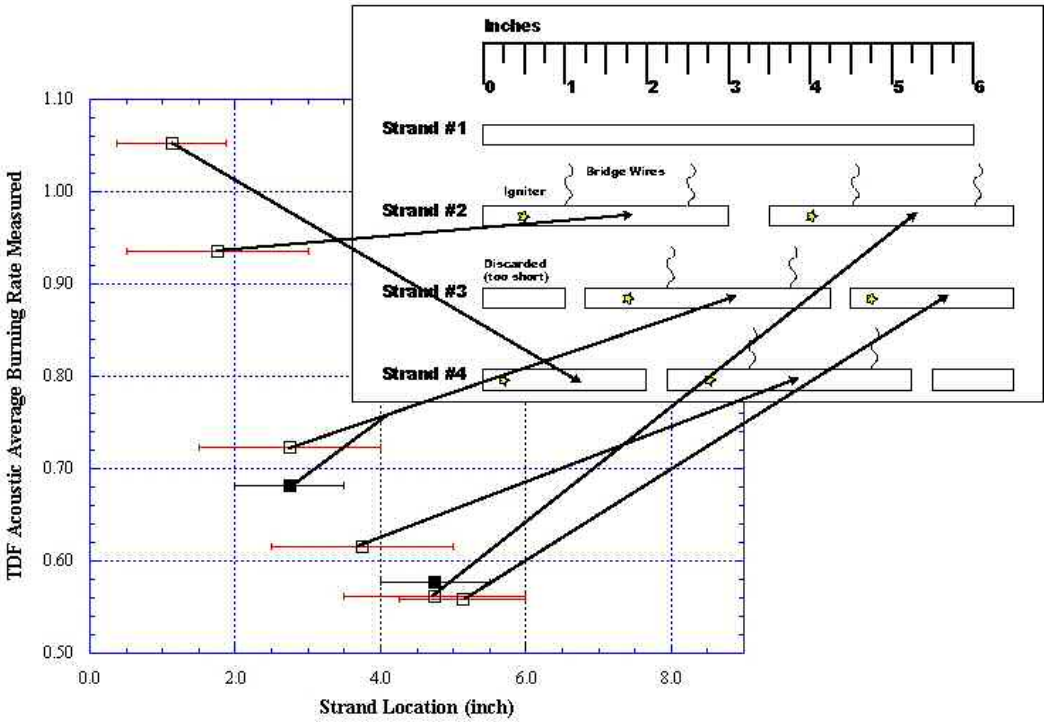

Figure 5-37. The bars on the plot represent the length over which the burning rate was determined—not uncertainty in location. The bars illustrate how testing of sequentially overlapping strands revealed the graded architecture.

The negative gradient in AP content was characterized by taking center strands from two extruded grains (designations TDF, VDB, etc. were for identification purposes) at locations offset by two inches as indicated in the top half of Figure 5-34. There was good agreement between the two grains as shown in Figure 5-38, and offsetting the sampling extended the range of characterization providing verification where the two overlapped. In the future a longer offset distance will be employed.

The grains that were processed with a positive gradient were sampled quite differently. A grain identification error during cutting resulted in four positive gradient grains being sampled at each of the four patterns in Figure 5-34. All samples were submitted for testing to verify repeatability of gradient architecture. It was found that the repeatability was very satisfactory, but more tests would be necessary to quantify it. The acoustic burning rate data from the positive gradient strands are plotted in Figure 5-39.

The mechanical measurements of burning rate agreed well and complemented the acoustic measurements. These data are plotted together in Figure 5-40.

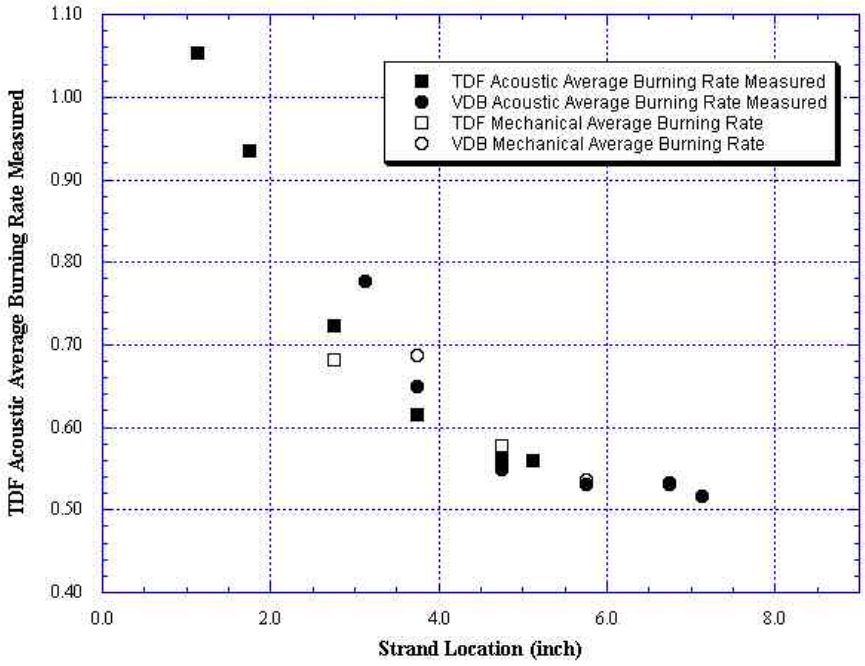

Figure 5-38. Strand burning rate results from two grains for negatively graded propellant.

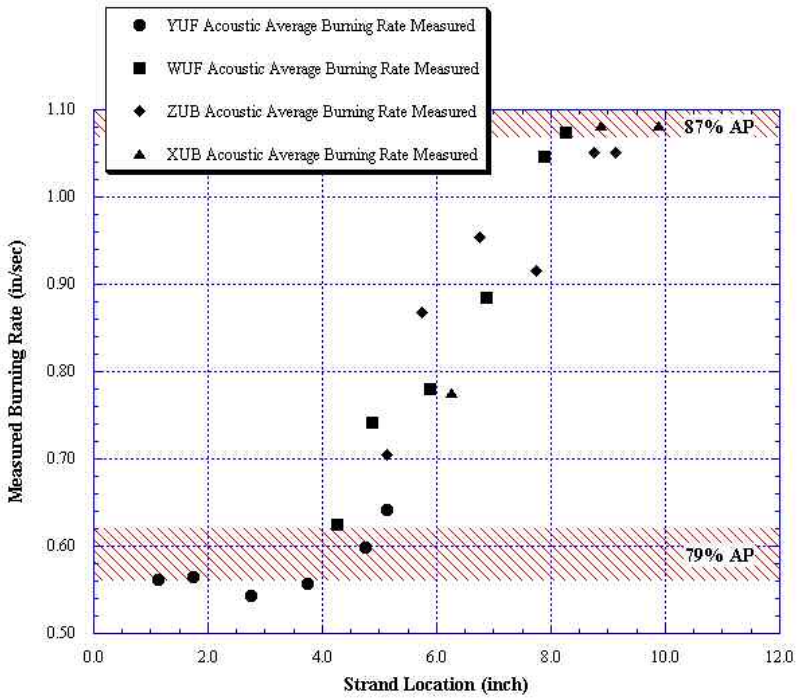

Figure 5-39. Strand specimens from four graded grains were subjected to acoustic burning rate strand testing to characterize the material response to a positive step change.

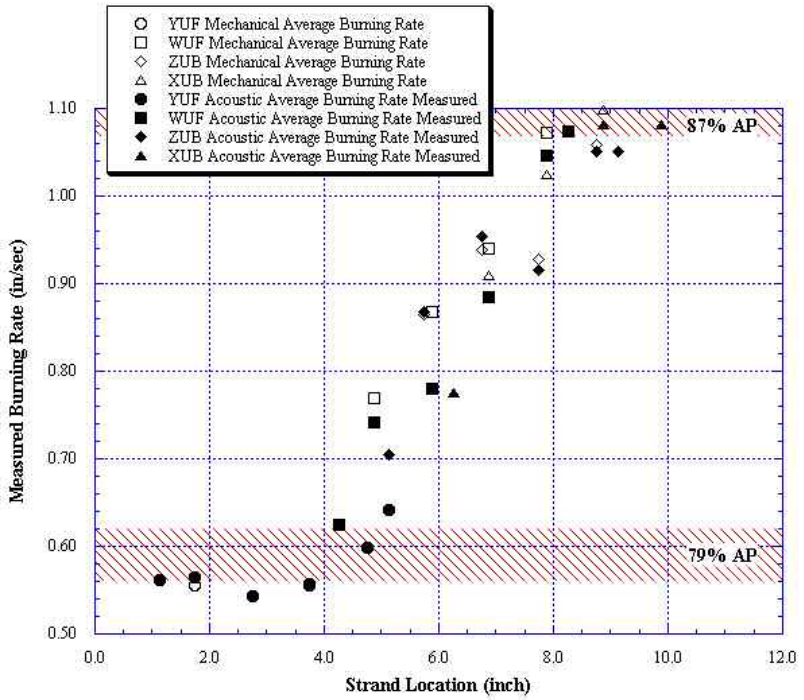

Figure 5-40. Mechanical burning rate measurements during the acoustic strand burning tests agree well with the acoustic responses.

The response in AP content of extruded propellant to a step change in AP feeding rate during twin-screw extrusion can be predicted using process models based on the RVD developed in Chapter 2. The zero inches reference point in Figures 5-37 and 5-38 was actually 14.875 inches from the leading end of the extruded grain. Using this and a value of 7.92 cm^2 for the cross-sectional area of the die, location was transformed into volume extruded. The burning rate responses for the positive step change were normalized to range from zero to one. The resulting transformation is plotted in Figure 5-41.

Evaluating the process models to describe the RVD for IH-AC3 propellant revealed that the shape factor from a fifth order description, $a_v = 66.3$, predicted the response in AP content due to a step change *disturbance*. A third order convolution model best described the gradient architecture using volume as the basis plotted in Figure 5-41.

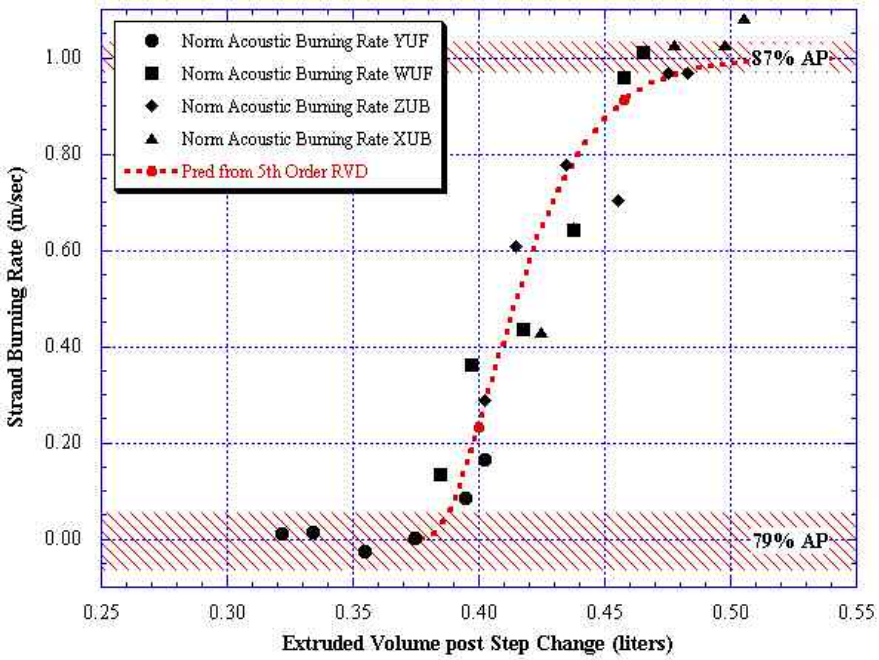

Figure 5-41. After a volume delay of 0.375 liters, the third order convolution step response in gradient architecture could be predicted using the shape factor from the fifth order RVD TSE process model.

From Figure 5-34, there was some indication from the dye that the gradient architectures for a positive and negative gradient may not be the same. However, comparing the burning rate data from the strand burning tests by spatial reflection of the data for the negative gradient, seen in Figure 5-42, the combustion properties for each gradient architecture appear to have similar spatial gradients. The correlation in these spatial gradients is a strong indication that the TSE process can create the same gradient architecture independent of the direction of the step change in the feed rate. This has important manufacturing implications, since it may not be necessary to go back to the original feed rate condition in order to generate the next gradient architecture. Therefore, in the production of graded composites using the TSE process, these results seem to indicate that gradient architectures can be simply and continuously reproduced with minimal accumulation of waste material.

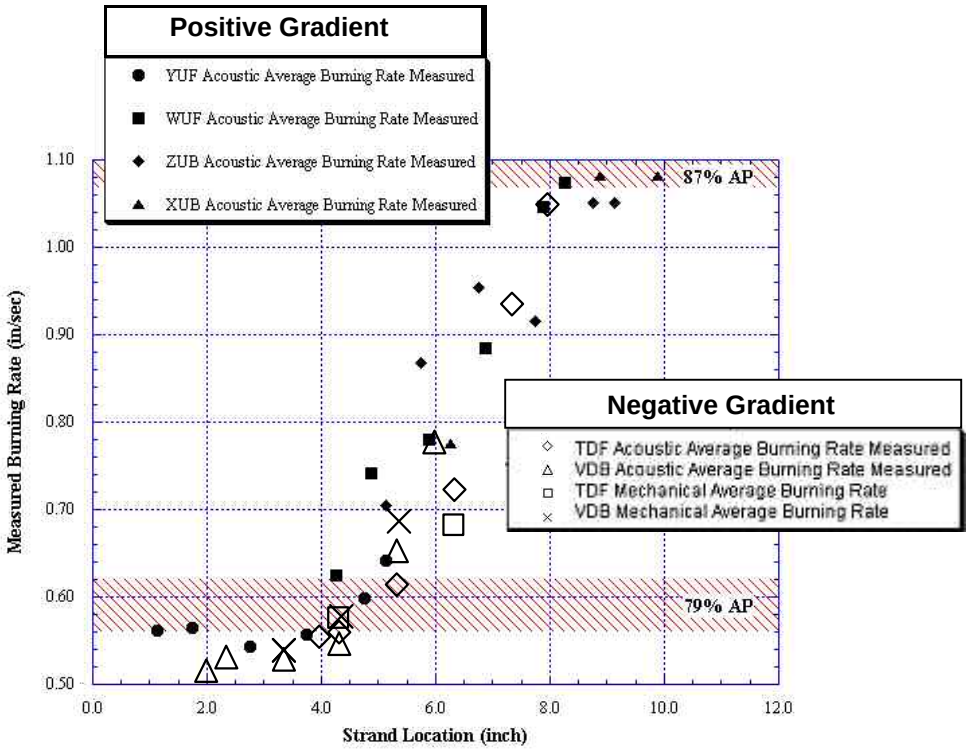

Figure 5-42. Comparison of the burning rate data from the strand burning tests for positive and negative gradients indicating that gradient architectures are similar

6.0 Microstructural Characterization of Energetic Materials

Equally important to quantifying the process in the transient state is to determine the effect on the microstructure of the extruded product as a function of position (or time). These process studies are currently underway concurrent with the development of techniques to quantify the microstructure. Generally homogeneity is highly desirable for any engineered product, and characterization methods have evolved to describe homogeneous products and deviations from homogeneity such as poor dispersion, voids, cracks, impurities, agglomerations, etc. FGMs by nature have designed microstructures that change with location, and therefore are non-homogeneous. Yet the inhomogeneity is still ordered. The characterization techniques must be quantitative, objective, and repeatable.

Furthermore energetic materials are an unusual class of composite to themselves. They are solid bodies consisting of a multimodal distribution of crystalline and sometimes metallic particles (referred to as filler) bonded to an elastomeric matrix. They are highly loaded with these particles, typically containing the highest amounts of filler physically possible. Often the bonding between the binder and filler is poor; although bonding agents are sometimes added to rocket propellants to improve mechanical properties under conditions of elastic loading. The additives are effective. But in response to mechanical damage such as sectioning with a razor or dry polishing, the larger particles are still easily displaced.

Quantitative techniques are most important to the research on FGMs. In the energetics literature and internal test reports, there is significant attention to quantitative characterization of powders as raw ingredients before compounding. However, characterization of photomicrographs of energetic materials tends to be qualitative and quite subject to bias. In the case of general composites, the methods of characterization described in the literature are common across material classes, such as, ceramics,

metals, and filled polymers. Common techniques include SEM (Nemati 1997) (Lee and Yee 2000) followed by optical stereological analysis (Russ 1986) (Kim, Mitomo et al. 1998) as well as various physical property measurements (Lee and Yee 2000). For graded composites, techniques such as ultrasonics (Marur and Tippur, 1998) and microhardness testing have been employed to characterize the gradient in mechanical properties associated with the microstructure of the gradient architecture.

As mentioned previously the functional gradient in rocket propellant will be achieved with degree of fill (volume loading) and/or coarse/fine ratio. In both cases, the result will be a change in the concentration of large particle size filler. This will be one approach to characterizing the gradient. A second technique that's bears some attention is referred to as texture analysis (Ohser, Steinbach et al. 1998). The procedure is based on the application of an algorithm to compute global characteristics of binary structures with linear filtering as the basis for the analysis. This is germane to FGMs because they consist of a binary structure, filler and binder. Ohser demonstrates his technique using an image of the microstructure for rolled stainless steel with ferrite and austenite phases. This technique yields many useful modes for characterizing images including specific line length and specific integral of curvature as well as the simple area fraction. Since Ohser's algorithm can be applied to any binary image, it should be applicable to SEM or optical microphotographs.

Consultation with microscopists in the enegetics industry will continue. The following photomicrograph appeared in an article (Bennett, Haberman et al. 1998) on non-shock ignition sensitivity of PBX-9501, a Department of Energy pressed explosive, Figure 6-1. While no reference to a specific method was given for the image's preparation, an acknowledgement was made to C. Skidmore and D. Phillips of Los Alamos National Laboratory. Personal contact with these gentlemen is proposed and will be pursued in regards to sample preparation and methods of analysis.

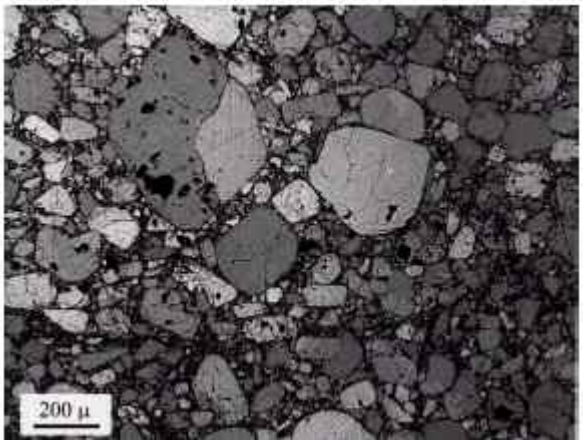

Figure 6-1. Photomicrograph of PBX-9501 as an Example of High Resolution and Excellent Constrast Between the Particles and the Matrix.

6.1 Sample and Surface Preparation

Preparation studies using inert propellant simulant in the FGM lab at UMD indicates that one promising method may be optical stereoscopy coupled with digital image analysis. Since the microstructure of an FGM varies with position, serial sectioning and sampling are necessary. The biggest challenge for highly filled polymer-bonded composites, i.e., solid rocket propellant, is particle loss (or pull-out) during cutting and polishing. The combination of hard and soft phases presents significant challenges. Improvement of the exposed surface is necessary to reveal the microstructure. However the more steps in the process and the longer the step, then the better the resolution and contrast of the filler at the expense of increasing filler loss. Figure 6-2 illustrates the effect of surface improvement.

Consultation with NAVSEAIHMD microscopist, Dr. S. Caulder, revealed that there is some concern that the process of surface preparation via dry polishing is causing damage to the specimen and introducing bias in the particle size distribution. Secondary back-scattering SEM images of a prepared surface reveal a large presence of fine particles as shown in Figure 6-3. Given that this simulant consists of 26.28 percent by weight fine particles, there is no way to determine if the particles are from the feed stream, artifacts of the dry polishing process, or attrition due to the mixing process. An experimental approach to address this issue is presented below.

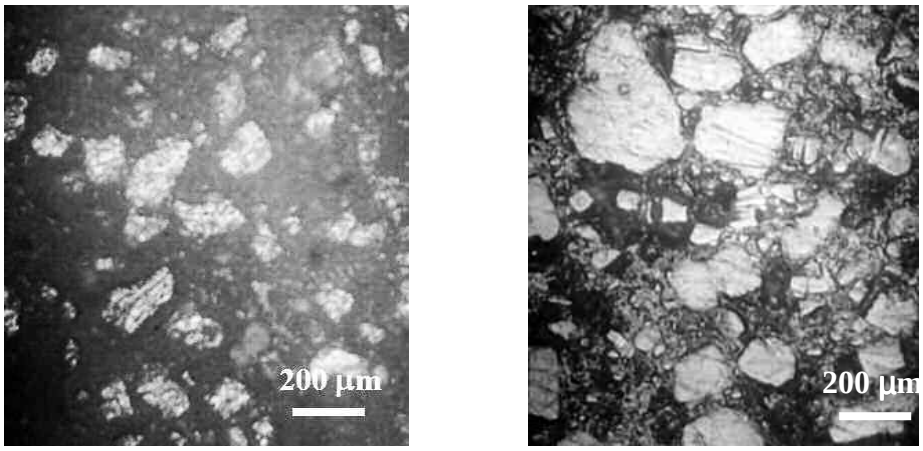

(a) (b)

Figure 6-2. Optical Photomicrographs of Inert Simulant for IH-AC3. (a) Unimproved Surface after Sectioning with Razor Blade. (b) Improved Surface after a Long Series of Polishing Steps.

Normally the sample should be cleaned with compressed air to remove any loose particles; this technique is quite effective with these types of samples as well. (Water is used for most materials across all industries; however, propellant fillers are often quite soluble in water.) Unfortunately it was determined in the FGM lab that compressed air has a tendency to remove loosely bonded large particles from the matrix. Compressed air was replaced with gentle air removal of loose dusts and followed by micro-cloth polishing; this technique has greatly reduced large diameter particle loss while still being effective in removing accumulated dusts from the polishing process.

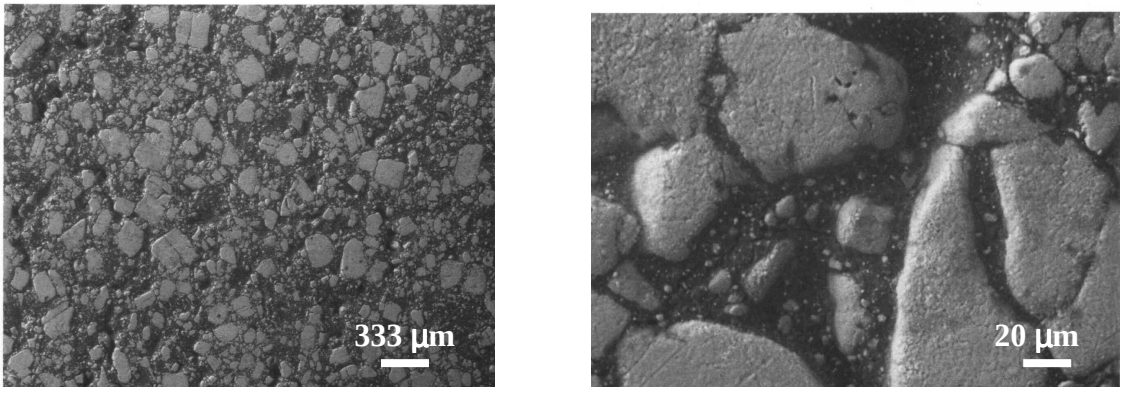

(a) (b)

Figure 6-3. SEM Photomicrographs of Inert Simulant for IH-AC3 with an Improved Surface under Relatively Low and Higher Magnifications. (a) Manification = 30x. (b) Magnification = 500x; Note the Very Small Interstitial Particles.

Using image thresholding, it was possible to obtain quantitative data from the optical and SEM micrographs. Upper gray level thresholding of the optical micrograph in Figure 6-2(b), seen in Figure 6-4, yielded a volume fraction of 0.51 for the solids loading. This value is less than the actual loading of 0.578 that was expected for a 70% by weight solids fill. Upper gray level thresholding of the SEM image in Figure 6-3(a), seen in Figure 6-5, yielded a value of 0.52, which was only 4% less. This indicates that the solids loading can be accurately determined using the sample preparation technique that was developed along with the thresholding image analysis of either optical or SEM micrographs.

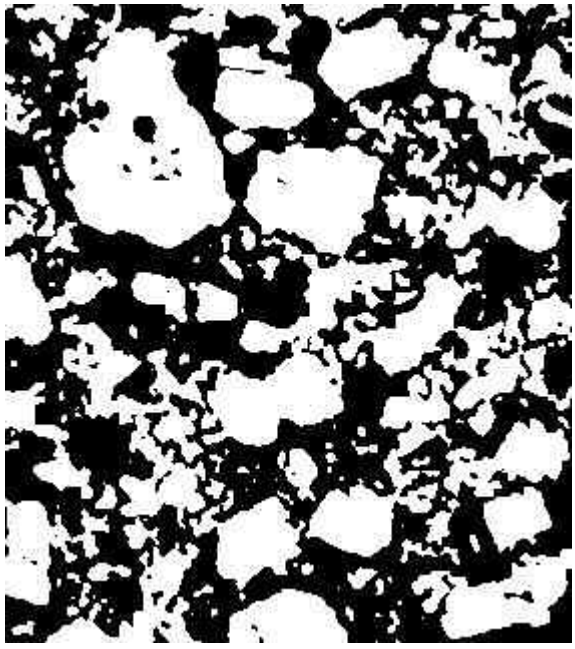

Figure 6-4. Upper gray level threshold of Figure 6-2(b) indicating location of particles.

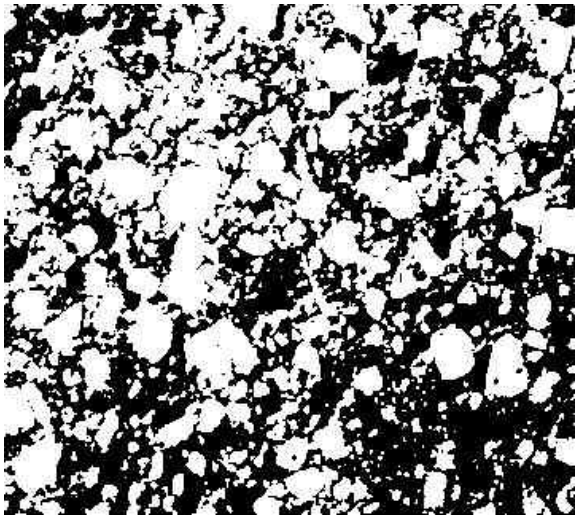

Figure 6-5. Upper gray level threshold of Figure 6-3(a) indicating location of particles.

6.2 Characterization of KCl/Elastomer Composites

After developing a technique for preparing and imaging the microstructures that evolve during TSE process for the inert propellant simulant in the extruder that was used for processing the IH-AC3 propellant, the KCl/Elastomer composite was examined. SEM micrographs in compositional mode were obtained for the 60% and 40% solids fill, as seen in Figures 6-6 and 6-7 respectively. The porosity measured using pycnometry and pyrolosis is readily observed in both micrographs. It is also clear that there are numerous small particles, as observed in the inert simulant. These particles were clearly identified as KCl by EDAXS analysis in the SEM. Unlike the inert stimulant for the IH-AC3, the presence of these particles is more of an indication that the KCl may be subject to attrition during the TSE process. As a consequence, there may be an effect of the TSE process on the particle size distribution in the graded composite.

Quantitative analysis was also performed on the KCl/Elastomer composites using SEM micrographs, which were slightly more accurate than the optical micrographs. To relate the solids loading by weight, m_p, to the volume fraction of particles, V_p, the following formula was used:

$$V_p = \frac{\rho_p m_p}{\rho_p m_p + \rho_m (1 - m_p)} \tag{56}$$

where ρ_p is the density of the particle material and ρ_m is the density of the matrix material. The volume fraction of porosity, V_o, can then be predicted using the density obtained from pycnometry measurements, ρ_{meas}, as follows:

$$V_o = 1 - \frac{\rho_{meas}}{\rho_p V_p + \rho_m (1 - V_p)} \tag{57}$$

This prediction can also be directly verified through pyrolysis measurements of m_p. The actual solids loading, V_{actual}, can then be predicted as follows:

$$V_{actual} = V_p (1 - V_o) \tag{58}$$

From thresholding the upper gray level of the SEM micrographs, as seen in Figure 6-8, the 60% by weight had an actual solids loading of 0.29, as opposed to a 0.38 from pycnometry and pyrolysis. This result is approximately 24% less than was expected. The darker particles were obtained by thresholding the lower gray level, as seen in Figure 6-9, to obtain a porosity measurement of 0.14, as opposed to the 0.05 from pycnometry and pyrolysis, approximately 120% more. The combined porosity and solids loading was 0.43 from the SEM micrograph, and 0.43 from pycnometry and pyrolysis, which indicates that the extra porosity is probably due to the 0.06 fraction of particles that were most likely removed during the grinding process due to a weaker interfacial strength between the Engage elastomer and the KCl than for the inert energetic simulant.

For the 40% by weight, which has a predicted solids loading of 0.22 from pycnometry and pyrolysis, the solids loading was 0.14 from a upper gray level threshold of the SEM micrograph, as seen in Figure 6-10. This value was approximately 36% less than the pycnometry and pyrolysis measurement. It was also somewhat consistent with the measurement from the 60% sample. The porosity was measured at 0.07 from the lower gray level threshold of the SEM micrograph, as seen in Figure 6-11. This value was approximately 17% more than the 0.06 measured from pycnometry and pyrolysis. Once again, the combined porosity and solids loading was 0.21 from the SEM micrograph and 0.28 from pycnometry and pyrolysis, where the removal of particles from the grinding process does not appear to be as severe. However, the image quality was not as sharp as the 60%, which made it more difficult to identify pores through thresholding. The image quality could also be responsible for the band of fine pores

seen near the top of the image, which was not observed in Figure 6-9. Therefore, the difference of 25% observed in the combined measurement may be attributed to the image quality. From these results, it can be concluded that the microstructural characterization can provide direct observation of the solids loading and porosity in the extruded composites. This demonstrates that the evolution of the gradient microstructure can be reliably ascertained from either microscopy or by pycnometry and pyrolysis.

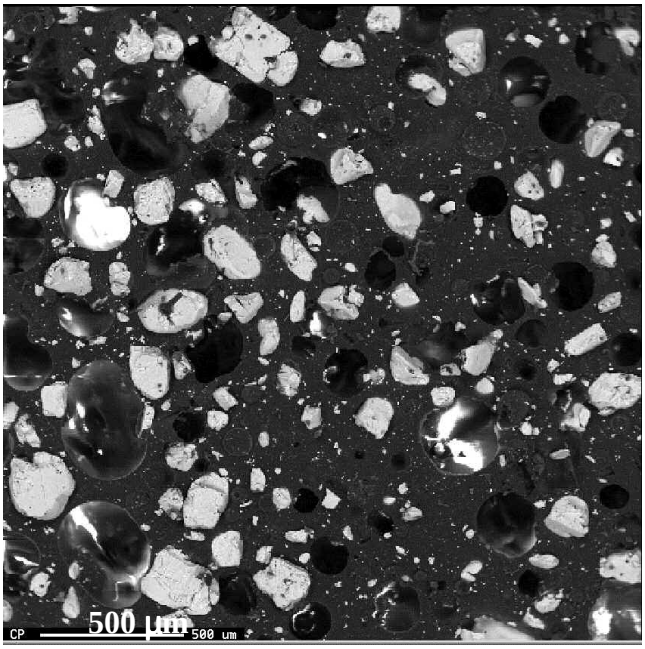

Figure 6-6. SEM micrograph of KCl/Elastomer composite with 60% solids loading.

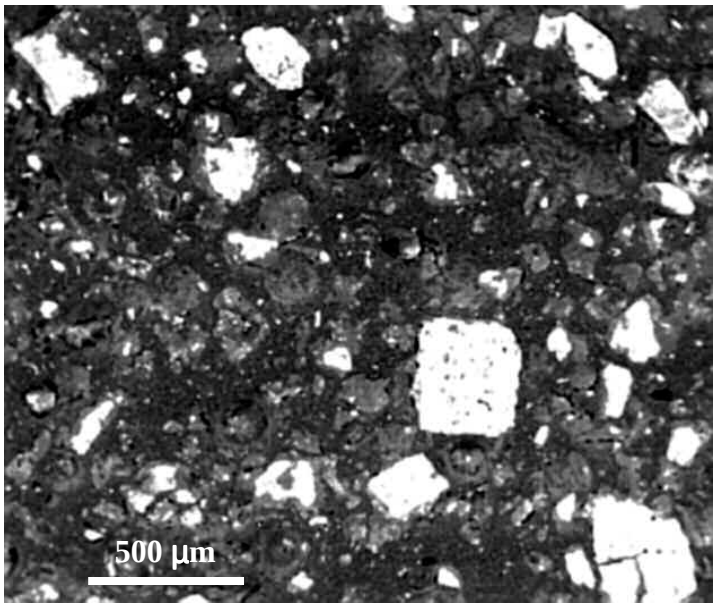

Figure 6-7. SEM micrograph of KCl/Elastomer composite with 40% solids loading.

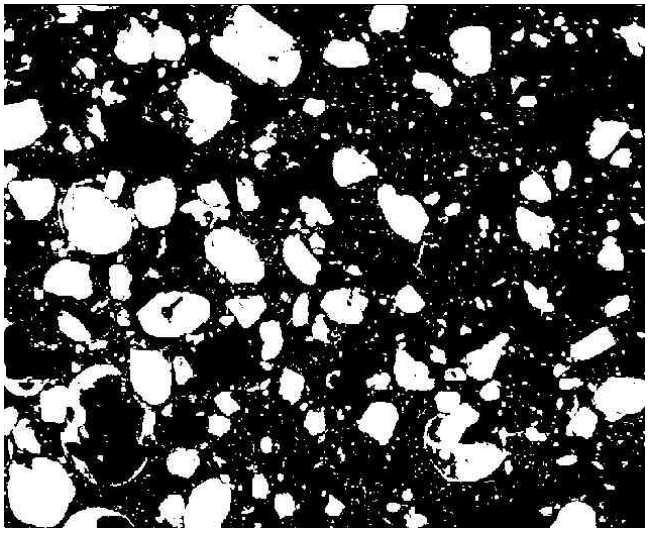

Figure 6-8. Upper gray level threshold of SEM Micrograph from Figure 6-6 indicating location of particles.

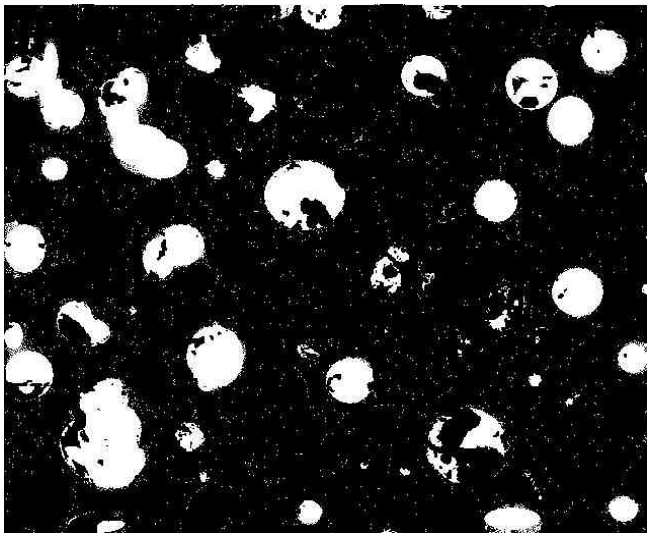

Figure 6-9. Lower gray level threshold of SEM Micrograph from Figure 6-6 indicating location of pores.

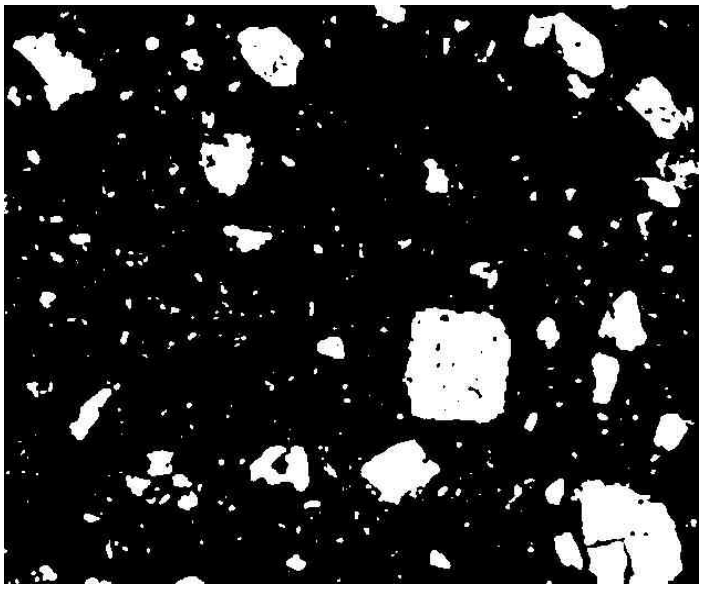

Figure 6-10. Upper gray level threshold of SEM Micrograph from Figure 6-7 indicating location of particles.

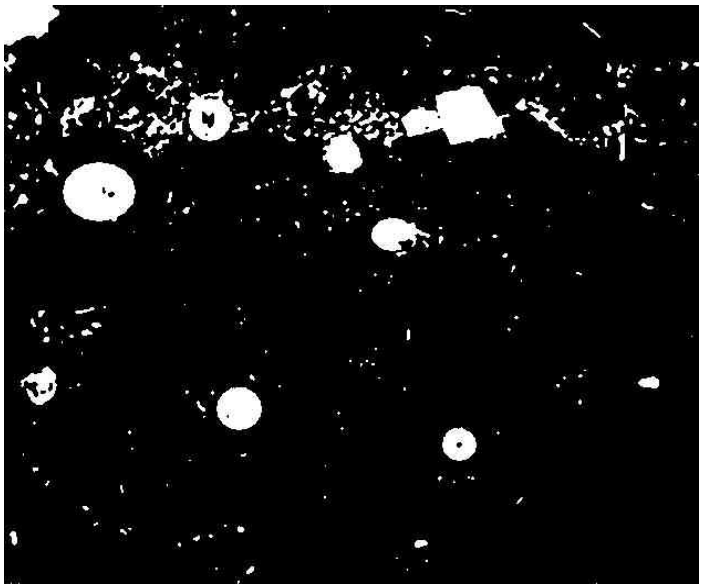

Figure 6-11. Lower gray level threshold of SEM Micrograph from Figure 6-7 indicating location of pores.

7.0 Fundamental Scientific and Technical Contributions

One of the technical challenges to developing functionally graded propellants has been the lack of a design methodology and manufacturing technology for processing continuously graded architectures in polymer composites. In this research effort, a novel continuous processing technology for fabricating functionally graded materials (FGMs) has been developed which was applied to both energetic and non-energetic materials. The continuous processing technology is known as Twin-Screw Extrusion (TSE), and was used in a transient operating condition to achieve gradient architectures.

Through the course of this research investigation, many fundamental scientific and technical contributions were made that advanced the understanding of how gradient architectures evolve in the TSE process. This knowledge is essential to developing an IDP that can ultimately serve as a tool for the designers and manufacturers of advanced polymer composites, in particular advanced energetics applications. Using the IDP, an entirely new methodology for designing energetic systems will be available for advanced energetics concepts, where the in-flight performance of a rocket motor (simply that part of a rocket consisting of the propellant grain, its case, and a nozzle) can be specified without having the constraint of geometrically complex designs that can not produce the desired performance either because of manufacturing or material limitations. Employing the process models that were developed in this research effort, the gradient architecture that achieves the specified performance can be easily predicted with or without geometric constraints in the IDP, as well as the operating conditions that are necessary to create it using a given manufacturing process.

Therefore, one of the most important contributions of this research effort has been the development of appropriate processing models that describe the relationship between operating conditions and the gradient architectures that evolve in the TSE process. The models define the limits in the TSE process restricting the evolution of the

gradient architectures that are created by the screw geometry and operating conditions, and therefore constrain the range for the architectural parameters over which the gradient architecture can be fabricated. However, for each TSE configuration (i.e., screw geometry, extruder type) the shape factor and order of the RVD must be determined experimentally in order to define these constraints using the process model developed in this research effort.

Through this research effort, fundamental questions relating to the operation of a twin-screw extruder in a transient state and to the microstructures of highly filled polymer composites that evolve during this process have been answered. These questions, originally posed in Chapter 1, have been answered as follows:

> 1. The effect of transient operating conditions during processing on the evolving gradient architecture of the extruded composite has been characterized using *in-situ* optical techniques and a posteriori physical property measurements.
>
> 2. This evolution has been predicted using a convolution process model based on Residence Time Distributions (RTDs) and Residence Volume Distributions (RVDs) for both energetic and non-energetic materials.
>
> 3. An approach for characterizing the gradient architecture in the extruded material has been developed based on pycnometry, pyrolosis, microscopy, and, for energetic materials, strand burning.
>
> 4. The burning rate performance for the gradient architecture has been determined over a wide range of compositions using a design of experiments approach, and has been used in the *a posteriori* modeling of the gradient architecture using the RVD determined from the *in-situ* optical measurements.

These answers have resulted in the following scientific and technical knowledge:

- The relationship between the gradient architectures that evolve in the TSE and the operating conditions for the extruder has been characterized through new process models based on RVDs and RTDs
- The applicability of RTD and RVD characterization of the TSE process has been extended from polymers to highly-filled polymer composites

- An approach for characterizing the gradient architecture has been developed based on physical property and microstructural measurements.
- The dependence of the burning rate performance on the compositions in the gradient architecture has been characterized

The research described in this thesis will also have a broader impact on commercial and military applications for both energetic and non-energetic of FGMs as follows:

- The new process models and characterized properties provide the basis for establishing an IDP for energetic materials that provides the operating conditions to meet a desired performance objective for a given energetic formulation and TSE configuration
- Establishes a new technology area for producing tailored energetic systems for commercial, as well as military, applications
- Establishes new techniques for fabricating FGMs using the transient attributes of continuous processing technologies
- Describes mixture experiments with operating conditions that are of great interest to energetics manufacturing facilities such as NAVSEAIHMD.
- Presents new characterization techniques for energetic and non-energetic extruded polymer composites

For these reasons, the quantitative residence time of the system becomes a convenient measurement of the cumulative effect of all process and material parameters on the transport and mixing of the material in the TSE process. In the volume domain, the residence distributions are independent of mass throughputs and degree of solids loading (over ranges tested) and only dependent upon screw geometry and operating conditions such as extruder screw speed or temperatures. Exploring models of lower and higher orders provided a much better description of the residence responses. The results of this research effort have shown that a convolution of a RD model with a step input yields a good prediction of the gradient architecture that evolves during the TSE process. Therefore, the normalized residence distribution function can be determined

from a small perturbation to the input of a twin-screw extruder, and then be used to predict the gradient architecture that can be fabricated in that extruder.

7.1 Processing of Inert Composites

Several research issues were addressed through the processing of inert composites in the UMD facilities. To model the TSE process for these materials, RTDs were fit to a second order process model based on the inverse Laplace transform of a model for two perfect mixers in series with a dead time. The second order model was found to fit the experimental data for inert composites much better than a first or third order model. It is important to remember that this process model permitted the process to be represented as an ideal abstraction of a physical process. However, the advantage of this representation was the capability of the process model to describe the behavior of a complex process with few parameters. Furthermore, the shape factors determined with the RTD fits were insensitive to composition being nearly the same for 40% or 60% solids fill. It is this insensitivity that makes it possible to predict the gradient architecture using the convolution model, and which indicates that the rheology of the material does not have a significant effect on the TSE process.

In-situ optical measurements tracked the evolution of the gradient architecture. Optical probes were placed near the end of the screws where the material entered the extrusion die. To predict the evolution of the gradient architecture using the RTD process model, shape factors from a second order RTD process model were used in a convolution with a first order response. While results for unfilled material exhibited good correlation between the measurements and predictions, the optical response for the filled material demonstrated a more significant variation. This was attributed to problems with transporting the tracer pellets in the TSE process when there is a large viscosity change associated with a step change in solids fill.

Graded inert composites were extruded using both slit and square dies. The slit die proved to be the most challenging to work with, since it introduced complex three-dimensional die effects into the evolving gradient architecture. The complex flow field was attributed to die entrance effects resulting from the compromised design of that die. It was expected that any die would have some measurable effect of material distribution within the evolving gradient structure due to shear-induced flow. This was seen with

each die in that the gradient would first appear in the center of the extrudate and spread outward as a function of time until the transition was complete—a two dimensional gradient. However, the gradient architectures produced using the square dies closely approached a one-dimensional gradient architecture, which was much less challenging to characterize using the approaches developed in this research effort. The three-dimensional effects attributed to the slit die likely contributed to the difficulties in characterizing the physical properties of the graded slit-shaped specimens.

To characterize the gradient architecture of the extruded inert composites, an approach based on physical property measurements was developed. This approach required complete destruction of portions of the gradient architecture through pyrolosis to quantitatively determine the content of solids. In addition, pycnometer measurements were used to characterize the density and determine the porosity of the samples introduced during the extrusion portion of the process. The porosity was determined to be approximately 5%. The porosity and solids loading was also directly confirmed for the extreme compositions in the gradient architecture using microscopy techniques. The gradient architectures determined using these measurements also correlated well with the gradient architectures determined using a posteriori optical measurements. These results indicated that the dispersed color concentrate was transported at the same rate as the KCl particles.

While RTD models were convenient to characterize process responses, e.g., on-line probes, die pressure, extrusion torque, RVD models necessary to describe the gradient architectures that were characterized in the extruded composite. The RVD models could be directly determined from the RTD models through a simple transformation using the volumetric throughput. To predict the gradient architecture, RVD shape factors were used from a single composition in the gradient architecture. Despite the variation in feed rates associated with each composition in the gradient architecture, the predicted gradient architectures correlated very well with the gradient architectures that were characterized. However, there was not a significant difference if either a first order or second order response was used in the convolution model.

7.2 Processing of Energetic Materials

There were a number of research issues for processing energetic materials that have been addressed for the first time in this research project. One is the determination of the residence distribution using an on-line method for an energetic material processed in an extruder in the United States. Worldwide there has been no data published on residence distributions with energetic materials. Additionally, it was also necessary to use a design methodology for a mixture experiment that incorporated process variables, also referred to as process factors, for determining the combustion properties of the material over the composition range spanned by the gradient architecture. These mixture experiments were confined to two AP feedstreams, which was more than sufficient for determining the appropriate composition for a single feed stream that was used in the fabrication of a gradient architecture for the strand burning tests.

The mixture experiments also provided the opportunity to settle a longstanding uncertainty in regards to experimental observations that suggested extruder screw rpm may influence the burning rate. Therefore, three mixture factors (coarse composition, coarse-to-fine ratio, and total solids loading) and one process factor (screw speed) were varied in the experiments. Despite the complex relationships between the physical limitations that are imposed on practical energetic formulations and the constraints that are imposed on the operating conditions for processing these materials in the twin-screw extruder, it is now possible to simultaneously predict the effects of formulation and operating conditions on the combustion properties using a response surface analysis to construct a statistical model.

Aside from the obvious benefit of revealing the full range of burning rates within the process and formulation constraints chosen, the response surface analysis provided invaluable insight in choosing directions in which to design gradient architectures. In that the propellant formulations associated with the gradient architecture had never before been produced or tested, the response surface analysis was necessary for selecting the factors that could be used to produce an appropriate gradient architecture using positive and negative step changes in the feed rates for a single feeder. Predictions of the burning rates for the extremes of the desired gradient and some intermediate points were made possible using the response surface analysis. From these predictions,

an estimate of the burning rate exponent could be calculated in order to determine the extremes that would not result in an explosion or flame-out. These conditions were then used to produce the first functionally graded rocket propellants for testing and characterization.

The results from the mixture experiments also indicated some alternatives for creating gradient architectures in energetic applications. Instead of varying the ingredients, it is possible to vary the screw rpm to control the variation in burn rate within the gradient architecture. It is also possible to consider deliberate and subtle changes in the screw rpm to impart particular nuances in the burning of the grains to compensate for burning rate anomalies that are currently present in homogeneous composite propellants.

The actual fabrication of the graded propellants represented the most complicated extrusion run performed to date at NAVSEAIHMD in the 13 plus years of the 40 mm facility because of the control room operations required to remotely execute the gradient formations and collections. The operations were so detailed that they required four people at four different stations in the control room. A flawless execution of the processing run with no upsets enabled all the grains to be produced in one day's work without having to conduct a refill of the AP hopper.

Measurements of the screw torque during the extrusion process correlated with *in-situ* optical measurements, which were modeled using a first order response with a shaped factor determined from a second order RTD process model. The optical measurements were able to detect the evolution of the gradient without tracer, unlike in the inert composite experiments. Measurements of die pressure were modeled using a second order response, while the pressure response due to the arrival of the gradient was consistent with the volume delay, v_d. Both the die pressure and torque exhibited a slight over-shoot as the die was cleared of lower viscosity propellant during the gradient extrusion. The second order RTD shape factors were powerful in that they were able to characterize color response, extrusion torque response, and die pressure. Furthermore, as with the inert composites, the RTD shape factor was insensitive to composition being nearly the same for either 79 or 87 percent solids loading.

For the extruded energetic material, the gradient architecture was characterized a posteriori using mechanical and acoustic strand burning tests. The results from these tests spanned the range of burn rates that were anticipated from the homogeneous tests, and correlated well with each other. However, unlike the inert polymers and composites, RTD data was best fit using a fifth order RTD process model. The shape factor from the RTD process model was then used in third order response for the convolution model to predict the gradient architecture determined from the strand burning tests, unlike the first order response used for the inert polymers and composites. Furthermore, it was determined that the gradient architecture evolved independent of the direction of the step change for the feed rate. This has important implications on the manufacturing of graded composites, since it implies that there is no need to return to the original feed rate first before a gradient architecture can be continuously reproduced, simplifying the production of the graded composites and minimizing waste.

8.0 Future Work

During the course of this research investigation, some interesting research issues have been uncovered that affect the TSE processing of continuously graded polymer composites. The results obtained using the inert polymer composite can be explored further using ideal simulants to determine processing effects on the composite micro-structure and on bimodal particle distributions. There are some future plans to test functionally graded IH-AC3 in a modified slab motor test. Also, some additional process equipment and analytical instrumentation would enhance future investigations. This future work is now discussed further.

8.1 Future Research Directions and Associated Areas of Research

The following are potential research directions and associate areas of research for future work:

1. Characterize two and three-dimensional die effects on the evolution of the gradient architecture during TSE processing.

2. Achieve a gradient architecture utilizing extruder screw speed alone or in conjunction with feeding rates.

3. Investigate microstructural characteristics that may be the mechanism responsible for the measured variations in burn rate due to changes in screw speed for a homogeneous formulation.

4. Explore non-destructive test methods, such as scanning acoustic microscopy, ultrasonics, Low-angle X-ray Scattering, or Magnetic Resonance Imaging, to characterize three-dimensional particle distributions in the microstructure of the gradient architecture.

5. Characterize the effects of larger variations in solids fill on the residence distributions, as well as variations due to changes in binder rheology.

8.2 Ideal Simulants for Determining Processing Effects on Composite Microstructures and on Bimodal Particle Distributions

The source of fine particles in the inert polymer composites will be investigated further in future studies that will consist of ideal simulants that consist of solids fill with a tightly controlled particle size. The filler would be screened through sieves to eliminate sizes below some nominal diameter such as 250 μm or a slim fraction between two screens. With this approach, it will be possible to differentiate the source of fine particles as either particle attrition during the TSE process or the sample preparation.

The ideal simulants also provide an opportunity to evaluate methods of preparation and microstructure examination and characterization. By providing a sample with a known volume loading and particle size distribution, the efficacy of each method and approach can be quantitatively determined. A similar argument is true for graded samples. The starting and stopping compositions will be known and can be verified. The specific nature of the gradient will be unknown but can be determined more easily under these controlled conditions. This data can be further evaluated and correlated with predictions by the RVD or RTD convolutions for a given screw geometry. For the same reasons, an ideal material will make it easier to provide more accurate measurements of compositional variations in the gradient architecture.

An accurate representation of a rocket propellant is a highly filled composite consisting of a bimodal distribution of small and large particle sizes. This can be achieved with an ideal simulant that has similar particle sizes. To produce ideal simulants, a distribution of large diameter KCl particle sizes can be fed as one feed stream. Using a second feeder, a second distribution of much smaller particle sizes can be fed. The graded compositions can then be achieved using a combination of overall solids fill and various coarse-to-fine ratios, as was done for the homogeneous formulations fabricated for burning rate characterization at NAVSEAIHMD.

8.3 Future Plans for Small Rocket Motor Testing

At the same time grains were being processed using the ZSK-40 TSE at NAVSEAIHMD for strand burning rate testing, additional functionally graded grains were produced for

future testing in small rocket motor hardware. Motor testing offers the most realistic measure of a propellant's combustion properties. The test provides thrust-time and pressure-time measurements to evaluate the propellant's performance in its intended operating environment, and verify new performance models being developed for the IDP. Once the performance model is verified, the IDP can be completed and the optimal gradient microstructure determined for future verification.

There were eight grains produced for small motor testing—three each of the two gradient directions and one each of the high and low AP homogeneous compositions. The extruded grain samples for rocket motor testing had the same geometry as those grains that were extruded and sectioned for strand burning—1.25 in. diameter and 30 in. length. The small motor test grain length must be 7.75 in. or less in length. The results of the strand burning rate data will be used to define location of the beginning and end of the gradient in the 30 in. sample.

8.4 Extension of Current Measurement Capabilities

For on-line sensors that operate in the time domain, it was necessary to fit the response using RTD parameters. With instrumentation to experimentally measure material flow rate at the die (or elsewhere internal to the extruder); one could transform the time-based responses to volume-based. Then the more general and preferential treatment of the on-line probe data in the volume domain (RVD) could be performed.

There are plans to continue to identify and evaluate instrumentation and analytical characterization methods to quantify local material properties. Two well established on-line techniques employed throughout industry are near-infrared (NIR) spectroscopy and densitometers. Micro-scale mechanical property test methods could be a general area of future investigation, although the data presented in this research effort is not encouraging. There may also be thermal methods that may be sensitive enough to characterize variations in thermal properties within the gradient architectures in polymer composites.

There is a desire to increase the accuracy for characterizing the combustion properties in the gradient architecture by obtaining measurements over lengths shorter than 1.5 in.—the shortest reliable length tested in this research effort. It would significantly enhance the accuracy to have resolutions lower than 0.5 in. More tests

using the acoustic strand burner apparatus could enable fine-tuning of the measurement conditions to also enhance the measurement accuracy, perhaps including an upgrade in software and hardware as well. It has been suggested that new tests could be developed, such as multiple bridge wires in series regularly spaced in close proximity, to characterize the gradient architecture in a single test. Another type of apparatus that has been suggested is a window bomb that would allow real-time video analysis of the burn front advancement. This would permit continuous measurements of the location of the burn front as a function of time, from which the burn rate can also be determined continuously by taking first derivatives of the measurements.

REFERENCES

ASTM (2002). D2240-02 Standard Test Method for Rubber Property-Durometer Hardness. West Conshohocken, PA, ASTM International.

Beauregard, M. R., R. J. Mikulak, et al. (1992). A Practical Guide to Statistical Quality Improvement: Opening Up the Statistical Toolbox. New York, Van Nostrand Reinhold.

Bennett, J. G., K. S. Haberman, et al. (1998). "A constitutive model for the non-shock ingnition and mechanical response of high explosives." J Mech Phys Solids **46**(12): 2303-22.

Booy, M. L. (1980). "Isothermal Flow of Viscous Liquids in Corotating Twin Screw Devices." Polymer Engineering and Science **20**(18): 1220-8.

Bruck, H. A., F. M. Gallant, et al. (2002). Development of a Novel Continuous Processing Technology for Functionally Graded Materials using an Inverse Design Procedure. 2002 SEM Annual Conference & Exposition on Experimental and Applied Mechanics, Milwaukee, Wisconsin, Society for Experimental Mechanics, Inc., Bethel, CT.

Bur, A. J. and F. M. Gallant (1991). "Fluorescence Monitoring of Twin Screw Extrusion." Polymer Engineering and Science **31**(19): 1365-1371.

Carvalheira, P., J. Campos, et al. (1996). Some rules for the design of high solid loading composite solid propellants and explosives. Energetic Materials-Technology, Manufacturing and Processing, Karlsruhe, FRG, Fraunhofer institut Chemische Technologie.

Cornell, J. A. (1990). Experiments with Mixtures. New York, John Wiley & Sons, Inc.

Cornell, J. A. (1995). "Fitting Models to Data from Mixture Experiments Containing Other Factors." Journal of Quality Technology **27**(1): 13-33.

Crosier, R. B. (1986). "Mixture Experiments: Geometry and Pseudo-Components." Technometrics **26**: 209-216.

Danckwerts, P. V. (1953). “Continuous Flow Systems: Distribution of Residence Times.” Chemical Engineering Science **2**(1): 1-18.

Dean, D. L. (1993). Tailoring Propellant Mechanical Properties via Processing. JANNAF Propellant Development and Characterization Subcommittee, Lawrence Livermore National Laboratory, Livermore, CA, CPIA.

Fogler, H. S. (1999). Elements of Chemical Reaction Engineering. Upper Saddle River, NJ, Prentice Hall.

Gallant, F. M. (2000). Continuous Extrusion of EX-101 Gun Propellant--A Green Munition. Indian Head, MD, Naval Surface Warfare Center Indian Head Division**:** 30.

Gallant, F. M., W. Newton, et al. (1999). Feeding Performance Studies for CPOCP Program Ingredients. Indian Head, MD, Naval Surface Warfare Center Indian Head Division**:** 41.

Gao, J., G. C. Walsh, et al. (1999). “Residence-Time Distribution Model for Twin-Screw Extruders.” American Institute of Chemical Engineering Journal **45**(12): 2541-2549.

Gao, J., G. C. Walsh, et al. (2000). “Mean Residence Time Analysis for Twin Screw Extruders.” Polymer Engineering and Science **40**(1): 227-237.

Gasner, G. E., D. I. Bigio, et al. (1999). “A New Approach to Analyzing Residence Time and Mixing in a Co-Rotating Twin Screw Extruder.” Polymer Engineering and Science **39**(2): 286-298.

Gocmez, A., C. Erisken, et al. (1998). “Mechanical and burning properties of highly loaded composite propellants.” Journal of Applied Polymer Science **67**: 1457-64.

Hicks, C. R. (1993). Fundamental Concepts in the Design of Experiments. New York, Oxford University Press.

Kim, Y.-W., M. Mitomo, et al. (1998). “Effect of Initial (α-Phase Content on Microstructure and Mechanical Properties of Sintered Silicon Carbide.” Journal of the American Ceramic Society **81**(12): 3136-40.

Kowalski, S. and J. Cornell (2000). “A new model and class of designs for mixture experiments with process variables.” Communications in Statistics-Theory and Methods **29**(9&10): 2255-2280.

Lee, J. and A. F. Yee (2000). “Micro-Mechanical Deformation Mechanisms in the Fracture of Hybrid-Particulate Composites Based on Glass Beads, Rubber and Epoxies.” Polymer Engineering and Science **40**(12): 2457-70.

Levenspiel, O. (1989). The Chemical Reactor Omnibook. Corvallis, Oregon, OSU Book Stores, Inc.

McLean, R. A. and V. L. Anderson (1966). “Extreme Vertices Design of Mixture Experiments.” Technometrics **8**: 447-456.

Mudalamane, R. (2002). Transient Behavior of Extruders. Department of Mechanical Engineering. College Park, MD, University of Maryland**:** 72.

Muscato, R., M. Michienzi, et al. (1999). Continuous Processing of Composite Propellant Program Live Processing. Indian Head, Maryland, Indian Head DIvision, Naval Surface Warfare Center**:** 40.

Naes, T., E. M. Faergestad, et al. (1998). “A comparison of methods for analyzing data from a three component mixture experiment in the presence of variation created by two process variables.” Chemometrics and Intelligent Laboratory Systems **41**: 221-235.

Nemati, K. (1997). “Fracture Analysis of Concrete Using Scanning Electron Microscopy.” Journal of Scanning Microscopies **19**(6): 426-30.

Newton, W., F. M. Gallant, et al. (1999). Preblending and Feeding Strategies for the Continuous Processing of Extruded Composite Propellant. Indian Head, MD, Naval Surface Warfare Center Indian Head Division**:** 30.

Nise, N. S. (2000). Control Systems Engineering. New York, John Wiley & Sons, Inc.

NOS (1968). Introduction of Propellant Technology. Indian Head, MD, Naval Ordnance Station**:** 181.

Ohser, J., B. Steinbach, et al. (1998). “Efficient texture analysis of binary images.” Journal of Microscopy **192**(Pt. 1): 20-8.

Piepel, G. F. and J. A. Cornell (1994). “Mixture Experiment Approaches: Examples, Discussion, and Recommendations.” Journal of Quality Technology **26**(3): 177-196.

Rampichini, S., D. Ruspa, et al. (2000). Acoustic Emission of Underwater Burning Solids Rocket Propellants. Combustion of Energetic Materials. K. K. Kuo and L. T. DeLuca. New York, Begell House, Inc.

Rauwendaal, C. (1986). Polymer Extrusion. Munich, Hanser.

Reddy, J. N. (1997). Mechanics of Laminated Composite Plates Theory and Analysis, John Wiley & Sons.

Russ, J. C. (1986). Practical Stereology. New York, Plenum Press.

Snee, R. (1975). “Experimental designs for quadratic models in constrained mixture spaces.” Technometrics **17**(2): 149-59.

Snee, R. and D. W. Marquardt (1974). “Extreme Vertices Designs for Linear Mixture Models.” Technometrics **16**(3): 399-406.

Staub, H., K. Neuenschwander, et al. (1989). Comparison of Continuous and Batch Processing in Respect of the Project of a New Single Base Propellant Plant. Joint International Symposium on Compatibility of Plastics and Other Materials with Explosives, Propellants, and Pyrotechnics, & Processing of Explosives, Propellants, and Ingredients, The Cavalier Hotel Beach Club and Convention Center, Virginia Beach, VA, ADPA.

Suresh, S. and A. Mortensen (1998). Fundamentals of Functionally Graded Materials: Processing and Thermomechanical Behavior of Graded Metals and Metal-Ceramic Composites. London, IOM Communications.

Thompson, R. and M. Michienzi (1998). On-line Quality Analysis System: On-Line Near Infrared (NIR) System. Indian Head, MD, Indian Head Division Naval Surface Warfare Center.